Drivers of Change in Haida Gwaii Kelp Forests: Combining Satellite Imagery with Historical Data to Understand Spatial and Temporal Variability

By

Lianna Gendall

B.Sc. University of Alberta, 2016

A Thesis Submitted in Partial Fulfilment of the Requirements for the

Degree of

MASTER OF SCIENCE

in the Department of Geography

©Lianna Gendall, 2022
University of Victoria

All rights reserved. This thesis may not be reproduced in whole or in part by photocopy or other means, without the permission of the author.

We acknowledge and respect the lək^{w}əŋən peoples on whose traditional territory the university stands and the Songhees, Esquimalt and W̱SÁNEĆ peoples whose historical relationships with the land continue to this day.

Drivers of Change in Haida Gwaii Kelp Forests: Combining Satellite Imagery with Historical Data to Understand Spatial and Temporal Variability

By

Lianna Gendall

B.Sc. University of Alberta, 2016

Supervisory Committee:

Dr. M. Costa, Supervisor (Department of Geography)

Dr. M. Hessing-Lewis, Committee Member (Hakai Institute)

Dr. Natalie Ban, Committee Member (School of Environmental Studies)

Abstract

Globally, kelp forests provide the foundation of temperate coastal ecosystems through the creation of three-dimensional habitat which supports many significant economic, cultural, and ecological species. With the increasing threat of local and global anthropogenic stressors including climate change, the long-term, large-scale monitoring of kelp forests is crucial in understanding the response of these foundation ecosystems to spatio-temporal drivers in a time of rapid global change. On the coast of British Columbia, Canada, kelp forests of *Macrocystis pyrifera* and *Nereocystis luetkeana* show highly variable patterns of change, however, lack sufficient time series data to truly understand trends, threats, and drivers. In particular, Haida Gwaii, an archipelago off the main coast of British Columbia, supports some of the most expansive kelp forests in the province. However, local Haida people have observed drastic declines at traditional harvesting sites leading to the prioritization of the management, monitoring and protection of these crucial ecosystems throughout their territory. Remote sensing technology now provides an effective way to track changes and trends in remote kelp forest ecosystems at large scales like that of the Haida Gwaii coastline. Specifically, Earth Observation satellite imagery of a variety of spatial resolutions exists back to the 1970s which can be leveraged for mapping kelp forest canopies through time. This research aims to quantify the distribution, variability, and drivers of change of Haida Gwaii kelp forests with the use of satellite imagery and historical data. Specifically, to address this goal, (i) we develop a methodological framework that enables the creation of a long-term dataset of kelp canopy area using archived multispectral satellite imagery from multiple satellite sensors that vary in their spatial resolution (0.5 m – 60 m) and temporal coverage (1973-2021). To do this, we combine a workflow of standardized remote sensing practices and an adaptable image-to-image object-

based classification approach to create the multi-satellite kelp mapping (MSKM) framework including an analysis of the impact spatial resolution has on the detectability of kelp forests and highlight ocean floor slope as a metric to understand uncertainties associated with using products from a range of spatial resolutions. In particular, we find that ocean floor slopes higher than 11.4 % led to high uncertainties when using medium-resolution imagery and as such, these areas were removed from further analyses. Next, (ii) we define changes in Haida Gwaii kelp forest canopy in association with drivers of change over the last 100 years using historical data (1867-1945) and medium- to high-resolution archived satellite imagery (1973-2021) at regional to local scales of analysis. Overall, kelp forest canopy area varied with low- and high-frequency climate indices where lower kelp forest canopy area occurred during warmer conditions. Additionally, patterns of kelp forests change varied across subregions where areas in the North showed considerable losses associated with a strong local gradient of sea surface temperature coupled with the cool to warm regime shift that occurred within the Pacific Decadal Oscillation in the late 1970s. In comparison, kelp forests in the cooler areas in the South showed long term resilience persisting for over a century throughout multiple heatwaves and regime shifts.

Table of Contents

List of Tables

List of Figures

Acknowledgements

I would like to acknowledge the Haida people on whose unceded traditional territory this research was conducted. It is with deep thanks to the Council of the Haida Nation and the Haida people, for allowing me to work on their beautiful, complex, and diverse territory which they continue to steward and protect since time immemorial.

First, I would like to thank my supervisor, Dr. Maycira Costa, for the guidance, care, laughter, and knowledge she has provided me over these past years. I would also like to thank my committee member Dr. Margot Hessing-Lewis for her mentorship and support especially in the facilitation of my trip to Haida Gwaii. Many thanks to my committee member, Dr. Natalie Ban for her kind encouragement and input on my thesis. Special thanks to the expertise and support provided by the Hakai Institute, especially the Geospatial team. I would also like to thank the many professionals, such as Dr. Lynn Lee, Stuart Crawford, and Joanne Lessard, whose knowledge and excitement for kelp forests, and ecology inspired me throughout this journey. I would like to extend thanks to Dr. Patrick Martone and Dr. Chris Neufeld for originally introducing me to the wonderful world of kelp through courses at the Bamfield Marine Science Center. I would like to thank Niisii Guujaw for first telling me stories of Haida Gwaii and sharing her love of her beautiful territory with me. Thank you deeply to Luba Reshitnyk and Sarah Schroeder not only for the kelp mapping mentorship but the much-needed support and life lessons along the way. Brian, many thanks for keeping me sane in and outside the lab. Thank you to my family and friends, especially my parents, for the continued emotional support along the way. Lastly, a massive thank you to my partner, Sam Starko, for the unwavering care, the shared steadfast love of kelp forest ecology and the endless ability to talk me through any crises that have led me here over the years

1.0 Introduction

1.1 Overview

Kelps (order Laminariales) form important coastal habitats, known as kelp forests, found across the world's temperate nearshore coastlines (Wernberg *et al.*, 2019) and support biodiverse, productive ecological communities (Johnson *et al.*, 2003; Krumhansl *et al.*, 2016; Wernberg *et al.*, 2019). Kelps play an integral part in temperate ecosystems and provide many ecosystem goods and services to humans (Filbee-Dexter & Wernberg, 2018). However, many threats, such as climate change, overfishing, invasive species and increasing harvest, threaten the health and persistence of kelp forests globally (Krumhansl *et al.*, 2016; Wernberg *et al.*, 2019; Bennion *et al.*, 2019). In particular, local anthropogenic stressors coupled with the increasing frequency and duration of oceanic heat stress events and storms as a result of global climate change threaten kelp forests (Dayton *et al.*, 1999; Easterling, 2000; Oliver *et al.*, 2018). Recent work highlights the variable and negative impacts of these conditions on the health, resilience and persistence of kelp forests worldwide (Wernberg *et al.*, 2013; Bell *et al.*, 2015; Filbee-Dexter *et al.*, 2016; Wernberg *et al.*, 2016; Krumhansl *et al.*, 2016; Filbee-Dexter & Wernberg, 2018; Pfister *et al.*, 2018; Schroeder *et al.*, 2019a; Starko *et al.*, 2019; Cavanaugh *et al.*, 2019b; Smale, 2020; Starko *et al.*, 2022).

Due to the increasing severity of threats, kelp forests show a declining trend of approximately 2 % per year globally (Krumhansl *et al.*, 2016). However, across their global distribution kelp forests show highly variable patterns of change highlighting the importance of understanding local to regional scale drivers in kelp forest dynamics across space and time. In particular, notable deterioration and losses have occurred in Western Australia (Wernberg *et al.*, 2013, 2016), California (Rogers-Bennett & Catton, 2019; McPherson *et al.*, 2021), Tasmania (Butler *et*

al., 2020), and Chile (Vega *et al.*, 2014; Hamilton *et al.*, 2022). Some losses result from rapid climate induce regime shifts like those documented in Western Australia which led to a 100 km range contraction of *Ecklonia radiata* and other losses result from the direct effect of anthropogenic factors such as the overharvesting of *Lessonia spp.* and *Macrocystis pyrifera* in Northern Chile, or the increased urban pollution in Kola Bay, Russia or New South Whales, Australia (Filbee-Dexter & Wernberg, 2018).

On the Pacific coast of Canada, British Columbia (BC), kelp forests are formed by *Nereocystis luetkeana* and *Macrocystis pyrifera*, which support a wide variety of commercially, recreationally, and culturally important fisheries such as Pacific salmon (*Oncorhynchus spp.)*, halibut (*Hippoglossus stenolepis*), sablefish (*Anoplopoma fimbria*), numerous species of rockfish (*Sebastes spp.)*, sole (*Lepidopsetta bilineata* and *Parophrys vetulus*), lingcod (*Ophiodon elongatus*), herring (*Clupea pallasii*), Dungeness crab (Metacarcinus magister) and the endangered Northern abalone (*Haliotis kamtschatkana*) (DFO, 2015; MaPP *et al.*, 2015). Moreover, *Macrocystis* and *Nereocystis* are important species to the many coastal First Nations residing on the West Coast of North America since time immemorial (Turner, 2001). For example, *Macrocystis* has been harvested along with herring roe in the spawn-on-kelp fishery for centuries (MaPP *et al.*, 2015), and *Nereocystis* stipes are traditionally used as anchor lines, fishing line, oil containers, and in the creation of bentwood cedar boxes (Turner, 2001). Due to the economic and cultural significance of kelp forests not only to First Nations but to many coastal communities in BC, managers and researchers are now prioritizing the monitoring and management of these important foundation ecosystems on the Pacific Coast of Canada (MaPP *et al.*, 2015).

Although patterns of change in kelp abundance and distribution vary substantially from region to region (Krumhansl *et al.*, 2016), the large-scale trends of kelp abundance in BC remain largely unknown. The recent meta-analysis by Krumhansl *et al.* (2016) reports that the North American Pacific Fjordland, which includes the coast of BC and Alaska, shows an increase in kelp abundance over time. However, this analysis is very limited in data coverage for the region. On the coast of North America, sea otters, key predators of sea urchins, were overharvested and functionally extirpated by the late 1800s, causing grazing-induced regime shifts from kelp forests to unproductive urchin barrens (Estes & Duggins, 1995; Filbee-Dexter & Wernberg, 2018). The longest, most robust time series of kelp forests to date on the BC coast documented the local re-introduction (1969) and spread of sea otters on the west coast of Vancouver Island which caused regime shifts back from urchin barrens to productive kelp forest ecosystems (Watson & Estes, 2011). However, sea otters have only been reintroduced to 25-33% of their historic range in BC (Nichol *et al.*, 2007), meaning that local increases in kelp forest abundance due to sea otter re-introduction cannot be equated to the entire coast of BC. In contrast, some local studies have highlighted recent declines in kelp forest ecosystems (Sutherland *et al.*, 2008; Schultz *et al.*, 2016; Burt *et al.*, 2018; Starko *et al.*, 2019). During the 2014-2016 marine heatwave, the mass mortality of sunflower sea stars, another sea urchin predator, led to declines in the abundance of *Nereocystis* in Howe Sound (Schultz *et al.*, 2016) and *Macrocystis* and *Nereocystis* on the central coast of BC (Burt *et al.*, 2018). Additionally, declines in kelp abundance were documented in response to the 2014-2016 marine heatwave in Barkley Sound on the west coast of Vancouver Island (Starko *et al.*, 2019, 2022), and a 25-35% decline in *Macrocystis* and *Nereocystis* biomass occurred from 1993 to 2007 in the Hakai Passage and Bradswell Group on the Central Coast (Sutherland *et al.*, 2008). Comparatively, a recent satellite-based study showed limited evidence

of kelp decline between 2004 to 2017 in the Cowichan Bay and Samsung Narrows area of the Salish Sea (Schroeder *et al.,* 2019a). Given this existing body of literature showing highly variable patterns of change across BC, the need for long-term and large-scale research to fully understand regional trends and drivers of kelp forests on the Pacific Coast of Canada is apparent.

The ability to monitor the distributions of kelp forests has dramatically improved with the emergence of new remote sensing technologies, such as unpiloted aerial vehicles (UAVs), aerial photography and high-resolution satellite imagery (Stekoll *et al.*, 2006; Cavanaugh *et al.*, 2010; Bell *et al.*, 2015; Pfister *et al.*, 2018; Schroeder *et al.*, 2019a; Schroeder *et al.*, 2019b; Nijland *et al.*, 2019; Bennion *et al.*, 2019; Mora-Soto *et al.*, 2020). Differences in the spectral properties of kelps and water allow sensors to distinguish floating kelp canopies at the surface of the ocean, in particular with the red-edge and near-infrared portion of the electromagnetic spectrum (Jensen, 1980; Schroeder *et al.*, 2019b). Specifically, multispectral high-resolution Earth Observation satellite imagery enables researchers to collect data at the spatial and temporal coverage needed to better understand regional kelp forest dynamics and trends (Schroeder *et al.*, 2019b; Bennion *et al.*, 2019). Medium-spatial resolution imagery from Earth Observation satellites have been available for the west coast of Canada since the late 1970s (~80 – 30 meters resolution via the Landsat series), and high-resolution imagery from the early 2000s (~ 2 – 10 m resolution via multiple satellites), allowing the investigation of the dynamics and trends of the kelp forests in BC (Nijland *et al.*, 2019). Even though satellite data are now available for the entirety of the BC coast, no large-scale, long-term studies exist. Furthermore, long-term trends in kelp forest persistence can be assessed by pairing pre-existing historical data with modern-day satellite imagery. Several independent historical data exist for the Haida Gwaii region dating back over a

century (Costa *et al.*, 2020; Blakley & Chalmers, 1973; Coon *et al.*, 1979; Howes *et al.*, 2001), making Haida Gwaii the ideal area for analysis of large-scale, long-term kelp forest changes.

1.2 Research Objectives

The main goal of this research is to quantify the distribution, variability, and drivers of change of Haida Gwaii kelp forests. Specifically, we address the goal with the following objectives:

(1) Develop a methodological framework that enables the creation of a long-term dataset of kelp distribution using archived multispectral satellite imagery from multiple satellite sensors that vary in their spatial resolution (0.5 m – 60 m) and temporal coverage (1973-2021).

(2) Define changes in Haida Gwaii kelp forest canopy and associated with drivers of change over the last 100 years using historical data (1867-1945) and medium- to high-resolution archived satellite imagery (1973-2021) at regional to local scales of analysis.

1.3 Thesis Structure

This thesis is separated into two papers to address the research objectives. The first paper (Chapter 2) provides a methodological framework developed to create a long-term dataset of kelp canopy area from archived medium- to high-resolution satellite imagery. The second paper (Chapter 3) uses the long-term time series developed as part of the first paper in conjunction with historical kelp data and environmental drivers to understand how kelp forests respond at different spatial scales in a period of rapid global change. Each of these papers was developed as independent publications, and as such, some information may overlap between the two. Lastly, the conclusion (Chapter 4) united these two papers and summarized the broad implications of this work.

1.4 Personal Relation to the Research and Place

As a descendant of colonial settlers (British) and immigrants (3rd generation Austrian) to Canada it is important to acknowledge my positionality of unearned privilege. Among the complex dynamics at play, I recognize that my history is marked with unjust settler colonial violence against Indigenous people of which Canada is built upon. Working on Haida territory and living on the territories of the Songhees, W̱SÁNEĆ and Esquimalt Nations, I aim to conduct myself in a way which decolonizes research, unlearns racial biases, and upholds first nations sovereignty. Specifically, this research falls under the permit 2020-004R of the Council of the Haida Nation, for approval to conduct research on their territory. In particular, this work aims to provide data to the Council of the Haida Nation for use in the management, monitoring and stewardship of the culturally, economically, and ecologically significant kelp forests of their region. Of significant importance, the origins of this work stem from the Traditional Ecological Knowledge of the Haida people highlighting the study region as a crucial kelp forest ecosystem under threat from local declines, and as such, it is critical to recognize that I am not the first to put forward the observations of declines made in this research.

2.0 A Multi-Satellite Kelp Mapping Framework: Time Series from Archived Satellite Imagery

2.1 Abstract

Even though kelp forests are a key marine habitat on the Pacific coast of Canada, how they change through time remains poorly understood. With the emergence of high-resolution satellite imagery in the 21st century, changes in kelp forest distribution can now be monitored across large scales through time. In this paper, we present a methodological framework using an object-based image analysis approach that enables the combination of imagery from multiple satellite sensors that vary in their spatial resolution and temporal coverage to reconstruct kelp trends. Additionally, the impact of spatial resolution on the detectability of kelp forests is described. The methodological framework comprises three main steps, 1) the compilation and quality assessment of satellite imagery, 2) the preprocessing of imagery, which includes a geometric correction, atmospheric correction, masking, band index/ratio production and image enhancements, and 3) an object-oriented classification accompanied by an accuracy assessment. Overall, this workflow was successful at producing accurate maps of kelp forest canopy from multiple sensors, with global accuracy scores ranging from 88% to 94%. When comparing the impact of resolution on the detectability of kelp forest canopy, less kelp was detected at lower resolutions and lower resolutions were less reliable at detecting small kelp beds in high slope areas. Based on the analysis, we suggest removing high slope areas (11.4 %) from time series analyses using high- to medium-resolution satellite imagery and that error, in this case up to 7 %, be taken into consideration when comparing kelp distributions from imagery at different resolutions in low-mid slope areas through time.

2.2 Introduction

Kelps, brown algae in the order Laminariales, are dominant habitat-forming organisms found in temperate nearshore ecosystems across approximately one-quarter of the Earth's coastlines (Wernberg *et al.*, 2019). Kelps create extensive aquatic forests that provide shelter and food for many ecologically and economically important marine species (Johnson *et al.*, 2003; Krumhansl *et al.*, 2016; Wernberg *et al.*, 2019) and provide a myriad of ecosystem goods and services, such as fisheries production, nutrient cycling and carbon removal, estimated at $684 billion US per year worldwide (Filbee-Dexter & Wernberg, 2018; Eger *et al.*, 2021). However, climate change, overfishing, pollution and increasing harvest threaten the health and persistence of kelp forests globally (Krumhansl *et al.*, 2016; Wernberg *et al.*, 2019; Bennion *et al.*, 2019). Recent work highlights the negative impacts of heatwaves on kelp forests (Wernberg *et al.*, 2013; Filbee-Dexter *et al.*, 2016; Wernberg *et al.*, 2016; Arafeh-Dalmau *et al.*, 2019; Cavanaugh *et al.*, 2019b; Smale, 2020) and loss of key predators, such as sea otters and sea stars, lead to overgrazing induced regime shifts from kelp forests to urchin-barrens (Dean *et al.*, 1984; Estes & Duggins, 1995; Filbee-Dexter & Wernberg, 2018; Burt *et al.*, 2018).

Kelp forests are dynamic by nature and show high inter-annual variability (Dayton *et al.*, 1999; Cavanaugh *et al.*, 2011a; Bell *et al.*, 2020). Considering that kelp forests are threatened across the globe but are highly variable through time, it is important to establish long-term time series to understand if and how kelp forests are responding to environmental conditions in a time of rapid global change (Wernberg *et al.*, 2016; Krumhansl *et al.*, 2016; Bell *et al.*, 2020). Historically, kelp canopy extent research is based on aerial surveys or physical field data collection, such as surveys by boats, snorkeling, or SCUBA (self-contained underwater breathing apparatus) diving (Cameron, 1915; Druehl, 1970; Dayton *et al.*, 1999; Sutherland *et al.*, 2008;

Krumhansl *et al.*, 2016; Bennion *et al.*, 2019). These survey techniques only cover small areas and are difficult to maintain long-term because of intensive labour requirements and high operating costs. Furthermore, these techniques remain logistically difficult due to the high seasonality and inter-annual variability of kelp forests, as well as their extensive distribution along complex remote coastlines with highly variable and sometimes extreme conditions, like the Pacific Coast of Canada (Yesson *et al.*, 2015; Schroeder *et al.*, 2019b; Bennion *et al.*, 2019; Smale, 2020).

Specifically on the Pacific Coast of Canada (British Columbia, BC), canopy-forming kelp forests are formed by *Nereocystis luetkeana*, and *Macrosystis pyrifera*, which support a wide variety of commercially, recreationally, and culturally important species (DFO, 2015; MaPP *et al.*, 2015). Only some local areas of the BC coast have been mapped at singular time points by provincial aerial surveys (Blakley & Chalmers, 1973; Field *et al.*, 1977; Coon *et al.*, 1978, 1979; Field & Clark, 1978; Sutherland, 1990, 1998, 1999; Sutherland *et al.*, 2008). Additionally, some local-scale studies have measured kelp extent through time but show highly variable patterns of change (Sutherland *et al.*, 2008; Watson & Estes, 2011; Burt *et al.*, 2018; Schroeder *et al.*, 2019a; Starko *et al.*, 2019, 2022) highlighting the need for large-scale, long-term monitoring initiatives to understand the extent of threats and assess kelp forest dynamics on the coastline of BC. In other areas of the Pacific coast, some successful aerial surveys have quantified kelp forest trends (North *et al.*, 1993a; Parnell *et al.*, 2010; Pfister *et al.*, 2018), but these aerial surveys remain operationally cost prohibitive at the scale of the BC coast.

With the enhancement of satellite imagery technology, the ability to monitor the distributions of kelp forests has dramatically improved, specifically with the increasing availability of high-resolution (<10.0 m) satellite imagery in the 21st century. Differences in the spectral properties of

kelp and water allow multispectral satellite sensors to distinguish floating kelp canopies at the surface of the ocean due mainly to kelp forests' high reflectance in the near-infrared range of the electromagnetic spectrum (Jensen, 1980; Schroeder *et al.*, 2019b). Many different methods of classification have been applied for mapping kelp, including manual, pixel-based (supervised, unsupervised, thresholds, spectral un-mixing) and object-oriented approaches (see summary by Schroeder *et al.*, 2019b). However, no standardized practices for kelp forest mapping have been developed and broadly accepted in the literature making the monitoring of kelp forests at large-scales difficult for non-remote-sensing experts (Bennion *et al.*, 2019).

Multiple factors influence the accuracy when using satellite imagery to map kelp forests. Glint, clouds, tide, bathymetry, coastline morphology, shadow, currents, waves, phytoplankton blooms and adjacency impacts can all negatively affect the ability to map kelp from satellite imagery (Britton-Simmons *et al.*, 2008; Schroeder *et al.*, 2019b; Nijland *et al.*, 2019; Cavanaugh *et al.*, 2021). In particular, many of these challenges increase in severity from south to north along the west coast of North America, such as increasing cloud cover, tidal amplitude, and coastal complexity (Cavanaugh *et al.*, 2021). Considering these challenges, the mapping of kelp forests using satellite imagery has been largely developed in California, where extensive offshore giant kelp forests are mapped using medium spatial resolution satellites, including Landsat and SPOT imagery from the 80s onwards (e.g., Augenstein *et al.*, 1991; Deysher, 1993; Cavanaugh *et al.*, 2010, 2011, 2019; Bell *et al.*, 2020). Several studies have adopted these methods developed in California to map kelp forest canopy in other areas of the world, e.g. South Africa (Anderson *et al.*, 2007), Oregon (Hamilton *et al.*, 2020), the Falkland Islands (Houskeeper *et al.*, 2022) and Canada (Nijland *et al.*, 2019), in areas where large kelp beds occur. However, using medium-resolution satellites to map kelp in BC remains challenging due to the presence of small fringing

kelp beds and the high topological complexity of the BC shoreline (Schroeder *et al.*, 2019b; Nijland *et al.*, 2019). In particular, when medium-resolution satellite imagery was used to map kelp beds on the Central coast of BC, between 28% to 75% of kelp forests that were present were missed due to the coarse resolution of the Landsat imagery used (Nijland *et al.*, 2019).

Over the last 50 years, the spatial resolution of Earth Observation satellite imagery has rapidly evolved. Medium spatial resolution imagery became available in the early 1970s (80.0 meters resampled to 60.0 meters via the Landsat 1-3 satellites) and continued to advance in the 1980s (30.0 meters via Landsat 4 on and 20.0 meters via the SPOT series). At the beginning of the 21st century, high spatial resolution imagery became commercially available (~ 2.0-10.0 m via Worldview, Quickbird, Geoeye, RapidEye, and SPOT 6/7 satellites), and, with the launch of the Sentinel-2 (10.0 m resolution) and PlanetScope dove (3.0 resampled from 3.7 m) satellites, the amount of available high-resolution satellite imagery has increased substantially over the last decade. Even though satellite data (archived and new) at different spatial resolutions is available globally, no large-scale, long-term study has taken advantage of data from multiple sensors to reconstruct kelp forest trends. Here, we present a methodological framework for mapping kelp forest-canopy areas from archived medium- to high-resolution satellite imagery using an object-oriented analysis approach and discuss the advantages and limitations of combining these data to reconstruct kelp distribution through time. Specifically, the impact of using satellite imagery acquired at different spatial resolutions to detect kelp forest canopy is explored, and suggestions for drawing appropriate conclusions when using multiple sensors are described. Here, we use a test site that supports both small fringing and large kelp forests located on the East coast of Haida Gwaii, BC, Canada, as a case study to develop a multi-satellite kelp mapping framework (MSKM framework). This MSKM framework will contribute to advancements in the remote

sensing of kelp forest canopies not only in BC, Canada, but will allow for trends to be understood in remote regions and ultimately help inform effective management strategies for the protection and longevity of kelp forest ecosystems globally.

2.3 Methods

2.3.1 Study Area

The test site for defining the MSKM framework is located in Haida Gwaii on the West Coast of Canada, in the unceded territory of the Haida Nation, whose relationship to the land and sea long predates colonial settlement and still exists to this day (Guujaaw, 2002; MaPP *et al.*, 2015). Haida Gwaii is a large archipelago with a complex coastline of approximately 4660 km in the Northeast Pacific Ocean (**Figure 1A** & B; Sloan & Bartier, 2000; Sloan *et al.*, 2015). Specifically, the study site spans roughly 800 km^2 on the Northeast Coast of Moresby Island, just west of Hecate Strait (**Figure 1C**). The two main features of this region are a large shallow bay to the North known as Gray Bay and a pronounced inlet between Moresby Island and Louise Island in the South known as Cumshewa Inlet.

Both dominant canopy-forming kelp species, *Macrocystis* and *Nereocystis*, are found in this region. *Macrocystis* grows year round, however, most growth occurs in the summer to early fall (Druehl, 1970; Dayton, 1985). *Nereocystis* is a perennial species that grows from late spring to early fall, with peak biomass occurring later in the summer and die-offs occurring in the late fall and winter (Springer *et al.*, 2007). Records from the 1800s from British Admiralty charts show large kelp forests in both Gray Bay and Cumshewa Inlet (Costa *et al.*, 2020a). Likewise, Haida highlight this region's importance for the harvest of giant kelp for the spawn on kelp herring roe fishery but remark significant declines of kelp forests in recent history in the Haida Marine Traditional Knowledge Volumes I, II and III (2007).

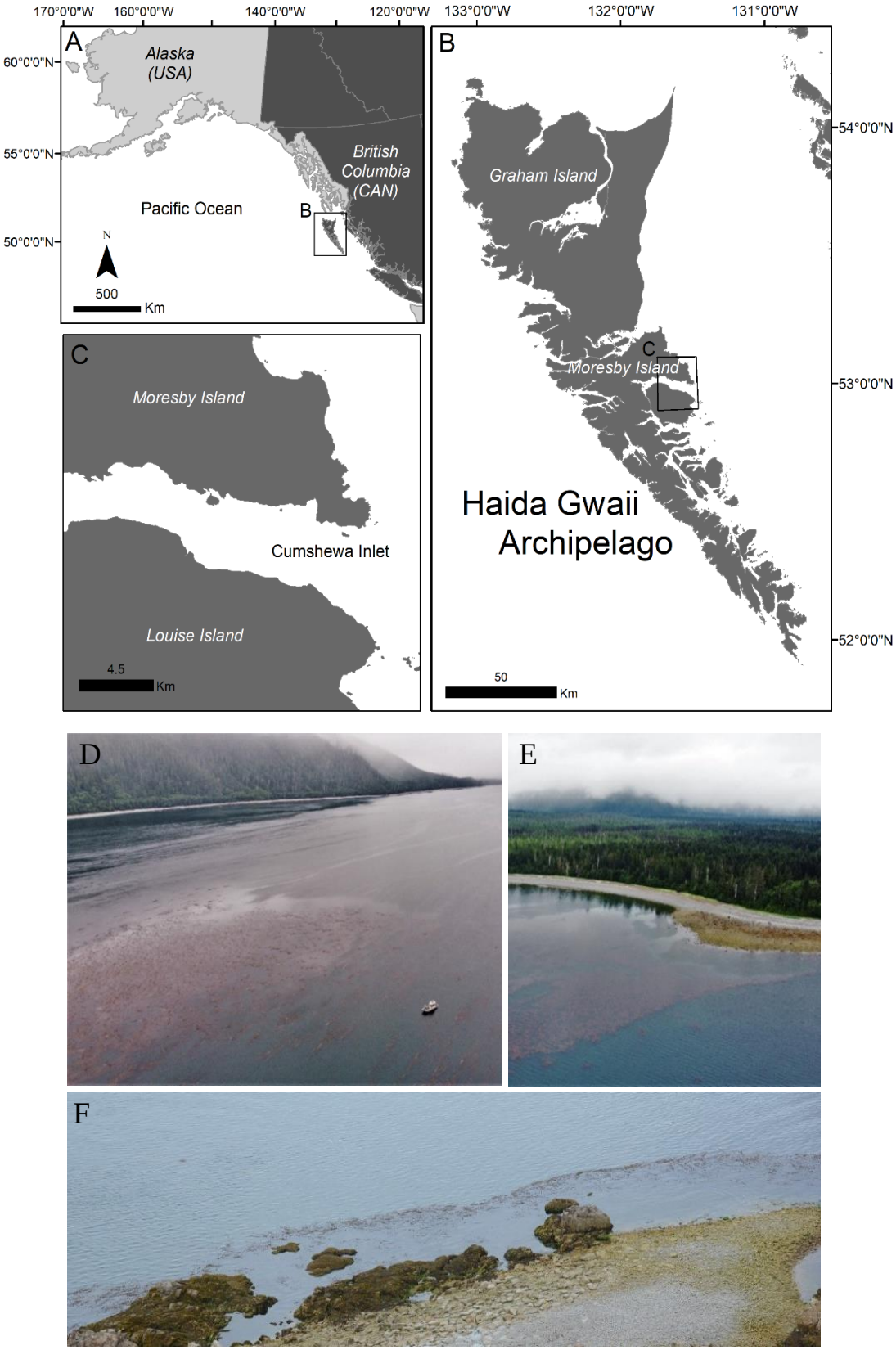

Figure 1. An overview of A) the Northwest coast of North America, the location of B) Haida Gwaii in reference to the British Columbia coast and C) the Cumshewa Inlet study area. The study site includes D) large offshore, E) large nearshore and F) small fringing nearshore kelp forests. Image source: D) & E) Lianna Gendall, F) Environment and Climate Change Canada

In this region, the complex bathymetry supports kelp forests in various sizes, from small fringing beds to large offshore beds that span kilometers. Large areas in Cumshewa Inlet and Gray Bay are characterized by very gradual sloping ocean floors, allowing for some of the most extensive kelp forests found in BC that are easily detectable with satellites of 60.0 m (resampled from 80.0 m) spatial resolution or better (**Figure 1E & F**). In contrast, this region also includes smaller, less detectable kelp forests that grow in narrow fringing beds along the steep slopping nearshore coastline (**Figure 1G**). These fringing kelp forests are generally characteristic of kelp forests found across the remainder of the BC coast (Stekoll *et al.*, 2006; Schroeder *et al.*, 2019a; Nijland *et al.*, 2019; Cavanaugh *et al.*, 2021). This range in kelp forest size makes this region an ideal area to define a framework for using different resolution satellites to map kelp forest canopy through time.

2.3.2 Methodological Framework

The MSKM framework is a workflow that allows researchers to compile robust temporal datasets of kelp forest canopy area through the evolution of medium to high-resolution satellites. The workflow consists of 3 main steps, including 1) imagery compilation and quality assessment, 2) preprocessing and enhancements, and 3) object-oriented image classification and accuracy assessment (**Figure 2**). To compare kelp distributions derived from multiple satellites

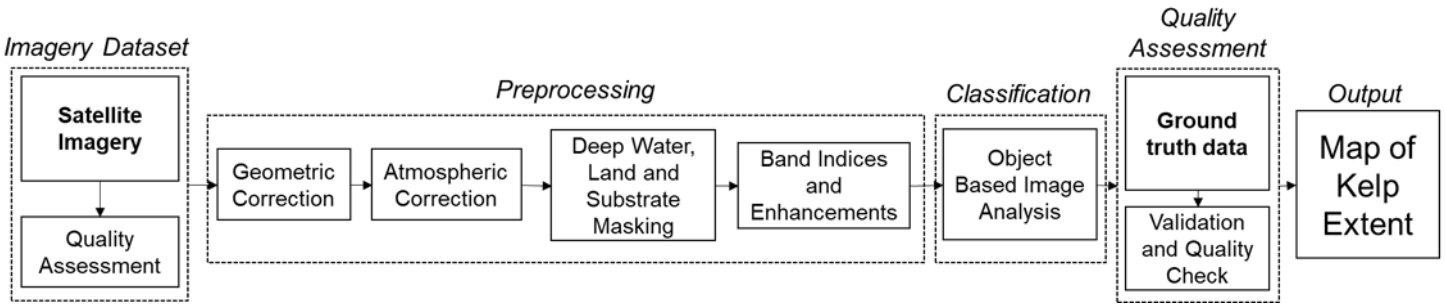

Figure 2. Workflow of methodological framework

with a range of spatial resolutions, we performed an analysis of the detectability of kelp at different spatial resolutions.

Step 1: Imagery Dataset

Archived high to medium-resolution (0.5 m – 60.0 m) multispectral satellite imagery was compiled from 20 different satellite sensors spanning from 1973 to 2021 through diverse sources, including open data, private data sharing agreements, and commercial acquisition (**Table 1**). Archived imagery is not necessarily collected during optimal conditions for kelp mapping, and therefore special consideration should be given to any factors that may lead to inaccurate kelp maps, such as clouds, tidal height, glint, shadow, haze, water turbidity, waves, algal blooms and time of imagery acquisition (Britton-Simmons *et al.*, 2008; Cavanaugh *et al.*, 2011; Pfister *et al.*, 2018; Schroeder *et al.*, 2019b). To minimize possible inaccuracies, a set of criteria were developed considering the categories for conditions for imagery acquisition to select good quality imagery to map kelp in the study region. the following categories were visually assessed and considered: glint, waves, shadows, clouds, month of acquisition, and tidal height. Each category was scored from 0-3, where the lower the score, the better quality the image. For instance, the criteria for ideal conditions consisted of an acquisition time between June and October, a low tidal height, and the minimal presence of glint, waves, shadow, and cloud within the nearshore areas where kelp is normally found within the imagery (Schroeder et al., 2019a, b) thus representing a score of 0. Once combined, images showing suboptimal conditions for kelp detection (overall criteria score ≥ 7) were removed from the dataset.

The spatial resolution of imagery ranges from medium resolution imagery in the 1970s (e.g., 60.0 m resampled from 80.0 m from Landsat 1-3) to more recent high-resolution imagery in the 21st century (e.g., 0.5 m pansharpened Worldview-2 imagery, 2.6 m Quickbird-2 imagery, and

3.0 m resampled from 3.7 m PlanetScope imagery) (Table 1). Importantly, this means that the quality score results should be framed within the context that more recent imagery is intrinsically more reliable for mapping kelp due to their higher spatial resolutions.

Step 2: Pre-processing

After selecting the optimal images for kelp mapping, we subjected images to standard preprocessing techniques, as described in the review by Schroeder *et al.* (2019). These techniques aim to reduce geometric and radiometric uncertainties and enhance the kelp spectral signal to improve classification accuracies.

Table 1. Medium- to high-resolution satellite imagery used to develop the methodological framework

SENSOR	*DATES*	*GROUND RESOLUTION*	*SWATH*	*REVISIT*	*BANDS*	*ATMOSPHERIC CORRECTION*	*BAND INPUTS FOR CLASSIFICATION*	*SOURCE OF IMAGERY*	*SOURCES FOR INDICES*
LANDSAT SERIES	**LS-7** 1999-2021	**30 m** multispectral 15 m panchromatic	170 km	16 days	OLI Blue 450-520 Green 540-600 Red 630-690 NIR 770-900 SWIR 1550-1750 SWIR II 2110-2290 Pan 520-680	Surface reflectance ready product	NDVI Green, Red, NIR	Freely Available from United States Geological Survey (USGS)	(Reed *et al.*, 2011; Cavanaugh *et al.*, 2011, 2013; Bell *et al.*, 2015, 2018; Nijland *et al.*, 2019)
	LS- 4-5 1984-present	**30 m** multispectral	170 km	16 days	TM Blue 450-520 Green 520-600 Red 630-690 NIR 770-900 NIR 1550-1750 MIR 2080-23500 Pan 520-900				
	LS-1-3 1972-1983	**60 m** multispectral (Resampled from 80 m)	170km	18 days	MSS Green 500-600 Red 600-700 NIR 700-800 NIR 800-1100	Rayleigh correction	NDVI Green, Red, NIR		
SENTINEL-2	2015-present	60m-**10m** multispectral	290 km	5 days	Coastal 443-463 Blue 490-555 Green 560-595 Red 665-695 Red Edge I 705-720 Red Edge II 740-755 Red Edge 1 783-803 NIR1 842-957 NIR2 865-885 SWIR 1380-1410 SWIR I 1910-2000 SWIR II 2190-2370	Surface reflectance ready product from SNAP Sen2Cor processor	NDVI Green, Red, NIR	Freely Available from United States Geological Survey (USGS)	(Mora-Soto *et al.*, 2020)
SPOT SERIES	**SPOT 4** 1989-2013	20m multispectral 10m panchromatic	60-80 km	5 days	Green: 500-590 Red: 610-680 Near IR: 790-890 SWIR 1530-1750 Pan 610-680	Rayleigh correction	NDVI Green, Red, NIR	Data sharing available to researchers through the Centre national d'études spatiales (CNES)	(Augenstein, 1991; Cavanaugh *et al.*, 2010; Casal *et al.*, 2011; Mora-Soto *et al.*, 2020)
	SPOT 5 2002-present	10m multispectral 5m panchromatic		2-3 days	Green: 500-590 Red: 610-680 Near IR: 780-890 SWIR 1580-1750 Pan 480-710				
	SPOT 6-7 2012-present	6m multispectral 1.5m Panchromatic		1-3 days	Blue 450-520 Green 530-590 Red 625-695 NIR 760-890 Pan 450-745			Purchased through Apollo Imaging Corp with academic discount	
GEOEYE-1	2008-present	1.84m multispectral 0.46m panchromatic	15.2km	2.6 days	Blue 450-510 Green 510-580 Red 630-690 NIR 780-920 Pan 450-800	Rayleigh correction	GNDVI Green, Red, NIR	Private data sharing agreement	Determined using M-Stat
QUICKBIRD-2	2001-2015	2.62m multispectral 0.65 panchromatic	15.2km		Blue 450-520 Green 520-600 Red 630-690 NIR 760-900 Pan 450-800	Rayleigh correction	GNDVI Green, Red, NIR	Private data sharing agreement	Determined using M-Stat
RAPID EYE SERIES	2008-present	5 m multispectral	77 km		Blue 440 - 510 Green 520-590 Red 630-685 Red Edge 690-730 NIR 760-850	Surface reflectance ready product	RE/Green Green, Red, RedEdge NIR	Available to researchers through Planet Labs Inc.	Determined using M-Stat
WORLDVIEW SERIES	**WV-3-4** 2014-present	1.24m multispectral 0.31m panchromatic	13.1km	1-3 days	Coastal 400-450 Blue 450-510 Green 510-580 Yellow 585-625 Red 630-690 Red Edge 705-745 NIR1 770-895 NIR2 860-1040 Pan 450-800	Rayleigh correction	RE/Yellow Green, Red, NIR Pansharpened without NIR Red/Green Green Blue	Private data sharing agreement	Determined using M-Stat (Schroeder *et al.*, 2019a, 2019b, 2020; Nijland *et al.*, 2019)
	WV-2 2009-present	1.84m multispectral 0.46m panchromatic	16.4km						
PLANETSCOPE DOVE SERIES	2018-present	3.0 m multispectral (Resampled from 3.7 m)	24 km – 32.5 km	Daily	Blue: 455 - 515 Green: 500 - 590 Red: 590 - 670 NIR: 780 - 860 Blue: 464 - 517 Green: 547 - 585 Red: 650 - 682 NIR: 846 - 888	Surface reflectance ready product	NIR/G Green, Red, NIR	Available to researchers through Planet Labs Inc.	Determined using M-Stat

Geometric correction - Geometric distortions occur in imagery due to errors during acquisition, such as variations in altitude, attitude, the velocity of the satellite, earth curvature, atmospheric refraction, and non-linearities in the satellite path (Jensen, 2005; Ayoub *et al.*, 2008). All selected images were checked for geometric distortions against the ESRI satellite base map in the WGS 1984 coordinate system, and those with distortions were georectified in ArcGIS using ground control points and the nearest neighbour interpolation (Jensen, 2005; Chang, 2009). However, where overlaps between imagery occurred, the overlapping images were georectified to the previous images to ensure the best match. The root mean squared error (RMSE) was calculated to evaluate the quality of the georectification, and a threshold of less than 2 pixels was deemed acceptable, except for the Landsat imagery, which was given an allowance of only 1 pixel due to the coarser spatial resolution.

Atmospheric correction - Following the georectification, the images were evaluated for radiometric/atmospheric issues. Atmospheric attenuation (scattering and absorption) introduces errors in surface reflectance values detected at the sensor and, therefore, may impact the band indices used and, consequently, the imagery classification outputs (Matthew *et al.*, 2000; Lin *et al.*, 2015). When possible, we attained atmospherically corrected images from imagery suppliers, as described in **Table 1**. For the other imagery, a simple approach considering a histogram shift determined by the Rayleigh scattering factor was applied based on methods described by Chavez (1988), hereafter referred to as the Rayleigh correction, given it primarily addresses Rayleigh scattering (Rayleigh, 1899). The scattering intensity is inversely proportional to the fourth power of the wavelength (λ^{-4}), meaning shorter wavelengths, such as blue and green wavelengths, are scattered more than longer wavelengths (Chavez, 1988). This method is based on the assumption that the darkest pixels in an image, such as shadowed areas or offshore deep-water areas, should

have no signal (null reflectance), but because of Rayleigh scattering, non-zero values are recorded (Chavez, 1988). To account for the Rayleigh scattering, these non-zero values are subtracted from the spectral signal of each specific satellite band. To assure the spectral relationship between bands remains accurate when correcting for Rayleigh scattering, the Rayleigh factor (λ^{-4}) is applied (Chavez, 1988). The initial step is to define the lowest reflectance value in the blue band acquired from the darkest (lowest reflectance) pixels within the image (B_c), which is consequently subtracted from each pixel in the blue band. Then, for each remaining visible band, the following equation is used to calculate the Rayleigh correction value (Rc).

$$Rc = \ ((1/(\lambda_b^4)\ /\ (1/(\lambda_{vis}^4))\ * B_C$$

Where λ_b represents the wavelength (nm) of the blue band, B_c represents the value subtracted from the blue band described above, and λ_{vis} represents the mean wavelength (nm) of whichever visible band the equation is being used to calculate the correction value for (e.g., 560 nm when correcting the green band of Geoeye 1). To ensure images were properly corrected, we produced spectral plots of water and kelp for a subset of imagery from each sensor and compared them to the known spectral plots for kelp and water from Schroeder (2019b), Bell *et al.* (2015) and Jensen (1980).

Deepwater, land, and substrate masking - Following the required corrections, images were subjected to (i) a lowest tide land mask, (ii) a deep-water mask and (iii) a soft substrate mask to eliminate areas where kelp is not found and to minimize processing time and false positives. Vegetation on land has a remarkably high near-infrared (NIR) reflectance compared to kelp (Sawaya, 2003; Wolter *et al.*, 2005), and therefore removing these features enhances the ability

to digitally differentiate kelp from water through contrast enhancement (Schroeder *et al.*, 2019a). We created the land mask using an object-based segmentation (Trimble eCognition Developer V8.64) on the imagery with the lowest tide. For each resolution of imagery used in this study, we added a buffer of 1 pixel to minimize adjacency impacts from the shoreline. To eliminate any areas where kelp was unable to grow (Druehl, 1978; Mumford, 2007), a 20-meter deep water mask was created using a bathymetry dataset from the Canadian Hydrographic Service (Davies *et al.*, 2019, Schroeder *et al.*, 2019b; Nijland *et al.*, 2019) Lastly, we masked shallow-soft sediment bottom, which is uninhabitable to kelp (Gregr *et al.*, 2019), using the BC Marine Conservation Analysis (BCMCA) benthic classes dataset (Ferdaña, 2006) and the DFO bottom patch model (Gregr et al., 2013).

Band indices/ratios and enhancements - The final task in the preprocessing workflow was to select the combination of bands and band indices/ratios that perform best in the classification step. In the literature, NDVI is standardly used to enhance floating kelp canopies in imagery from the Sentinel-2, Landsat, and SPOT satellites (Augenstein *et al.*, 1991; Cavanaugh *et al.*, 2010, 2011a, 2013; Reed *et al.*, 2011; Casal *et al.*, 2011; Bell *et al.*, 2015; Schroeder *et al.*, 2019b; Nijland *et al.*, 2019; Mora-Soto *et al.*, 2020; Table 1). As such, NDVI was used to enhance imagery collected by these satellites. For any imagery acquired by a sensor that had not previously been used for kelp detection in the literature at the time of processing, the m-statistic, a measure of class separability (Kaufman & Remer, 1994), was calculated for all possible band indices and ratios. A high m-statistic represents high separability between two classes. For each sensor, we combined the 2-3 highest scoring band indices or ratios with the visible bands and visually assessed the combinations to choose which provided the best overall classification

results (**Table 1**). The selected bands, band indices and ratios were then linearly enhanced to maximize the spectral signal of kelp forests for the final input into the classification.

Step 3: Classification

An object-based image analysis (OBIA) was used based on the recommendation for classifying kelp forest canopy from Schroeder *et al.*, (2019b). The OBIA approach combined a multiresolution segmentation followed by supervised nearest neighbour classification using the Trimble eCognition Developer Software (V8.64) to classify kelp canopy within the imagery. The final enhanced bands, band indices and/or band ratios for each image were subjected to a multiresolution segmentation (Scale: **Table 2**, Shape: 0.3, Compactness: 0.5) to group similar pixels into objects. From those objects, training classes corresponding to kelp, submerged kelp/understory seaweed, water, glint/waves, cloud, shadow, and shallow water, were defined using expert knowledge. **Figure 3** shows examples of the most common classes used in the OBIA. Note that not all classes were present in all imagery. In particular, some classes, such as glint/waves and submerged kelp/understory seaweed were indistinguishable in the medium resolution satellite imagery. Because classes varied by image, the feature space optimization function in the Trimble eCognition Developer Software (V8.64) was used to mathematically calculate the best number and combination of object features, such as the spatial, spectral, and contextual information (e.g. mean of bands/band indices, standard deviation of bands/band indices, maximum difference across all values of all bands/band indices), to separate classes based on training samples (Gupta & Bhaudauria, 2014). This tool compares features of different sample classes to find the optimal combination that produces the largest average minimum distance between samples to be used when categorizing the remaining image objects into those given classes (Gupta & Bhaudauria, 2014). The ability of the FSO chosen features to separate

classes was evaluated based on the analysis of boxplots and three-axis scatter plots of the top three selected features for a subset of images. Following this evaluation, we performed a nearest neighbour classification using the optimal features defined by the feature space optimization tool to categorize the remaining image objects into their respective classes. Before validation, the outputs were visually subjected to a quality assessment using a knowledge-based approach where erroneous classifications were manually reclassified in ArcGIS. Lastly, for the validation step, the outputs of the classification were turned into two binary classes: kelp (1) and all other classes (0).

Table 2. Different scale factor used to determine object size in the segmentation step of classification

Resolution	***Sensor***	***Scale***
0.5	**Aerial Imagery, Pansharpened Worldview**	**40**
2-3	**Quickbird, Worldview**	**30**
4	**PlanetScope**	**28**
5	**Rapid Eye**	**25**
6	**Spot**	**20**
10	**Spot**	**10**
20	**Sentinel**	**7**
30	**Landsat 4-8**	**5**
60	**Landsat 1-3**	**5**

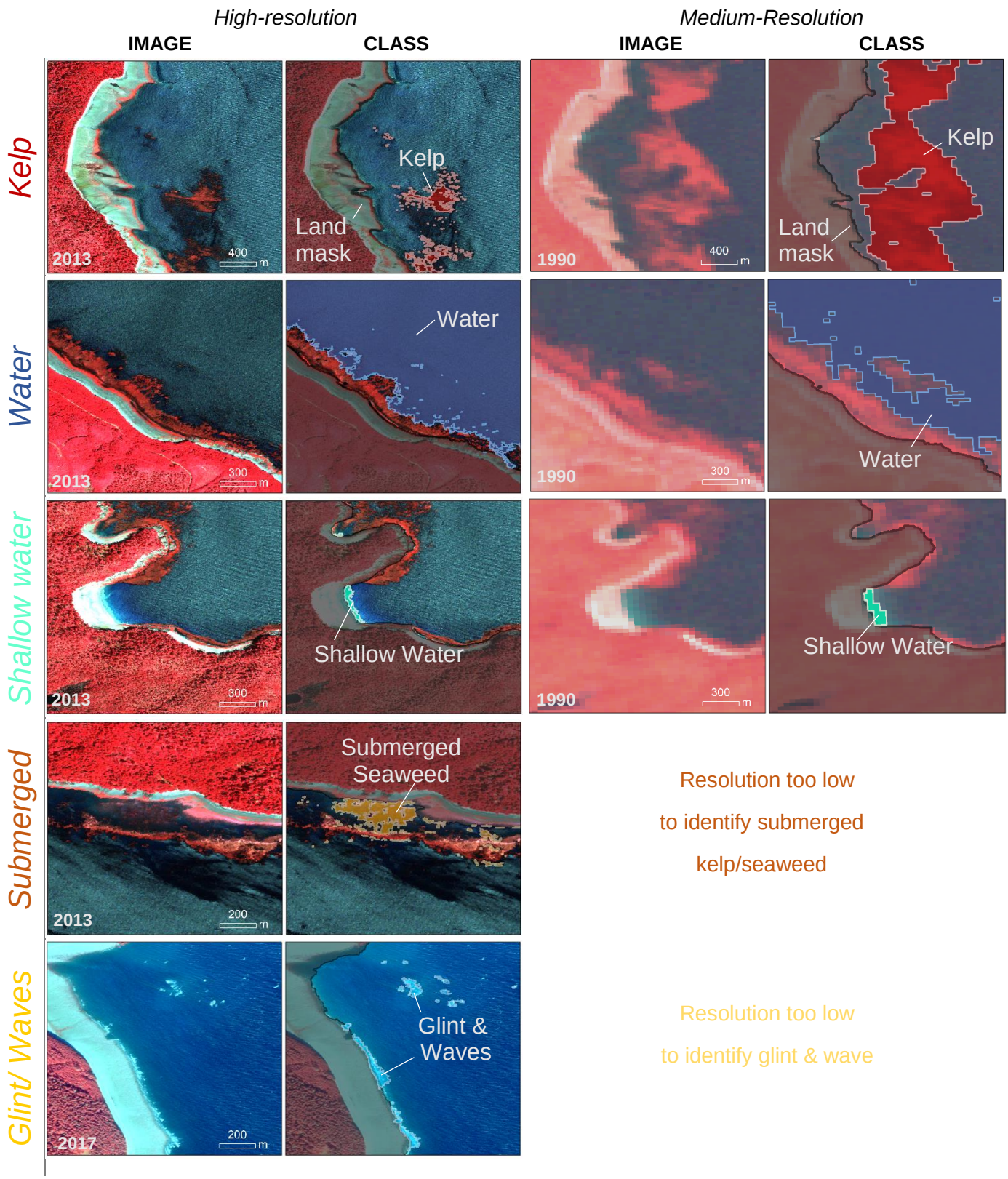

Figure 3: Most common class types used in the Object-based classification for high resolution (Quickbird-2 image from 2013 and 2017 at 2.6 m resolution) and medium resolution (Landsat image from 1990 at 30.0 m resolution) satellite imagery

Step 4: Quality Assessment

For the classification validation, *in situ* kelp data and historical survey data for the region were compiled. Ideally, ground-truth data should be collected at the time of satellite imagery acquisition (Schroeder *et al.*, 2019b). However, if no ground-truth data are available, other forms of data can be used to validate the classification, such as past surveys that show the location of kelp forests (Cavanaugh *et al.*, 2010; Olivero *et al.*, 2016) or expert knowledge based on reflectance values (Schroeder *et al.*, 2019a). For our dataset, we compiled two forms of validation data: (i) *in situ* and (ii) archived data (**Figure 4**). *In situ* data, including drone images, drop quadrat photos, above water photos, and remotely operated underwater vehicle footage were acquired in August 2021, a day after PlanetScope imagery acquisition. Archived surveys comprised of oblique photos from an aerial survey performed by Environment and Climate Change Canada (ECCC) in 2015, multiple years of SCUBA surveys (1990, 1994, 2007, 2012, 2017) from the Department of Fisheries and Oceans Canada (DFO) (Boldt *et al.*, 2020), and the kelp shoreline classifications from an aerial survey conducted in 1997 by ShoreZone were obtained. All validation data was combined into a dataset of spatial points and classified as either kelp present or absent. Specifically, for the DFO Scuba surveys, data was simplified from species specific data (*Macrocystis* and *Nereocystis*) to kelp forest presence and absence and similarly, for ShoreZone data, shoreline segments were simplified from species (*Macrocystis* and *Nereocystis*, or both) and density specific measures (patchy or continuous coverage) to kelp forest presence and absence. For the archived aerial images from ECCC, a random subset of images were visually assessed as having kelp forests present or absent for the validation. All validation data were compared to the classification produced from imagery in the matching year to produce measurements of accuracy. By breaking down the accuracy assessment into user's, producer's and global accuracy, errors of commission (false-positives), omission (false-

negatives) and overall accuracy respectively were assessed (Congalton, 1991). No archived validation data was available during the years of acquisition for the three highest resolution satellites included the dataset, so in order to validate products from Quickbird-2, Geoeye-1 and Worldview-2 satellites, the ECCC oblique photos were used with the assumption that some errors would be associated with possible yearly variability.

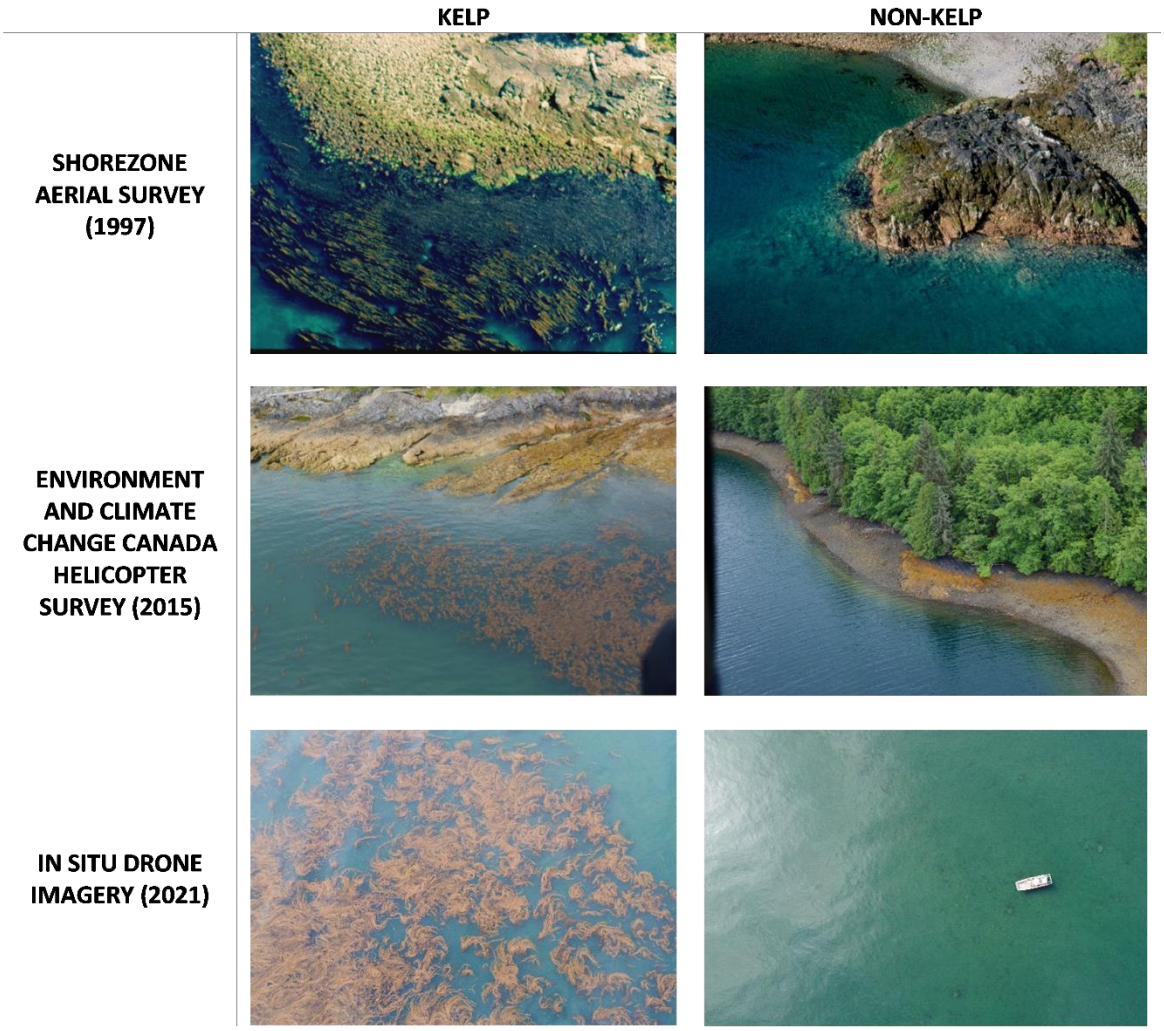

Figure 4. *In situ* and archived data for accuracy assessment of the classification. Not shown are the DFO SCUBA surveys

2.3.3 Spatial Resolution Analysis

Here, we further evaluate the impact of spatial resolution on the detectability of kelp forest canopy in satellite imagery at different scales. First, we quantify the spatial resolution's impact

on the total kelp canopy area. Next, we use a segment-based approach as the aerial units for analysis within which we calculate the associated ocean floor slope as percent rise and define the relationship between slope and kelp bed size to understand the detectability of kelp forests at a finer spatial scale across the test site region. The following steps were adopted in this analysis:

Step 1: Images from Quickbird (2.6 m resolution), RapidEye (5.0 m resolution), and Sentinel-2 (10.0 m resolution) were resampled using bilinear interpolation to the different resolutions matching the time series database used in this research (6.0 m, 10.0 m, 20.0 m, 30.0 m, 60.0 m; Table 1) following Nelson *et al.*, (2009) and Tian *et al.*, (2020). Sentinel-2 was included in the analysis to address possible interpolation errors (Titus & Geroge, 2013) associated with resampling high-resolution imagery from Quickbird-2, and RapidEye to 20.0 m, 30.0 m, and 60.0 m resolutions. The original and resampled images were classified using the OBIA method described above. To ensure that images from the same sensor remained comparable, we used the same areas to train the classifier for each set of down-sampled images. After the classification of the resampled images, the overall kelp forest canopy detectability across the entirety of the study region was analyzed by calculating the percent of kelp area detected at each resolution as a percent of the kelp area detected at the original image's resolution.

Step 2: A 1 km segment-based approach was used as the areal unit to evaluate the kelp forest canopy area detected across resolutions at different ocean floor slopes (see **Figure 5** for the delineation of segments). This segment-based approach is often used in temporal analysis of remote sensing-derived kelp forest canopy to minimize differences caused during acquisition and due to kelp forest seasonality and movement of kelp beds from tides and currents (Pfister *et al.*, 2018; Schroeder *et al.*, 2019a; Berry *et al.*, 2021). Because this approach is often used in temporal analyses, here, we adapted this approach to quantify the impact ocean floor slope (as a

proxy for kelp bed size) has on the detectability of kelp forests spatially across the region. This analysis is based on the premise that ocean floor bathymetry often limits the size of kelp forests (Gregr *et al.*, 2019; Nijland *et al.*, 2019), and therefore can be used as a proxy for the size of kelp forest. Due to the complex bathymetry and presence of large offshore and nearshore kelp beds in our study area, segments were created in two categories based on bathymetry: shoreline (slope greater than 3 %) and flat (slope of less than or equal to 3 %) segments (**Figure 5**) adapted from Berry *et al.* (2003). The two segment categories were created using 20-meter bathymetry data from CHS (Davies *et al.*, 2019). The shoreline segments, characterized by nearshore kelp beds, were created along 1 km where lengths of the shoreline extending to the 20 m bathymetry line in areas where the slope was greater than 3 %. The flat segments, characterized by extensively large kelp beds that extended kilometers offshore, were broken up along 1 km segments from the outside border of the flat area (slope less than 3 %), moving inwards so that every segment was approximately the same size as an average fringing shoreline segment (**Figure 5**).

Step 3: Further, our analysis is based on the understanding that the kelp beds growing in high slope areas are generally fringing beds, and consequently difficult to map with lower resolution imagery (Nijland *et al.*, 2019). To test the assumption that high slope areas support only small fringing kelp beds the relationship between ocean floor slope and kelp bed size (measured as canopy area in m^2) was explored. For each segment, the mean slope was calculated using the 20-meter bathymetry data from CHS (Davies *et al.*, 2019), and a kelp forest 'bed' was defined as a continuous patch of kelp forest where kelp forest objects in the classification were connected.

Step 4: Based on the results of the slope and kelp bed size analysis, we divided segments into 2 broad slope categories: low-mid slope areas (0-11.3 %), which included all flat segments and some shoreline segments which support large kelp beds, and high slope areas (11.4-37.0 %), only including shoreline segments which support small kelp beds. Next, percent area change was compared across resolutions in each slope category.

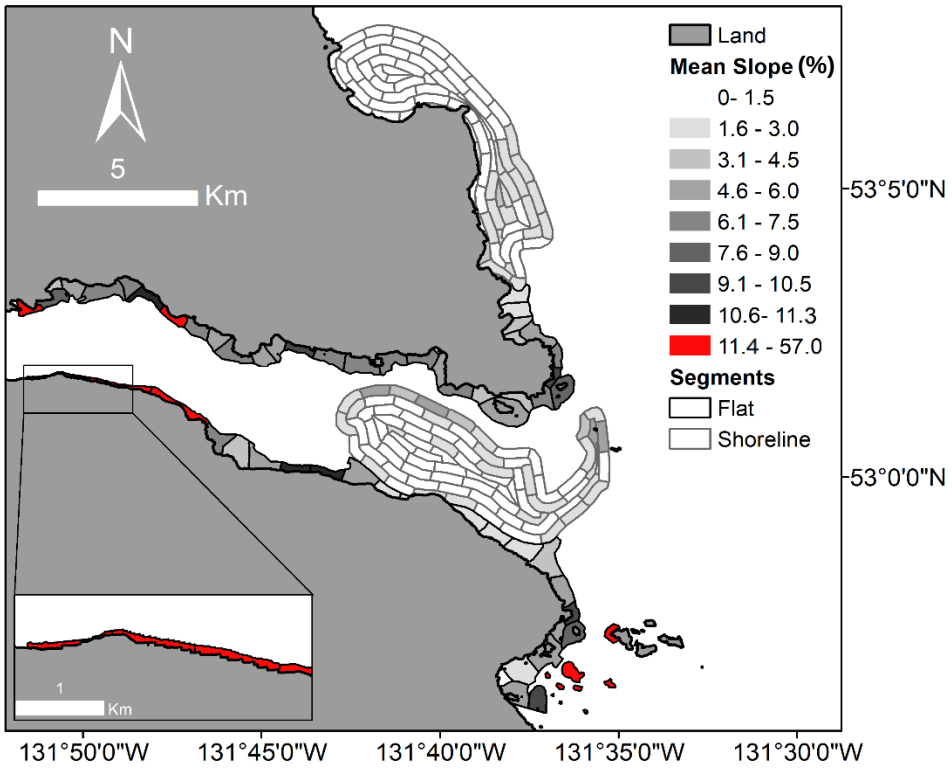

Figure 5. Map of approximately 1 km segments categorized by type, shoreline or flat, categorized into 2 main categories based on each segments mean slope: low-mid (0-11.3 %) shown in greyscale and high (11.4-37.0 %) shown in red

2.4 Results

2.4.1 Imagery Quality Assessment

Out of hundreds of archived images examined across the many different sources (**Table 1**), a total of 52 images were selected during the quality assessment step that span from 1973 to 2021. No good quality images were found for a total of 13 years, with most gaps in imagery occurring prior to 2005, including 1975, 1978-1981, 1983, 1987, 1993, 1995, 1996, 2003, and 2004. Landsat was the only freely available satellite imagery provider before 2004 and thus the preferred choice for imagery, and in particular, Landsat-7's scan line corrector failure in 2003 (Markham *et al.*, 2004) led to no available images for 2003 and 2004. For years following 2005, a variety of high-resolution imagery (2.0 – 20.0 m) were compiled ranging from a single Spot 4 image (20.0 m) to numerous images from Quickbird-2 (2.6 m), Geoeye-1 (1.8 m), Worldview (1.8 m), PlanetScope (3.0 m resampled from 3.7 m) and RapidEye (5.0 m) satellites. In addition to the high-resolution satellite imagery, we included a single nadir RBG aerial image (0.5 m spatial resolution) from the Canadian Hydrographic Service in the dataset because of the lack of good quality high-resolution satellite imagery in 2007.

The 52 archived images selected through the criteria were acquired in various conditions, leading to a range in quality scores (**Table 3)**. The largest proportion of imagery (46%) were acquired during optimal conditions for kelp forest canopy mapping. Among the defined criterion, more often, high tides or the presence of glint and cloud in imagery led to lower scores than waves and haze (**Table 3**). Notably, in some years, no low tide imagery was available because of the high tidal exchange that occurs in Haida Gwaii (Thomson, 1981), leading to 33% of images ranked in the lowest category for tides (over 5 m). These images were still included in the time series dataset because kelp forests were readily visible upon inspection.

Table 3. Summary of image quality criteria where percent (%) is the proportion of the 52 images that fall into each category

Quality	*Cloud (%)*	*Tide (%)*	*Glint (%)*	*Waves (%)*	*Timing (%)*	*Haze (%)*	*Quality*	*Score*	*Percent (%)*
0	79	31	52	96	92	77	*Optimal*	*<1*	46
1	10	17	42	4	8	12	*Good*	*2 to 3*	37
2	10	19	4	0	0	6	*Okay*	*4 to 5*	15
3	2	33	2	0	0	6	*Acceptable*	*6*	2

2.4.2 Preprocessing

Considering the selected imagery used for further analysis, a total of six images needed geometric correction: one from Landsat-1 and all imagery from Quickbird-2 and Geoeye, resulting in a RMSE within the 2-pixel threshold (average RMSE: Quickbird-2: 4.49 m, Geoeye-1: 3.61 m, Landsat-1: 16.48 m). For the next step, Rayleigh correction was applied to imagery from Landsat 1-3, Quickbird-2, SPOT 5-7 and Geoeye-1; images acquired by the other sensors (Sentinel-2, RapidEye, PlanetScope, and Landsat 5) were deemed usable because they were provided in atmospherically corrected products. After Rayleigh correction, generally, our results showed that kelp and dark water pixels were reduced to zero or just slightly above in the blue band compared to the original values (**Figure 6)**. For the green band, pixels values decreased by approximately half, and by approximately a third in the red band (**Figure 6)**, conforming with the shape of kelp spectra and water spectra from in situ hyperspectral measurements of kelp and water spectra presented in Schroeder *et al*. (2019b), Bell *et al.* (2015) and Jensen (1980).

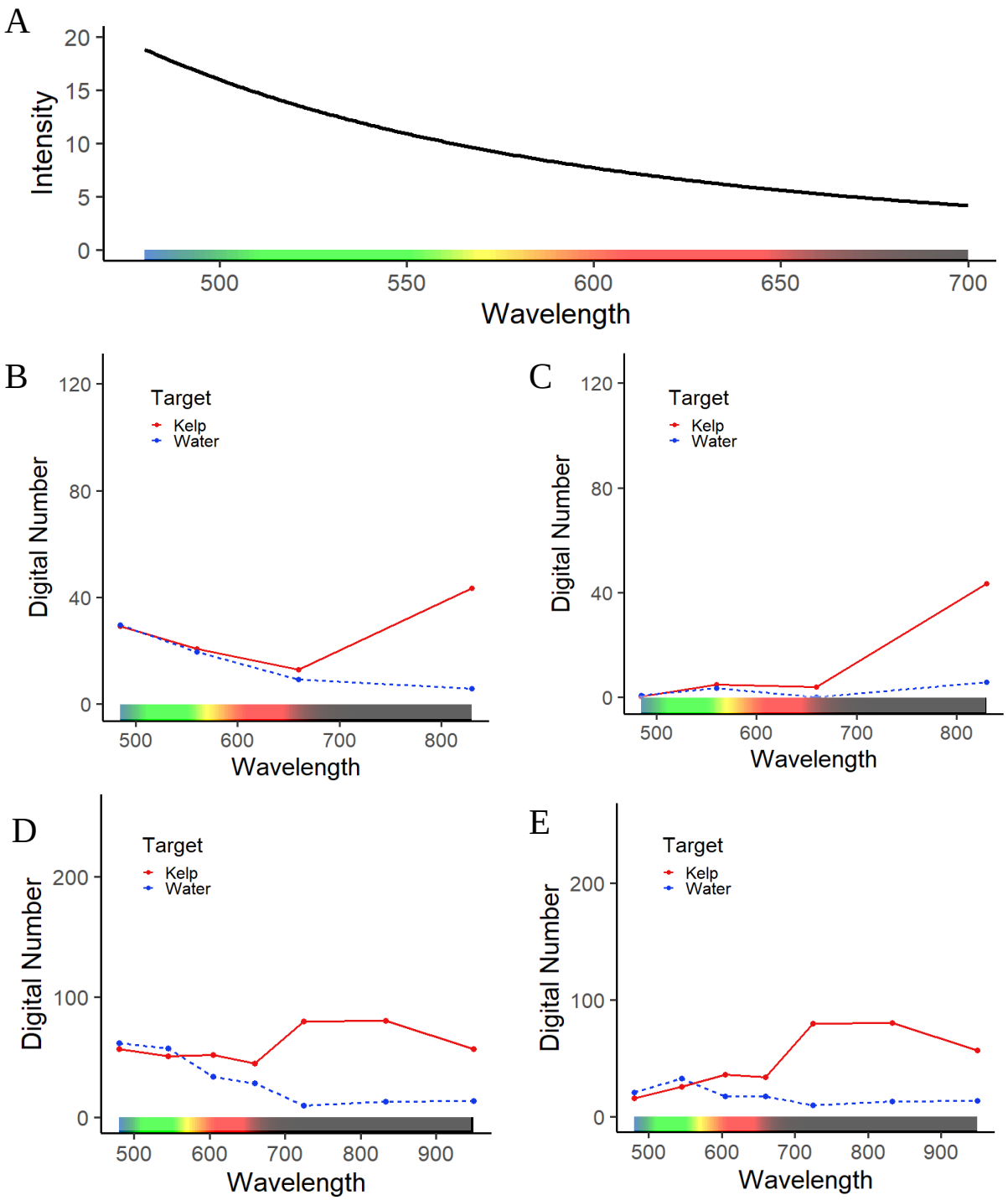

Figure 6. Examples of spectra before and after performing the Rayleigh Correction using the A) Rayleigh scattering curve to atmospherically correct imagery. B) & C) show a Quickbird-2 image before and after correction and D) & E) show a Worldview-3 image before and after correction. Note the magnitude of the digital number varies between sensors.

After geometric and Rayleigh corrections, the different spectral indices were evaluated based on the m-statistics for separability of kelp from other targets. Among the available spectral indices, the m-statistic results showed different optimal indices for the different satellites (**Table 4**). For Geoeye-1 and Quickbird-2 imagery, a normalized vegetation index with the green band (G-NDVI) instead of the red band had the highest separability (> 1.44). While for PlanetScope imagery, a simple ratio combination of the near-infrared and green bands showed the highest separability (>11.34). Lastly, for satellites that included a red edge band, RapidEye and Worldview, a simple band ratio of red-edge over green (>1.69) and red-edge over yellow (>2.72), respectively, was best at separating kelp from water. We then used the statistically selected indices and bands as the input data for the object-oriented classification.

Table 4. Summary of the m-statistic of different band indices and ratios for kelp and non-kelp classes observed in the imagery during band selection (R: red, Y: yellow G: green, B: blue, RE: rededge, NIR: near infrared, G-NDVI: NDVI with green instead of red, RE-NDVI: NDVI with rededge instead of NIR, B-NDVI: NDVI with blue instead of red, B-RE-NDVI: NDVI with blue instead of red and rededge instead of NIR, G-RE-NDVI: NDVI with green instead of red and rededge instead of NIR).

SATELLITE	KELP-WATER		KELP-SHALLOW WATER		KELP-SHADOW		KELP-GLINT/WAVES	
WORLDVIEW-2	**RE/Y**	3.19	NIR1/B	4.91	**RE/Y**	2.72	-	-
	RE-NDVI	2.96	NDVI	4.63	RE-NDVI	2.32	-	-
	NIR2/Y	2.51	G-NDVI	4.43	RE/R	1.99	-	-
GEOEYE-1	**G-NDVI**	6.58	B-NDVI	6.58	-	-	B-NDVI	28.59
	NIR/G	6.52	NDVI	6.52	-	-	NDVI	13.66
	B-NDVI	1.44	**G-NDVI**	1.44	-	-	**G-NDVI**	4.74
QUICKBIRD-2	**G-NDVI**	9.81	NIR/R	15.80	**G-NDVI**	7.46	-	-
	NIR/R	7.34	**G-NDVI**	9.85	NIR/G	6.95	-	-
	NIR/G	7.24	NIR/G	7.08	NDVI	5.02	-	-
PLANETSCOPE	**NIR/G**	14.02	**NIR/G**	11.34	-	-	**NIR/G**	19.63
	NIR/R	8.55	NIR/R	7.53	-	-	NIR/R	8.81
	NDVI	7.55	NDVI	7.32	-	-	NDVI	7.39
RAPIDEYE	**RE/G**	1.69	NIR/R	31.74	-	-	NIR/R	12.00
	B-RE-NDVI	1.46	NIR/G	11.23	-	-	NIR/G	10.81
	G-RE-NDVI	1.42	RE/R	9.11	-	-	RE/R	10.17

2.4.3 Classification & Accuracy Assessment

Here the results are presented according to the order of the various decision processes for the classification and validation. In an object-oriented classification approach, after the initial segmentation step (see Methodological Framework Step 3: Classification), we used the feature space optimization tool of eCognition to define the combination of object features that best differentiate classes. In this study, the possible object features include the mean and standard deviation of the input bands and band indices, as well as more complex derivatives of the input bands and band indices, as in the mean difference to neighboring objects for all bands and band ratios and the maximum difference between all bands and band indices within a given object.

Based on the samples defined by the user, the selection of object features is chosen independently for input into the nearest neighbour classification. Specifically, the feature space optimization function defines the best combination of object features that gives the highest possible separability (lowest overlap) between classes, as illustrated by the example of features chosen to classify a Quickbird-2 image from the dataset (**Figure 7)**. In this particular case, the feature space optimization tool chose the standard deviation of G-NDVI (**Figure 7A**), the mean G-NDVI (**Figure 7B**), and the maximum difference between all bands and band indices (**Figure 7C**) to differentiate kelp from submerged seaweed/kelp, glint/waves, and water sample classes. In this example, mean G-NDVI alone can differentiate kelp from all other classes present in the image. However, the feature space optimization chose both the standard deviation of G-NDVI and the maximum difference between all bands and band indices because, when combined, they can differentiate among all classes (**Figure 7D**). Although only the top three features are shown in **Figure 7**, the feature space optimization tool can suggest numerous features to improve the separability among classes, and, in the majority of cases, the feature space optimization tool

selected more than 3 and less than 10 features depending on the image. Specifically, the top features varied considerably depending on the input bands and band indices of each sensor, the classes and samples selected within the imagery, but generally, the mean of the red-edge band, near-infrared band and/or the band indices were selected by the feature space optimization tool to separate kelp from other classes.

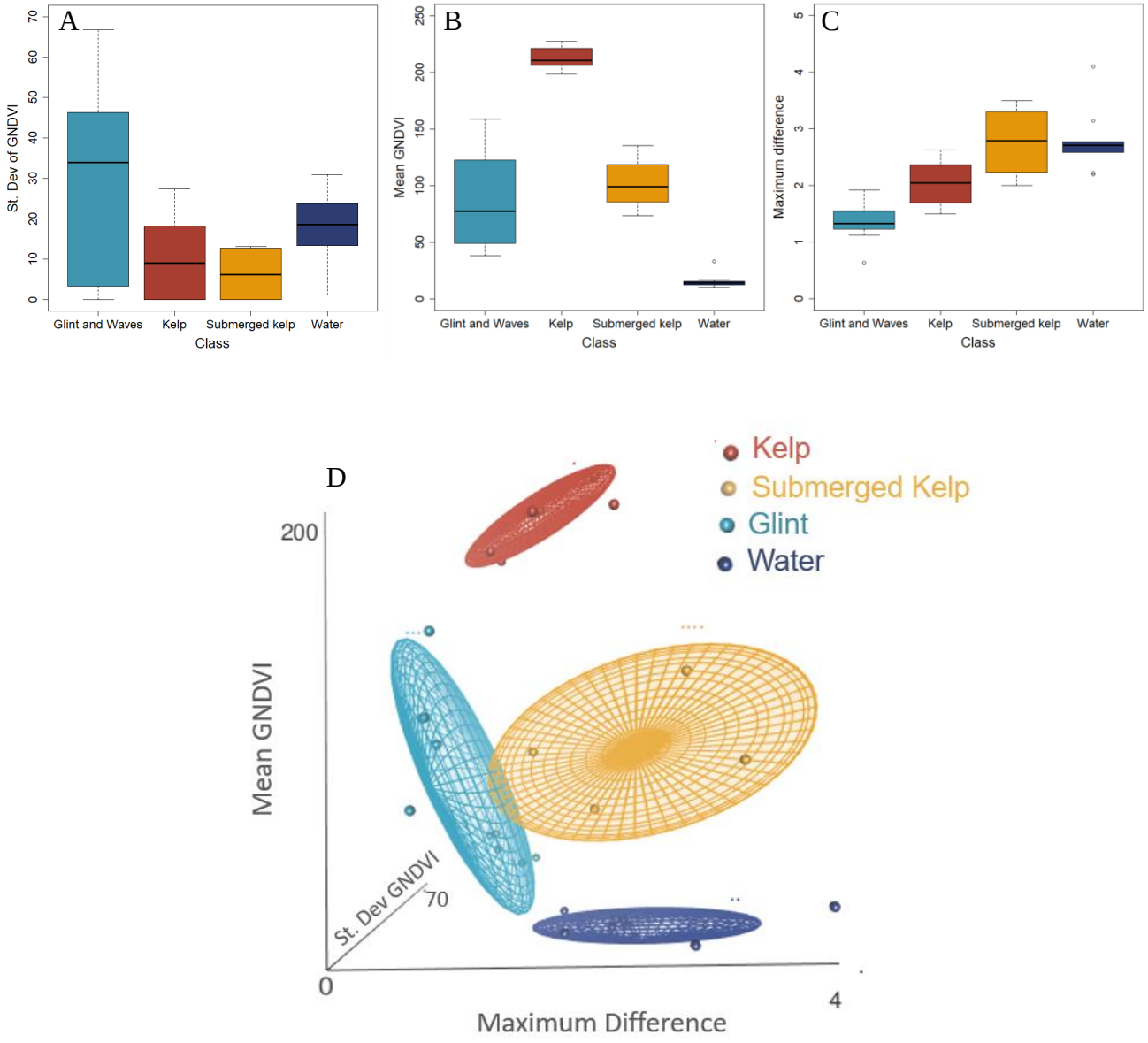

Figure 7. Boxplot of the top three features chosen by the Feature Space Optimization (FSO) tool: A) the standard deviation (St. Dev) of GNDVI, B) mean GNDVI and C) the maximum difference between all (G, R, NIR and GNDVI) input bands. D) Three-axis scatter plot of the top three features chosen by the Feature Space Optimization (FSO) tool showing separability of classes. Example of FSO was done with a Quickbird-2 image.

After selecting the optimal features, we ran the classification according to the nearest neighbour algorithm, followed by an evaluation of the classification results, considering user's, producer's, and global accuracies (**Table 5**). The overall global accuracy for all sensors ranged from 88 to 94 % (**Table 5, S1-5**). Generally, both producer's and user's accuracy for both kelp and non-kelp classes were high, with the highest errors in the non-kelp user's accuracy category corresponding to kelp misclassified as water. These errors were characteristic of areas where kelp was either relatively sparse, partially submerged, or in thin fringing beds along the shoreline (See example in **Figure 8A**). Specifically, we achieved high global accuracy (94%), user's accuracy (100%) and producer's accuracy (92%) for kelp for the 2021 Planet satellite image classification. However, we received a lower user's accuracy (70%) for non-kelp targets, where some areas of sparse and partially submerged clusters of kelp in the field data were misclassified as water (See example in **Figures 8A & B**). Examples of the range in size and density of correctly identified kelp forests are illustrated in **Figures 8C & D**. Lastly, we found no apparent differences when comparing the accuracy assessments that used concurrent and non-concurrent data for Quickbird-2, Geoeye-1, and Worldview-2 (**Table 5**).

Table 5. Summary of the accuracy assessment where user's accuracy (%) refers to how often classes (non-kelp and kelp) on the map are actually present in situ and producer's accuracy (%) refers to how often real features (non-kelp and kelp) on the ground are correctly classified on the maps.

Timing	*Satellite (Resolution)*	*Kelp User's Accuracy*	*Kelp Producer's Accuracy*	*n=*	*Non-Kelp User's Accuracy*	*Non-Kelp Producer's Accuracy*	*n=*	*Global Accuracy*	*n=*
Concurrent	**PlanetScope**	100	92	171	70	100	30	94	201
	Spot 7	100	88	64	86	100	48	93	112
	Landsat-5	97	82	113	64	92	39	89	152
	Aerial	100	83	6	75	100	3	88	9
	Rapid Eye	100	88	7	100	100	1	88	9
Non-Concurrent	**Quickbird-2**	90	96	47	95	89	45	92	92
	Geoeye-1	95	89	64	77	89	27	89	91
	Worldview-2	98	84	50	85	98	46	91	96

Figure 8. Examples of A) and B) kelp that was misclassified as water, and examples of C) and D) kelp that was correctly classified during the accuracy assessment. Image sources: A) & D) Environment and Climate Change Canada, B) & C) Gendall, L.

For the classification evaluation, it is important to consider that the number of validation data varies among the datasets. On average, we used 124 validation points (85 kelp points and 39 non-kelp points) for the validation of each sensor's product, except for products derived from Rapideye and the aerial imagery. For these, only 9 validation data points were available for each, and thus even though we achieved high accuracy, caution about the results is recommended. Further considerations are related to the impact of the spatial resolution of the different satellites on the accuracy results. For instance, the lowest resolution satellite included in the validation, Landsat-5 at 30.0 m, had similar accuracy to the higher resolution satellites (**Table 4**), but

classifications of Landsat-5 imagery did produce the lowest measure of user's accuracy for non-kelp targets (64%). Specifically, steep areas nearshore, which support smaller thin fringing beds, were misclassified as water, or omitted due to the low-water mask's coarse resolution. However, in general, there was no evident significant impact on the accuracy measurements and the spatial resolution of imagery, showing that this methodological framework performs well across the different spatial resolutions of imagery included in this study.

2.4.4 Resolution Analysis

Figure 9 illustrates the relationship between pixel size and the mixing of the spectral signature of different features within a pixel. Specifically, within a pixel resolution (for instance, 30.0 by 30.0 meters for Landsat 5), the kelp spectral signature is averaged with the spectral signature of other classes in close proximity (e.g., water), decreasing the ability to accurately map kelp forests as pixel size increases (**Figure 9**). In particular, as resolution decreases, kelp and water spectrum are mixed, and specifically for the near-infrared wavelengths, a lower reflectance signal is retrieved (**Figure 9G**). In the example presented in **Figure 9**, at 60.0 m resolution, the object-based classification can no longer differentiate the kelp signal from the surrounding water (**Figure 9G**) since the spectral signal of the small kelp bed is no longer discernable from the surrounding water signal.

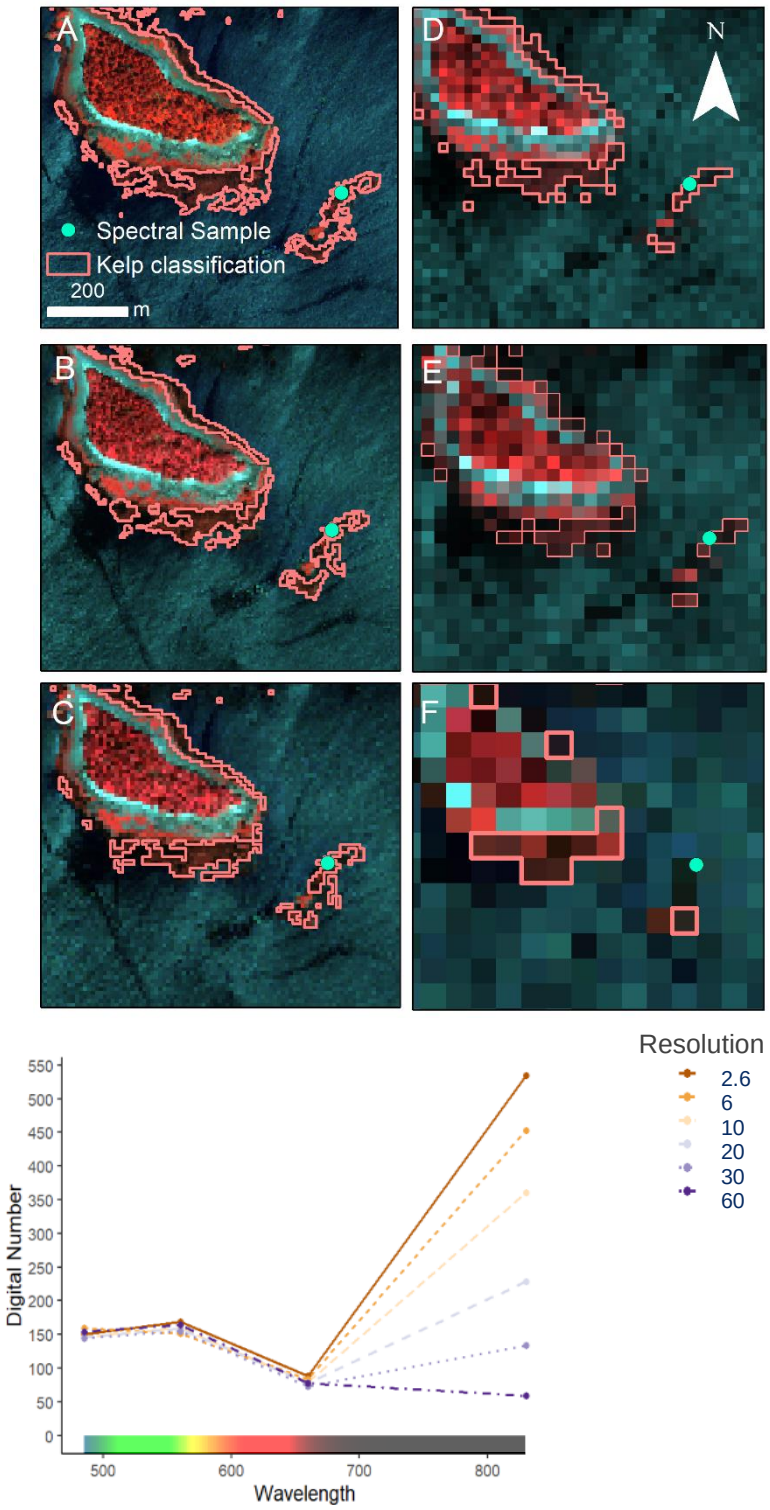

Figure 9. Clips of the same location of A) the Quickbird-2 image at 2.6 m resolution down sampled to B) 6.0 m, C) 10.0 m, D) 20.0 m, E) 30.0 m, and F) 60.0 m with G) showing the spectra measured at the sample location at each resolution. Kelp classification is shown as a kelp outline and. Images are false color infrared showing land vegetation and seaweed (including kelp) as red, rock/sand as light blue and water as dark blue to black.

The pixel mixing issues generally decrease the ability to correctly classify kelp when using medium-resolution imagery; however, this depends on the size of the kelp bed and proximity to the coast. We show that generally, most downgraded resolution images produced aerial kelp canopy within 9 % of their image's original detected kelp canopy area (**Figure 10**), except for the Quickbird-2 (**Figure 10A)** and RapidEye (**Figure 10B)** images downgraded to 20.0 m (QB20, RE20, respectively) and 30.0 m (QB30, RE30). QB30 and RE30 showed 25% and 29%, and QB20 and QB30 showed 17% and 12% less kelp area than detected in the original images. Here, it is difficult to differentiate the effect of the interpolation method used to downgrade the imagery from the actual impact of the spatial resolution on the kelp classification results. The further an image is downgraded away from its original resolution, the more likely artifacts or errors from the interpolation methods may occur (Titus & Geroge, 2013). For example, downgrading high-resolution Quickbird-2 (2.6 m) and RapidEye (5.0 m) images to medium resolutions (20.0 m, 30.0 m and 60.0 m) likely results in more blurring and edge halos than what would likely occur within an image actually acquired at medium-resolution (Titus & Geroge, 2013). This possible issue is minimized by avoiding data analysis by downgrading high-resolution to medium-resolution, and instead, considering downgrading the Sentinel-2 image from 10.0 m (SE10) to 20.0 m, 30.0 m and 60.0 m (SE20, SE30, SE60, respectively). **Figure 10C** shows that the total area of kelp remained almost unchanged when downgrading the medium resolution Sentinel-2 image from 10.0 m to 20.0 m, 30.0 m, and 60.0 m. Given this possible source of uncertainty associated with the interpolation method, further analyses only use Quickbird-2 and RapidEye imagery downgraded to 5.0 and 10.0 m, and the Sentinel-2 image downgraded to 20.0 m, 30.0 m, and 60.0 m. The spatial resolution and kelp area analysis, in

summary, showed that across the entire case study region that the detectability of kelp forest canopy area remained relatively unchanged (within 9 %) when downgrading high resolution imagery from Quickbird-2 (2.6 m) and RapidEye (5.0 m), to 6.0 m and 10.0 m and from Sentinel-2 (10.0 m) to 20.0 m, 30.0 m and 60.0 m.

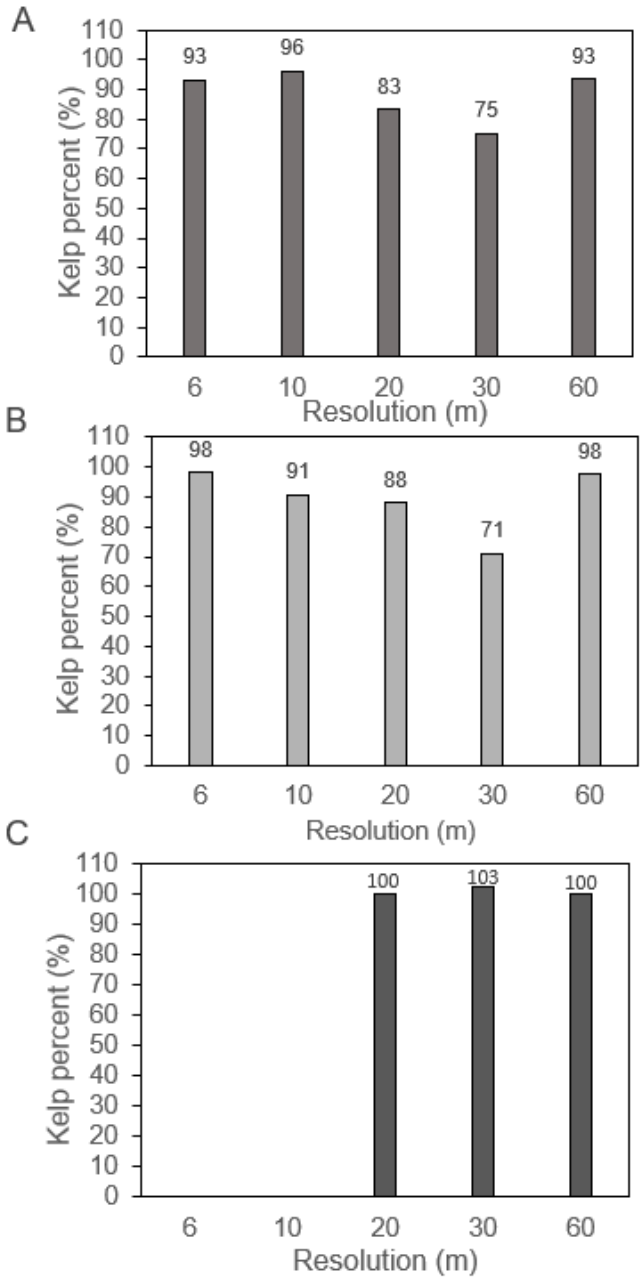

Figure 10. Change in kelp extent as a percent of the kelp extent derived from the original image plotted by resolution for A) Quickbird-2 (original resolution: 2.6 m), B) RapidEye (original resolution: 5.0 m) and C) Sentinel-2 (original resolution: 10 m)

Next the question remains: can ocean floor slope be used as a proxy for the size of kelp beds, and therefore restrict the detectability at different spatial resolutions spatially across the region? **Figure 11** shows the relationship between kelp bed size produced from the three original images included in the spatial resolution analysis (Quickbird-2, RapidEye and Sentinel-2) and ocean floor slope associated with each segment. Generally, areas of low-mid slope (0-11.3 %) were associated with both small (<17 000 m^2) and large kelp beds (≥17 000 m^2), whereas high slope (> 11.4) areas were only associated with small fringing kelp beds (<17 000 m^2). This difference in kelp bed size leads to differences in kelp forest detectability at different spatial resolutions

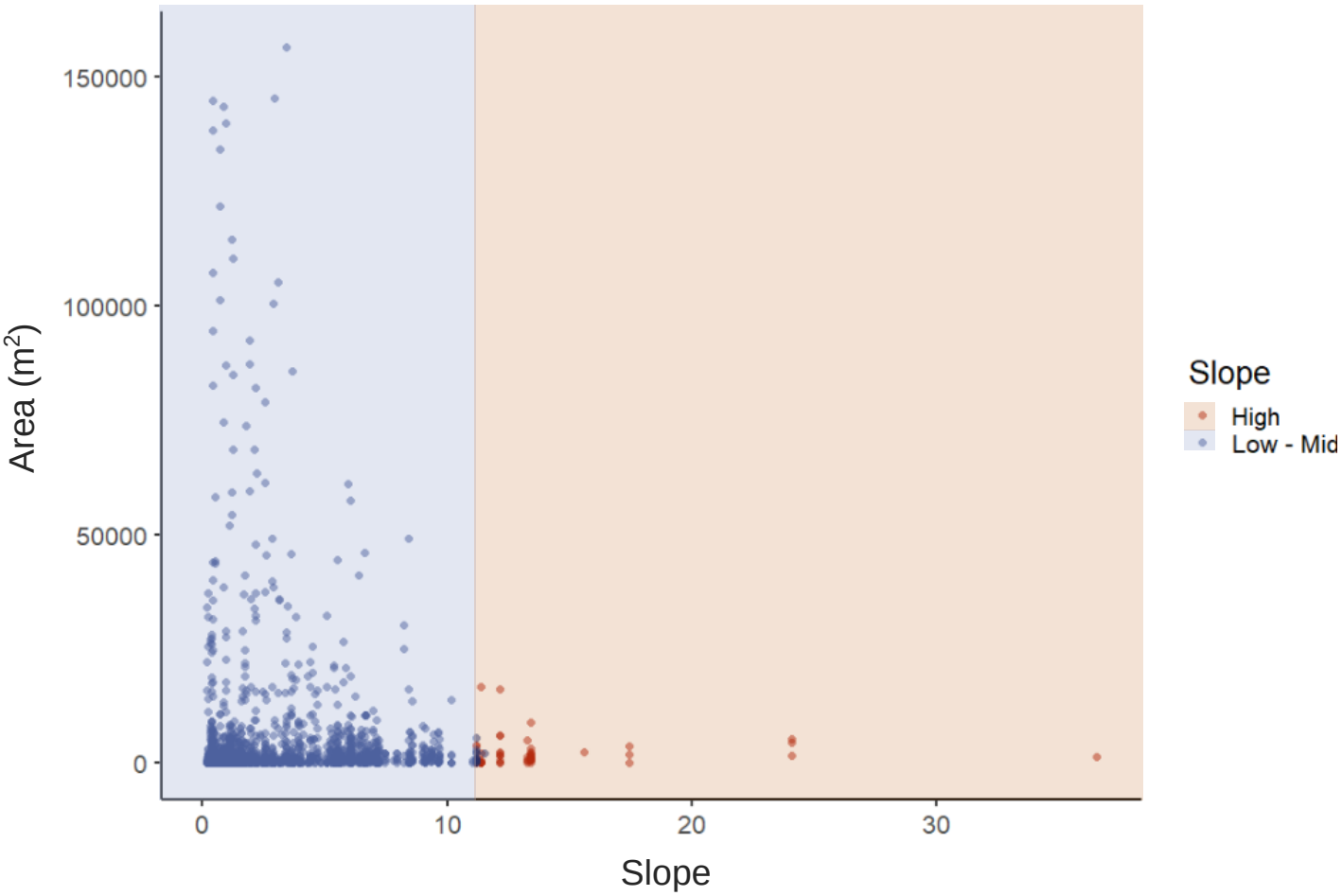

Figure 11. Area of kelp bed by segment slope where blue represents all kelp beds found within the low to mid-slope category (0-11.3 %) and orange represents high slope area (11.4-37.0 %)

across the region. For instance, as shown in **Figure 12** low-mid slope areas exhibited a lower percent difference (within 7 %) of kelp extent area between the various imagery resolutions than the high slope areas (up to 50%) overall. In particular, the differences in kelp aerial extent in high slope regions were much more pronounced in the downgraded medium-resolution imagery (SE20, SE30 and SE60) than the high-resolution imagery (QB6, QB10, RE6 and RE10). These results allowed us to restrict the use of medium-resolution imagery to map kelp only in areas of mid-low slope, i.e., imagery resolution between 20.0-60.0 m is not recommended for high slope areas where fringing-small kelp beds dominantly occur. Further, high-resolution imagery (2.6-10.0 m) can be used to map kelp in low-mid and high slope regions.

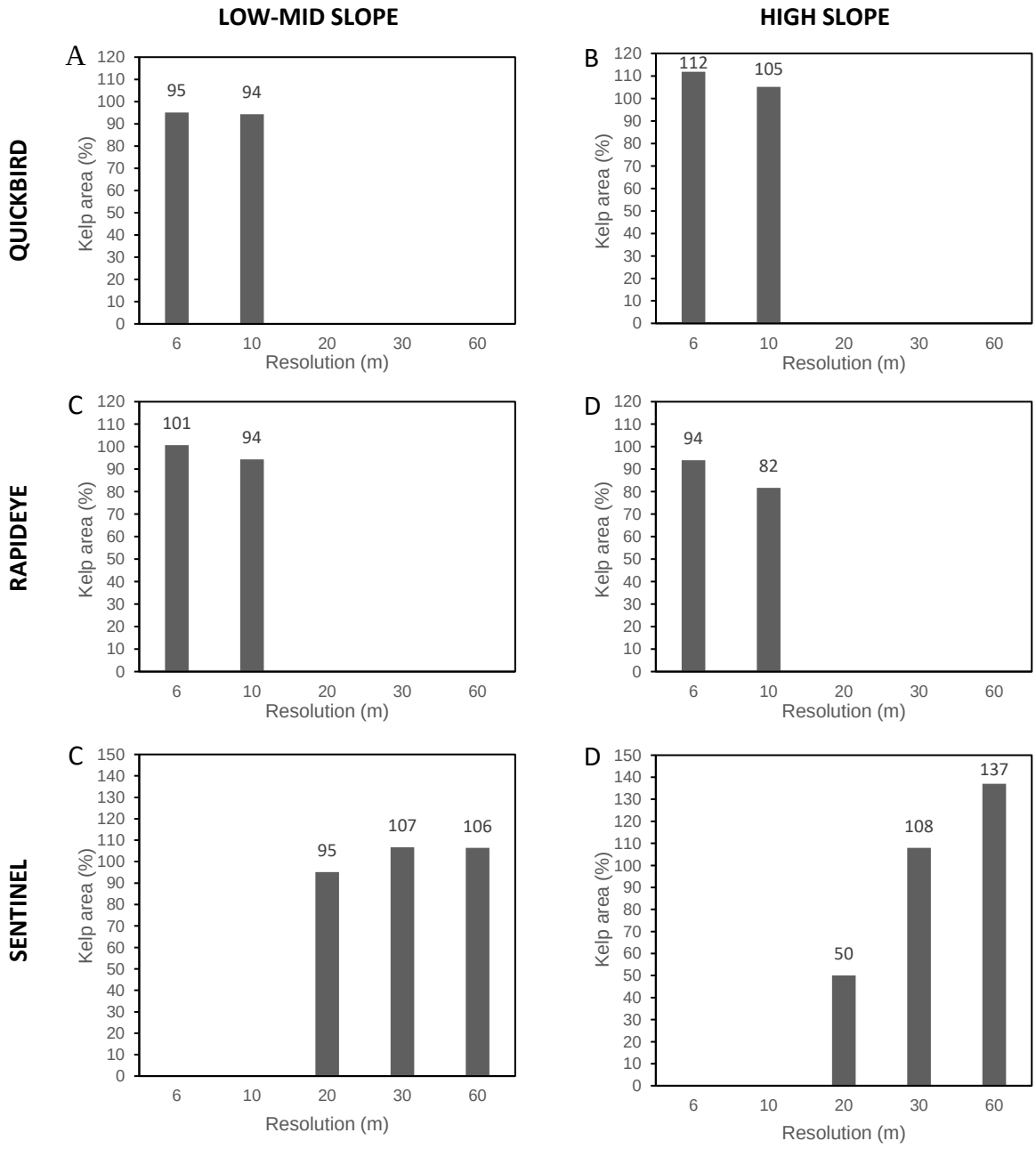

Figure 12. Change in kelp forest canopy area as a percent of that derived from the original image plotted by resolution separated into low-mid (and high slope categories for Quickbird-2 (original resolution: 2.6 m), RapidEye (original resolution: 5 m) and Sentinel-2 (original resolution: 10 m)

2.5 Discussion

With advances in remote sensing technology, opportunities to map and monitor important ecosystems across large scales through time are increasing. The Landsat series offers the best tool to map kelp forests at a single resolution (30.0 m) back through time (Cavanaugh et al., 2010, 2011b, 2013; Nijland et al., 2019; Bell et al., 2020; Finger et al., 2021). However, the ability to use medium-resolution imagery to accurately map changes in kelp forests area through time remains difficult in regions with small fringing kelp beds, such as the Pacific coast of Canada and Oregon (Nijland *et al.*, 2019; Hamilton *et al.*, 2020a). Here, we developed a framework combining standardized practices and adaptable methods to produce time series of accurate maps of kelp forest canopy areas from satellite imagery acquired at various spatial resolutions. We also showed that the ability to map kelp forests at different imagery resolutions can vary spatially based on ocean floor slope, and thus this metric can be used to highlight areas of uncertainty. Herein, we make a case for the workflow, discuss the impact of spatial resolution on kelp detection, summarize the recommendations for researchers when using the MSKM framework (**Table 6**) and more broadly consider the limitations and applications of the research.

2.5.1 Methodological Framework: Standardization and Adaptability

During this time of rapid ecological change, new approaches to bridge the gap between the advancements in satellite imagery technology and the growing field of ecosystem management and protection are required (Cavanaugh *et al.*, 2021). Specifically, Earth Observation data can help managers understand how important, yet data-poor regions may be changing and highlight areas in need of the establishment of monitoring, restoration and/or protection programs. Here, combining standardized (e.g., quality criteria, Rayleigh correction) and adaptable (e.g., OBIA classification) methods in the MSKM framework streamlines the process of creating kelp forest

maps from a wide variety of satellites while minimizing errors so that researchers can understand past and present changes in kelp forest ecosystems and make well-informed decisions in the future**.**

In remote sensing, Earth Observation satellite data has become readily available, and users often face confusion when trying to determine which satellites to use to produce the best results for their given application (Alavipanah *et al.*, 2010). In this paper, we highlighted some of the most well-known sensors for mapping kelp forests, such as the Landsat, SPOT and Sentinel-2 satellites (e.g., Cavanaugh *et al.*, 2011b; Mora-Soto *et al.*, 2020; Bell *et al.*, 2020), while also presenting some new cost-effective high-resolution options such as imagery from the RapidEye, the Worldview, and the PlanetScope dove satellite series, which add valuable data into the kelp mapping field with their coverage since 2008, 2009, and 2018, respectively. In addition to the choice of satellites, having a specific set of criteria when choosing what images to use is crucial in minimizing the time and cost associated with building time series (**Table 6**) (Alavipanah *et al.*, 2010; Nahirnick *et al.*, 2019; Schroeder *et al.*, 2019a). We demonstrated one possible set of criteria that can be used to minimize errors associated with environmental conditions and the timing of satellite imagery acquisition. Note that the criterion should always be selected based on the specific area of interest. In particular, other factors that could lead to the erroneous classification of kelp forests in satellite imagery are land adjacency effects, high currents independent from tides, water turbidity, and the presence of algal blooms (Cavanaugh *et al.*, 2021). Our analysis did not consider these because they were largely absent in our study region. However, challenges such as cloud cover, higher tidal amplitude and lower sun angles increase in severity as latitude increases along the west coast of North America (Cavanaugh *et al.*, 2021), and in our case study region, clouds and higher amplitude tides often limited the availability of

good quality images. As such, some mid to high tide images (2.0 m – 5.0 m above chart datum) were included based on a visual assessment of the imagery. Nijland et al. (2019) found a loss of kelp canopy area up to 42% when comparing a 2.0 m tidal height difference on the Central Coast of BC. Additionally, Timmer *et al.* (in prep) found that small kelp beds in Unpiloted Aerial Vehicle (UAV) imagery decreased by roughly 22.5% per meter of tidal height increase. In contrast, Cavanaugh *et al*., (2010, 2011) found that tides of 2.0 m difference had little to no impact on satellite-derived kelp biomass measurements in California where giant kelp forms large offshore beds similar to those found within the case study region used to develop the MSKM framework.

Once a good quality imagery database is created, users are faced with many inconsistent and complex approaches to correct systematic errors in remotely sensed data, such as atmospheric attenuation and geometric distortions (Young *et al.*, 2017; Schroeder *et al.*, 2019b). In order to keep the workflow streamlined and easy to use, we propose a simple geometric and atmospheric correction method that can be applied to imagery acquired by various different sensors (**Table 6**). For georectification, we found that a simple 1st order polynomial, which considers systematic and random distortions in images (Bannari *et al.*, 1995; Jensen, 2005; Ayoub *et al.*, 2008) properly addressed any geometric distortions present in imagery.

For the atmospheric correction, the Rayleigh correction method provided a quick, simple, yet effective approach, to correct the impacts of atmospheric scattering in imagery from different sensors. There are numerous atmospheric correction methods that range from simple techniques like the Rayleigh correction method (Chavez, 1988) to the more complex algorithms that need supplemental data, including atmospheric models and, ideally, *in situ* measurements (Cooley *et al.*, 2002; Pflug & Main-Knorn, 2014). Other researchers, for instance, have effectively used

models such as the Fast line-of-sight Atmospheric Analysis of Hypercubes (FLAASH) (Schroeder *et al.*, 2019a) and the Atmospheric and Topographic Correction (ATCOR) (Nijland *et al.*, 2019). Nonetheless, these methods can often under/overcorrect values when parameters are not adequately chosen, making it challenging for non-remote sensing experts to use, and problematic when applied over large bodies of water (Camacho, 2006; Yang *et al.*, 2021; Richter & Schlapfer, 2021). Ideally, for mapping kelp, when possible, imagery should be downloaded as atmospherically corrected products such as in Hamilton et al. (2020), Mora-Soto et al. (2020), Bell et al. (2020), and Houskeeper et al. (2022). For example, the United States Geological Survey's (USGS) provides Landsat Analysis Ready Data (ARD) products (Zhu, 2019) and the Planet Skysat provides Surface Reflectance (SR) products (Frazier & Hemingway, 2021). However, when these products are not readily available, adhering to a simple method that only requires within-image information is recommended to prevent errors related to inconsistent methods or data input. We found that the adopted Rayleigh correction method resulted in similar kelp and water spectra as those in Schroeder et al. (2019b), Bell et al. (2015) and Jensen (1980). And, more importantly, the shape of the kelp and water spectra from the corrected Landsat 1-3, Quickbird-2, SPOT 5-7 and Geoeye-1 images were akin to those of the atmospherically corrected products of Sentinel-2, RapidEye, PlanetScope, and Landsat 5-7 images included in the time series, allowing confidence on the use of the various band indices and ratios in the next step of the analysis.

Numerous band ratios and vegetative indices have been used to enhance kelp in satellite imagery (Schroeder *et al.*, 2019b), most notably, the normalized difference vegetation index (NDVI), which was initially used to detect healthy land vegetation (Tarpley *et al.*, 1984) has been co-opted for floating kelp forest detection (Augenstein *et al.*, 1991; Cavanaugh *et al.*, 2010; Cui *et*

al., 2012; Dierssen *et al.*, 2015; Schroeder *et al.*, 2019b; Nijland *et al.*, 2019; Hamilton *et al.*, 2020a). Based on the literature, NDVI has been effectively applied to Sentinel-2, Landsat, and SPOT satellite imagery to differentiate kelp from other classes. Alternatively, based on the m-statistics analysis and similar to Schroeder *et al*. (2019b), we found that the NDVI with the green band (G-NDVI) instead of the red band performed better, most likely because of less noise in the green band than in the red band when visually inspecting the imagery. Additionally, indices that included the red-edge band outperformed other indices, likely associated with the ability to detect submerged kelp better with the red-edge band than with the near-infrared band (Timmer *et al.*, 2022). Considering these factors, within an image pixel, there is likely a spectral signal mixture of submerged and floating kelp canopy with water, consequently, users should consider that the red-edge indices may produce a higher reflectance signal or slightly more kelp area than non-red edge indices depending on the properties of the kelp forest (percent submerged, depth, size, density, species). Although different band indices were chosen in our analysis, the overall accuracy of kelp maps produced remained high across all satellites, indicating the viability of using multiple band indices to enhance kelp forest extent in various imagery.

Among the many different forms of classification, a commonly used method, the multiple endmember spectral mixture analysis (MESMA), has been effectively used for mapping kelp forests in Landsat imagery. MESMA is a pixel-based approach, which linearly models the amount of kelp and seawater in each pixel using one kelp pixel endmember and multiple water pixel endmembers (Cavanaugh *et al.*, 2010, 2011a; Hamilton *et al.*, 2020a; Bell *et al.*, 2020; Friedlander *et al.*, 2020; Finger *et al.*, 2021; McPherson *et al.*, 2021). In comparison, the OBIA approach presented herein and first used by Schroeder *et al.*, (2019a,b) to map kelp forests, is based on clustering pixels into objects before the classification. The advantages of using the

OBIA approach proposed in this MSKM framework are related to less computational power, less consideration of imagery noise commonly found in pixel-based classifications, and the ability to mimic visual interpretation of features in an image (Baraldi & Boschetti, 2012; Evans *et al.*, 2013). The OBIA approach negates the necessity of normalization between images often needed when using pixel-based approaches (Schroeder *et al.*, 2019a,b), and most importantly, the feature space optimization tool allows for the classification to be optimized on a per image basis. Of note, given our goal to produce highly accurate kelp maps for areas comprising medium and large-size kelp beds, the approach suggested here is a supervised classification method and needs some expert knowledge to determine good training samples for the classifier in any given area.

Across all sensors, the MSKM framework resulted in high overall global accuracy (88 to 94 %) when compared to the range (59-94%) documented in the literature (Casal *et al.*, 2011; Schroeder *et al.*, 2019b; Nijland *et al.*, 2019; Hamilton *et al.*, 2020a). It is important to note that different sources of validation data were used to evaluate the classification results, including field observations concurrent with imagery acquisition, data acquired from airplane and SCUBA surveys, matched for the same year, and some not matching the same year. However, for using all these different data sources, expert knowledge was always embedded prior to the accuracy assessment to minimize the use of erroneous classification outputs when comparing with validation data. Generally, the errors of omission and commission showed that most errors occurred at medium-resolutions where sparse and narrow fringing beds along steep shorelines were misclassified as water or omitted due to the coarse resolution low water mask, similar to Nijland *et al.* (2019) indicating that the relationship between imagery spatial resolution and kelp bed aerial extent has to be considered to highlight mapped areas with high uncertainties.

2.5.2 Impact of Resolution & Drawing Appropriate Conclusions

The MSKM framework presented here incorporated the analysis of a large range of satellite imagery with different spatial resolutions (0.5- 60.0 m) to build the longest time series possible, including data from the 70's to present-day from medium to high-resolution satellites. Generally, although the imagery resolution differed by magnitudes, the mapped kelp area at the regional level did not largely differ among resolutions. However, at a finer spatial scale, we found that kelp mapped at high slope areas were more impacted at coarser resolutions. A few researchers have shown that the spatial resolution of satellite imagery and the conditions during acquisition can affect the detectability of kelp in satellite imagery (Britton-Simmons *et al.*, 2008; Schroeder *et al.*, 2019b; Nijland *et al.*, 2019; Cavanaugh *et al.*, 2021). Here, we propose the addition of a new parameter, ocean floor slope, to define the limitations of mapping kelp from different resolution imagery. Particularly, the comparison between kelp bed size and slope showed that high slope areas mainly support small kelp beds, leading to more uncertainty when mapping with medium-resolution imagery (up to 50%). For instance, we noticed that for medium-resolution imagery (e.g., Landsat) smaller kelp beds are not accurately discernible due to the reflectance signal mixing of kelp and water within pixels. We also found that although small kelp beds are present in low-mid slope areas, the mapped kelp canopy area did not differ substantially among resolutions (< 7 %). This is likely because even though some small kelp beds are missed in the classification of medium-resolution imagery, the area of the large kelp beds generally compensates for the missing small kelp beds. Based on these factors, we suggest that regions with slopes higher than 11.4 % should either be mapped only with the high-resolution imagery or excluded from comparisons between high-resolution and medium-resolution imagery (**Table 6**). Additionally, for time series kelp change analysis, we recommend that users consider that a certain percent of kelp area differences among years can be attributed to errors due to resolution,

Table 6. Summary of the recommendations outlined in the discussion for researchers applying the MSKM framework to create long-term time series of kelp forest canopy area

MSKM FRAMEWORK RECOMMENDATIONS	
QUALITY CRITERIA	Have a set of quality criteria adapted for the specific area of interest when choosing what images to use minimizes the time and cost associated with building archived imagery time series. Things to consider in the development of criteria for a given area: 1. Peak biomass for acquisition timing 2. Aim for low tidal heights 3. Minimize cloud cover and haze 4. Minimize glint and waves 5. Minimize low sun angles and shadows 6. Minimize adjacency effects
GEOMETRIC & ATMOSPHERIC CORRECTIONS	When possible, attain imagery as atmospherically and geometrically corrected products and when not possible use simple approaches such as a simple 1st order polynomial shift for geometric correction and the Rayleigh correction method to adjust atmospheric scattering and attenuation.
BAND INDICES/RATIOS	Use a measure of class separability such as the m-statistic to determine the best combination of band indices and ratios to use for each sensor.
CLASSIFICATION	To classify kelp within different imagery from different satellites use an adaptable OBIA classification with the help of the feature space optimization tool to minimize errors and attain high accuracy scores. Of note, expert knowledge is required to choose samples to train the classifier and a visual quality assessment of the classification should be done to minimize erroneous classifications prior to the accuracy assessment.
ACCURACY ASSESSMENT	When possible, collect *in situ* validation data. However, if no ground-truth data are available, other forms of data can be used to validate the classification, such as past surveys that show the location of kelp forests or expert knowledge based on reflectance values.
RESOLUTION	The ability to map kelp forests at different imagery resolutions can vary spatially based on ocean floor slope, and thus this metric can be used to highlight areas of uncertainty. Based on the Haida Gwaii test area: 1. We suggest that regions with slopes higher than 11.4 % should either be mapped only with the high-resolution imagery or excluded from comparisons between high-resolution and medium-resolution imagery. 2. We suggest that changes up to 7 % be taken into consideration when comparing kelp distributions from imagery at different resolutions in low-mid slope areas. Special attention should be given to the detection limits at different resolutions when applying the MSKM framework in new areas, thus we suggest performing similar resolution analyses and adjusted the ocean floor slope threshold accordingly, especially if segment size and kelp forest density, and species vary significantly from those presented in this study.

and not attributed to true changes in kelp extent. Within our region, we suggest that changes up to 7 % be taken into consideration when comparing kelp distributions from imagery at different resolutions in low-mid slope areas (**Table 6**).

2.5.3 Challenges and Broad Applications of the Methodological Framework

A few challenges and limitations remain when using this proposed MSKM framework, including imagery characteristics and environmental conditions at the time of imagery acquisition that cannot be accounted for, the small sample size used in the resolution analysis and the size of the segment used as the unit of analysis. In particular, when using this framework in new areas, special consideration should be given to these limitations in addition to the type of species present and the density of kelp forests in the region. The spatial resolution analysis and subsequent recommendations were conducted with rigorous methodological criteria; however, the analysis was limited to samples of imagery from only three different satellites. We acknowledge that the sample size is limited, and other satellite-associated variables beyond spatial resolution, including spectral resolution, signal-to-noise ratio, and satellite vicarious calibration, also play a role in detectability (Trishchenko *et al.*, 2002; Teillet & Ren, 2008; Schroeder *et al.*, 2019b). Within these considerations, the different satellites/bands employed in this study generally have similar band location and bandwidth. Specifically, the images and bands chosen for the resolution analysis from Sentinel-2, Quickbird-2 and RapidEye cover most of the bands used in the dataset to derive kelp from satellite imagery (**Table 1**).

In addition, we were unable to quantify the impact that different environmental conditions such as haze, shadows, glint, currents, or tide have on the detectability of kelp at different imagery spatial resolutions. These impacts are challenging to isolate and account for because they may differ largely based on location, species type, density, and time of acquisitions. Consequentially,

we suggest researchers should always aim to minimize these impacts by selecting the best possible images using the quality criteria presented within the MSKM framework. Moreover, when using the MSKM framework, researchers should consider the species and density of kelp forests present within their region and how this could impact the detectability in satellite imagery. Specifically for our region, kelp beds are generally dense regardless of the bed size and species, thus conforming with the presented MSKM framework. For other regions where sparse kelp forests dominate or areas containing solely bull kelp forests, special attention should be given to the detection limits at different resolutions, and the ocean floor slope threshold may be adjusted when using medium-resolution imagery.

The resolution analysis allows for a conservative approach when drawing conclusions from time-series of kelp forest canopy extent derived from different satellites. Additional research in the future may include defining correction factors like the tidal correction factor applied by Bell *et al*., (2020) to minimize the effects of the different spatial resolutions on the mapped kelp area. For this, we recommend multiple replicates of comparisons between satellite images collected at different spatial resolutions in similar conditions over the same location within a short time frame. Furthermore, it is important to note that our unit of analysis was ~1 km segments. In the literature, the size of segments for kelp time series analyses vary substantially (e.g., 100 m in Schroeder *et al.*, 2019a, 8 km in Pfister *et al.*, 2018, 1 km in Berry *et al.*, 2021), and as such, special consideration should be given to the scale of future analysis and further explorations of the relationship between resolution and kelp detectability are advised if the unit of analysis (segments length) for future work significantly differs from those presented in this study.

Many methods exist to detect kelp from satellite imagery; however, most focus on compiling time series using a single type of sensor, which can limit either the spatial resolution of imagery

available to create long-term time series (i.e., 30.0 m Landsat imagery from 1984 onwards) or with the use of high-resolution satellite imagery the length of time series is limited considerably. The MESMA approach (described above) was developed to use Landsat imagery from 1984 onwards to detect large offshore beds of kelp in California (Cavanaugh et al., 2010, 2011a; Bell et al., 2020; McPherson et al., 2021). Similarly, this method has been used to map *Macrocystis* in the Southernmost part of Argentina (Friedlander et al., 2020) and *Nereocystis* off the coast of Northern California (Finger et al., 2021) and Oregon (Hamilton et al., 2020). However, when this approach was used to map kelp beds on the Central coast of BC, between 28% to 75% of kelp that was present in the shoreline areas was missed due to the medium-resolution nature of the Landsat imagery (Nijland *et al.*, 2019). Recently, a similar method using 10.0 m Sentinel-2 data was created by Mora-Soto *et al.*, (2020), and although this method solves some of the issues associated with the 30.0 m resolution of the Landsat data, a serious limitation with the Sentinel-2 data repository is that it only dates back to 2015. In contrast, the methodology presented here enables kelp trends to be understood with high-resolution data back to the early 2000s and medium-resolution data back to the 1970s. The methods proposed by Cavanaugh et al., (2010), Nijland et al. (2019), Mora-Soto et al., (2020) and the one shown here, when integrated with the growing availability of higher-resolution imagery such as the PlanetScope dove satellite series (available since 2018), will streamline the monitoring of kelp forests into the future and will continue to allow scientists to better understand large-scale trends in kelp forests in a time of unprecedented kelp loss globally.

Global threats to kelp forests are on the rise, and numerous declines in kelp forests have already been documented in the 21st century (Filbee-Dexter & Wernberg, 2018). For example, a 95% decline in giant kelp forests in northern California occurred during the onset of the sea star

wasting epidemic and the 2014-2016 marine heatwave (Rogers-Bennett & Catton, 2019; McPherson *et al.*, 2021). Mass declines of multiple kelp species across the globe have occurred in Baja California (Arafeh-Dalmau *et al.*, 2019), Japan (Tanaka *et al.*, 2012; Kumagai *et al.*, 2018), Australia (Johnson *et al.*, 2011; Wernberg *et al.*, 2013; Smale & Wernberg, 2013; Vergés *et al.*, 2016; Carnell & Keough, 2019; Layton *et al.*, 2020), Oman (Coleman *et al.*, 2022), Norway (Rinde *et al.*, 2014), Spain (Piñeiro-Corbeira *et al.*, 2016; Casado-Amezúa *et al.*, 2019), Chile (Vega *et al.*, 2014; Hamilton *et al.*, 2022) and the Atlantic coast of Canada (Filbee-Dexter *et al.*, 2016). Even prior to the advent of high-resolution satellite imagery, changes in kelp forest ecosystems were documented. For example, a temporary loss of giant kelp forests occurred in Baja California during the 1997-1998 heatwave (Ladah *et al.*, 1999), and giant kelp forests in southern California already showed signs of instability and vulnerability to climate forcing following the North Pacific regime-shift in 1977 (Parnell *et al.* 2010). During this time of rapid change, the framework proposed here allows changes in kelp extent to be mapped in challenging to monitor areas using high-resolution data but also enables understanding trends back through time by integrating medium resolution data to elongate timelines. As such, for any given area, this methodological framework enables the compilation of time series data from both periods (pre and post the advent of high-resolution satellite imagery) without needing to compromise the temporal scale or resolution of the time series.

2.6 Conclusion

Globally, threats to kelp forest are on the rise; however, locally kelp forest show highly variable patterns of change (Krumhansl et al., 2016; Wernberg et al., 2019). This study highlights that with the advancement in Earth Observation satellite technology, archived satellite imagery can be leveraged for the monitoring of crucial kelp forest ecosystems using medium resolution

imagery from the 70s onwards (Landsat and SPOT) and more recently, using high resolution imagery (e.g., Worldview, RapidEye, Planet) from the early 2000s onwards. With considerations of kelps highly dynamic nature, kelp forest ecosystems need long-term large-scale monitoring to robustly understand kelp forest trends through time. Building on past remote sensing kelp mapping methodologies, the MSKM framework allows for the creation of kelp forest-canopy timeseries by combining archived medium- to high-resolution satellite imagery and in this study, we demonstrate that through standardized practices (i.e., the image quality criteria, geometric and Rayleigh correction) and adaptable image-to-image methods (i.e., band index/ratio selection and OBIA) accurate maps of kelp forest canopy areas can be produced. We acknowledge that differing resolutions have an impact on the amount of kelp detected in a given image and that when using this framework, we suggest using ocean floor slope as a metric to highlight areas of uncertainty in kelp detectability. We show that only high-resolution imagery should be used to map kelp in areas with ocean floor slopes higher than 11.4 %, however in low-mid slope (0-11.3 %) areas that support larger kelp forest comparison can be made across medium- to high-resolution imagery. However, errors associated with resolution, in our case about 7%, should be taken into consideration when comparing kelp extent derived from different resolution imagery in the future. The proposed framework will enable researchers to understand more accurately the recent trends in kelp extent using high-resolution imagery that spans the last two decades while still being able to understand larger changes detectable with medium-resolution imagery prior to the early 2000s. Creating these long time series of kelp forest canopy area using the MSKM framework can facilitate the monitoring and protection of important nearshore kelp forest habitats from emerging threats in this time of rapid global change and when coupled with

environmental driver data and/or climate prediction modelling can highlight regions of kelp forest risk and resilience globally.

3.0 A Century of Loss & Resilience: Understanding the Spatio-Temporal Drivers of Haida Gwaii Kelp Forests

3.1 Abstract

Canopy kelps are dominant habitat-forming organisms in nearshore temperate ecosystems that provide shelter and food for many ecologically important species, supporting cultural practices and fisheries. High-resolution satellite imagery can quantify the distribution of kelp forests over large areas like the Haida Gwaii coastline and establish datasets necessary to detect change over time. Kelp monitoring for the Pacific Coast of Canada is at its inception and the drivers of change remain poorly understood. Our goal is to use satellite imagery alongside historical and environmental driver data to quantify and understand patterns of change in an important kelp forest region of Haida Gwaii, British Columbia, Canada by: 1) assessing changes in kelp forest canopy area using high to medium resolution satellite imagery (1973-2021) and historic data from British nautical charts (1867-1945), and 2) assessing regional climate indices and local drivers to understand the spatio-temporal trends in kelp forest canopy area. Overall, patterns of kelp forests area varied across the study region with some areas showing considerable losses while others showed long term resilience. The loss of kelp forests occurred in the North of the region where approximately 60% of the total maximum kelp forest area previously documented disappeared. This disappearance correlates with a regime shift that occurred in the late 1970s from a cool to warm period in the Pacific Decadal Oscillation exacerbated with the high local sea surface temperatures experienced in the North of the region. In contrast, more sheltered and cooler subregions showed high variability and overall resilience where kelp forests have persisted over a century. These spatial and temporal scale-dependent results highlight how local environmental gradients can cause unexpected losses in areas well within species range limits

and highlight the need for long-term datasets to capture trends in highly variable foundation species through time.

3.2 Introduction

Ecosystems such as kelp forests, mangroves, coral reefs, and seagrass meadows are foundational parts of nearshore environments that support biodiversity, provide habitat to many important organisms, sequester blue carbon, and deliver ecosystem goods and services to people around the world. The International Panel on Climate Change (IPCC) oceans and cryosphere report (Pörtner *et al.*, 2019) highlights these foundation ecosystems as vulnerable and threatened by not only global climate change but local and regional scale stressors. Coastal areas are amongst the most densely populated regions globally, contributing to coastal ecosystem declines driven by pollution, eutrophication, erosion, invasive species introduction, dredging and coastal development (Crain *et al.*, 2009; Lu *et al.*, 2018). With climate change, not only does the long-term persistent warming of the ocean play a key role in the loss of coastal habitats, but the increased local variability can lead to long-term temporal degradation and lower resilience in the face of climate perturbations. More specifically, the increasing frequency and intensity of marine heat waves – discrete periods of anomalously warm water - has severely impacted the health and persistence of coastal ecosystems globally (Smale, 2020). Losses, gradual deterioration and higher variability of key habitat-forming organisms such as corals, seagrasses, mangroves and kelp forests can have cascading impacts on the complete functioning of nearshore ecosystems (Smale *et al.*, 2019) and further damage the global capacity to mitigate climate change with coastal ecosystem-based solutions in the future (Pörtner *et al.*, 2019).

Canopy-forming kelps, such as *Nereocystis luetkeana*, and *Macrocystis pyrifera*, are foundation species that make up three-dimensional habitats and support numerous marine

species, cultural practices, and diverse fisheries (Turner, 2001; Krumhansl *et al.*, 2016; Wernberg *et al.*, 2019; Cavanaugh *et al.*, 2021). Globally, these ecosystems are threatened by rising sea surface temperatures, marine heatwaves, invasive species, increased harvesting and the loss of key trophic species such as sea otters and sunflower sea stars (Smale *et al.*, 2013; Krumhansl *et al.*, 2016; Teagle *et al.*, 2017; Filbee-Dexter & Wernberg, 2018; Wernberg *et al.*, 2019; Cavanaugh *et al.*, 2021). Loss of kelp forest habitats has been documented in multiple regions following recent marine heatwaves, and the loss of key predators has led to overgrazing-induced regime shifts from kelp forests to unproductive urchin barrens (Dean *et al.*, 1984; Estes & Duggins, 1995; Wernberg *et al.*, 2013, p. 201; Filbee-Dexter *et al.*, 2016; Wernberg *et al.*, 2016; Filbee-Dexter & Wernberg, 2018; Burt *et al.*, 2018; Arafeh-Dalmau *et al.*, 2019; Cavanaugh *et al.*, 2019b; Rogers-Bennett & Catton, 2019; McPherson *et al.*, 2021).

Long-term, large-scale, spatio-temporal datasets are needed to monitor and consequently protect these critical coastal ecosystems; however, these datasets are often costly and hard to produce (Cavanaugh *et al.*, 2021). With advances in remote sensing technology over the past half-century, long-term time series of Earth Observation satellite imagery can now be leveraged to track and understand changes in coastal ecosystems (Klemas, 2010). Satellites have been used to map mangrove-salt marsh regime shifts (e.g., Cavanaugh *et al.*, 2019a), assess mangrove resilience to sea level rise (e.g., Duncan *et al.*, 2018), monitor seagrass habitat loss (e.g., Hossain *et al.*, 2015; Nahirnick *et al.*, 2020), measure seagrass blue carbon biomass (e.g. Sani *et al.*, 2019) and understand changes in kelp forest ecosystems in many regions of the globe (e.g. Cavanaugh *et al.*, 2011; Bell *et al.*, 2020; Schroeder *et al.*, 2019a,b; Nijland *et al.*, 2019; Bennion *et al.*, 2019; Beas-Luna *et al.*, 2020; Hamilton *et al.*, 2020; Mora-Soto *et al.*, 2020). Alongside the ability to map ecosystems through time, satellites can be used to capture environmental and

biological drivers, such as sea surface temperature, salinity, surface chlorophyll concentration, and turbidity (e.g., Thomas *et al.*, 2002; Klemas, 2010; Dogliotti *et al.*, 2015; Suchy *et al.*, 2019; Giannini *et al.*, 2021), which can be used in conjunction with time series data to understand how coastal ecosystems are responding to the effects of global climate change (e.g., Thurstan *et al.*, 2015; Bell *et al.*, 2020; Suchy *et al.*, 2019, 2022; Hamilton *et al.*, 2020; Venello *et al.*, 2022).

On Canada's Pacific coast, *Nereocystis* and *Macrocystis* forests support a wide variety of commercially, recreationally, and culturally important species (DFO, 2015; MaPP *et al.*, 2015). Moreover, *Nereocystis* and *Macrocystis* are vital species to coastal First Nations for their use in the cultural production of food, tools, materials, and medicines (Turner, 2001). Although global threats to kelp forests are on the rise (Krumhansl *et al.*, 2016; Wernberg *et al.*, 2019), an understanding of the long-term, large-scale trends in kelp forest change on the Pacific coast of Canada is lacking. The province of British Columbia (BC) has a long coastline, over 25,000 km (Nijland *et al.*, 2019), and not all regions have been mapped. In many areas, kelp mapping has been periodic, with singular time points (Blakley & Chalmers, 1973; Field *et al.*, 1977; Coon *et al.*, 1978, 1979; Field & Clark, 1978; Sutherland, 1990, 1998, 1999; Sutherland *et al.*, 2008). In other regions, local scale studies exist that measure kelp forest distribution through time but show highly variable patterns of change (Sutherland *et al.*, 2008; Watson & Estes, 2011; Burt *et al.*, 2018; Schroeder *et al.*, 2019a; Starko *et al.*, 2019, 2022), highlighting the need for large-scale, long-term datasets. Specifically, for the northern region of BC, including Haida Gwaii, no continuous historical kelp dataset exists. A number of independent surveys of kelp forest have occurred in the Haida Gwaii region of the Pacific Coast of Canada dating back over a century, including nautical chart data from the late 1800s and early 1900s (Costa et al., 2020), some provincial surveys from the 1970s and an aerial shoreline survey in the 1990s (Blakley &

Chalmers, 1973; Coon *et al.*, 1979; Howes *et al.*, 2001). The Council of the Haida Nation (CHN) and the British Columbia (BC) provincial government both emphasize the need for the monitoring and protection of kelp forests, a key ecological feature that provides many economic, cultural and ecological services to the people of Haida Gwaii (Sloan & Bartier, 2000; Haida Marine Traditional Knowledge Study Participants *et al.*, 2011; MaPP *et al.*, 2015), thus requiring procurement and analysis of kelp distribution time series (Cavanaugh *et al.*, 2021). In particular, Haida people have highlighted the importance of the Cumshewa and Flagstaff region on the East coast of Moresby Island as a crucial ecological and cultural area of kelp forest habitat for harvesting, management and monitoring (Haida Marine Traditional Knowledge Study Participants *et al.*, 2011; MaPP *et al.*, 2015)

This study aims to create a long-term time series of kelp forest canopy area to understand the spatial-temporal trends and drivers of change in kelp forest ecosystems in Haida Gwaii, BC, Canada. Specifically, we address the following questions: 1) At what spatial and temporal scales are directional trends in kelp forest canopy area observed? 2) How do both regional and local environmental conditions drive the observed spatio-temporal dynamics? To answer these questions, we used medium- to high-resolution archived satellite imagery (1973-2021) and historical data (1867-1945) to reconstruct kelp forest canopy area through time and examined trends at different temporal and spatial scales. At the temporal scale, we investigated kelp forest trends across the complete satellite time series (1973-2021) and separated into two temporal subsets of the time series: one of the medium-resolution satellite imagery (1973-2004, 30-60 m) and the other of the high-resolution satellite imagery (2005-2021, $\leq$ 20 m). At the spatial scale, we explored changes in kelp forest canopy area at the regional, subregional, and local scales. At the regional scale we defined trends across the entire Cumshewa to Gray Bay study region (800

km^2), whereas at the subregion scale, we evaluated five areas experiencing similar local conditions. At the local scale, kelp forest persistence was investigated on a segment basis. In this study, resilience, in other words recovery and resistance as described by Hodgson *et al.* (2015), refers to areas that show no declining long-term trend through time or, at the local scale, high or variable persistence rates with recovery in the face of climatic perturbations and local stressors. Next, we assess areas of resilience and loss over more than a century by comparing the historical nautical chart data with the satellite time series at the subregional scale. Lastly, we assessed the relationship between kelp forest canopy area and regional indicators of climate to understand the drivers of kelp forest change, and collected *in situ* data, including substrate, dominant understory, seaweed, and urchin presence, to further evaluate the differing patterns observed across the region.

Some of the most extensive kelp forests on the Pacific Coast of Canada occur in Haida Gwaii (Jenkins & Britt, 1972; Sloan & Bartier, 2000; Costa *et al.*, 2020b). As such, the results presented here directly contribute to many regional initiatives considering the spatial management of this key coastal habitat in BC, including the Marine Plan Partnership for the North Pacific Coast (MaPP) – (http://mappocean.org/), the Coastal Environmental Baseline Program – (https://www.dfo-mpo.gc.ca/science/environmental-environnement/cebp-pdecr/index-eng.html), Marine Protected Area Network process in Northern Shelf Bioregion – (http://mpanetwork.ca/bcnorthernshelf/), thus leveraging the future protection and management of kelp forests not only in this region but across the Pacific coast of Canada. Moreover, as the longest and most temporally continuous study of canopy-forming kelp forest area dynamics in Canada, this study fills a gap documented in the global distribution of threats to kelp forests and

contributes to the understanding of what drives the variable responses kelp forests have to climate change globally (Krumhansl *et al.*, 2016; Wernberg *et al.*, 2019).

3.3. Materials & Methods

3.3.1 Study System

Haida Gwaii is a large archipelago located off Canada's mainland Pacific coast (**Figure 13**). Haida Gwaii is the unceded territory of the Haida Nation, whose relationship to the land and sea has existed since time immemorial and continues to this day (Guujaaw, 2002; MaPP *et al.*, 2015). This region is characterized by a cool, nutrient-rich, temperate marine environment supporting extensive kelp forests (Blakley & Chalmers, 1973; Coon *et al.*, 1979; Peterson *et al.*, 2007; Haida Marine Traditional Knowledge Study Participants *et al.*, 2011). Following an ecosystems-based management approach, the coordinated and cooperative management of the marine environment surrounding Haida Gwaii is undertaken by the CHN, the BC and the Canadian governments (MaPP *et al.*, 2015). The Haida Gwaii Marine Plan, approved in 2015 following the 2007 Strategic Land Use Agreement between the CHN and the provincial government, provides a detailed framework for the joint management and protection of the marine and coastal ecosystems of Haida Gwaii. This framework highlights kelp forests as an essential part of the ecosystem needed to sustain and support healthy Haida Gwaii communities (MaPP *et al.*, 2015).

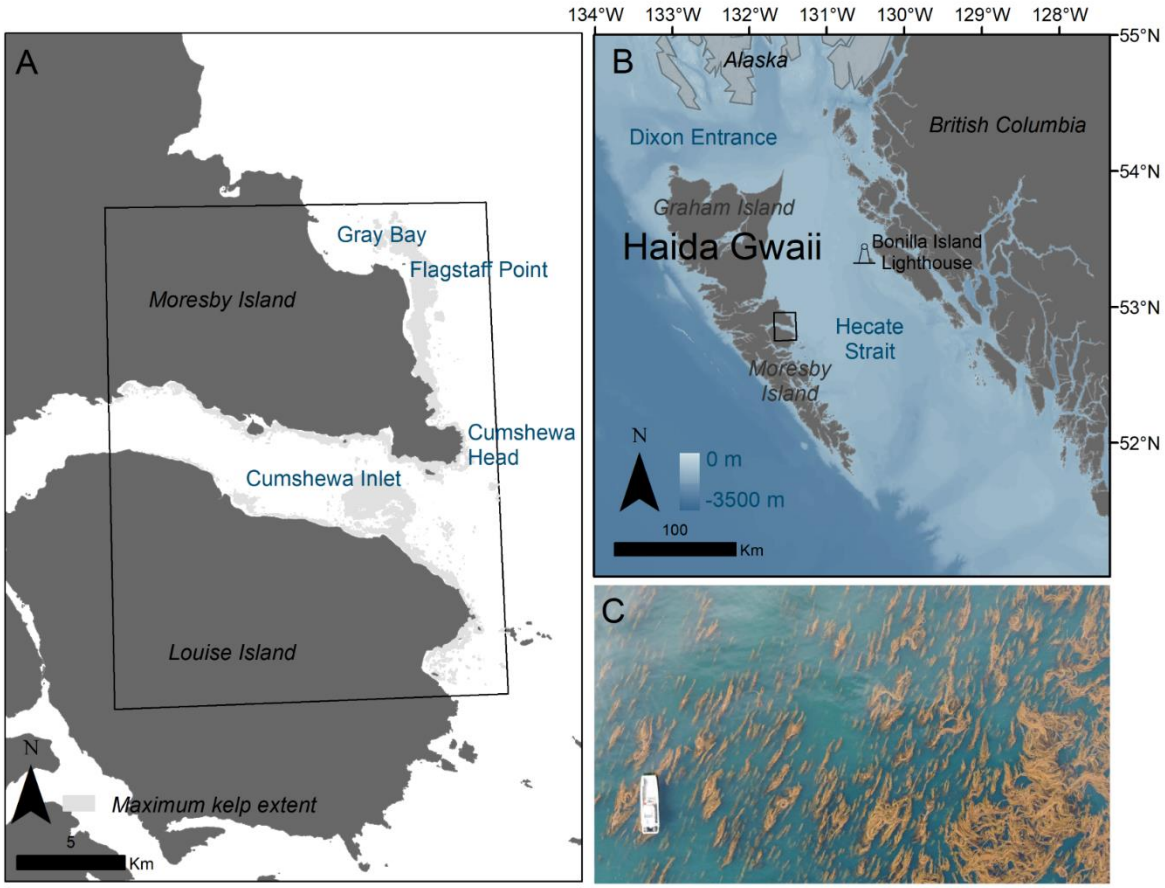

Figure 13. Overview of study region, A) Haida Gwaii kelp forest time series study region (outlined in black solid line) with maximum kelp forest canopy area across the complete time series (1973-2021) in gray. B) shows an overview map of Haida Gwaii archipelago in relations to the mainland coast of British Columbia and Alaska showing bathymetry in meters (m) below chart datum and the location of the Bonilla Island Lighthouse used to calculate SST anomalies and C) showing an example of the size and density of giant kelp forests found within the study region in relation to 32-foot research vessel.

As part of the Haida Gwaii archipelago, the study region spans roughly 800 km^2 on the Northeast Coast of Moresby Island, covering Gray Bay in the North and Cumshewa Inlet in the West (**Figure 13**). Hecate Strait, a shallow soft sediment shelf, exists to the east of the study region, separating Haida Gwaii from the mainland coast. Haida people describe this region as an important area for the harvest of *Macrocystis*, specifically for the spawn on kelp herring roe fishery (in Haida: k'aaw), however, notable declines of *Macrocystis* canopy were documented by Haida harvesting in the region (Haida Marine Traditional Knowledge Study Participants *et al.*, 2011). Moreover, these extensive kelp forest ecosystems support an abundance of valuable species, such as herring (*Clupea pallasii*), salmon (*Oncorhynchus spp.)*, halibut (*Hippoglossus*

stenolepis), rockfish (*Sebastes spp.)* and a variety of shellfish (Blakley & Chalmers, 1973; Haegele & Hamey, 1981; Haggan *et al.*, 2007; Haida Marine Traditional Knowledge Study Participants *et al.*, 2011). The kelp forests within the study region are generally dominated by large dense *Macrocystis* forests (**Figure 13C**); however, patches of *Nereocystis* forests are found to a lesser extent throughout the region, particularly concentrated around Cumshewa Head.

3.2.2 Data compilation

We created a time series of kelp aerial canopy extent by compiling archived medium- to high-resolution multispectral satellite imagery from 1973 to 2021 and historic kelp data from British Admiralty nautical charts from the late 1800s to early 1900s (Costa *et al.*, 2020b). We compiled key environmental drivers available and known to influence kelp abundance at the regional and local scale including fetch, wind, tidal currents, local SST, regional SST anomalies, the Pacific Decadal Oscillation (PDO), the El Nino Southern Oscillation (ENSO), the North Pacific Gyre oscillation (NPDO), and *in situ* observations in the summer of 2021 of substrate type, understory seaweed community and sea urchin presence.

Kelp forest canopy time series

Satellite-derived kelp time series (1973-2021) – We used the methodological framework presented in Chapter 2 (see Figure 2, Chapter 2) to compile a time series of kelp forest canopy aerial extent across approximately 50 years. The methodology framework consisted of three main components, which are briefly described below: 1) imagery compilation and assessment, 2) imagery preprocessing and 3) classification and validation.

An archived dataset of high to medium resolution (0.5 m – 60 m) multispectral satellite imagery (1973 to 2021) from a total of 20 different satellites was compiled through various

sources (**Table 7**). The quality of the dataset was defined based on a quality control approach considering important criteria, including clouds, tide, haze, waves, glint, and the month of imagery acquisition (Schroeder *et al.*, 2019b; Cavanaugh *et al.*, 2021). From this analysis, images showing suboptimal conditions for kelp detection were removed from the dataset. Only one or two images were collected per year, acquired during peak biomass (between July and early October), to create the time series due to the lack of available high-quality historical archived satellite data for this region. A total of 52 images were selected, spanning 36 years from 1973 to 2021 (**Table 7**), predominantly from July and August. Although we acquired some images from later in the growing season, no apparent trend in kelp forest area was associated with acquisition timing. An analysis of the impact of resolution described in Chapter 2 (see section 2.4.4) demonstrated that small fringing kelp forests found in high slope areas were difficult to detect, which led to uncertainties when mapping kelp forest canopy area from a variety of different resolution satellite imagery. Because of these uncertainties, we removed high slope areas (>11.4 %) that support a very small proportion (0.01%) of the overall kelp forest canopy area of the region from the analysis. Two high slope areas remained in the dataset because they fell within a few decimal points of areas considered high slope and including them allowed for more spatial continuity of the data.

Following imagery assessment, we performed geometric correction of the imagery using 1st order polynomial shifts and applied the Rayleigh correction method to atmospherically correct images (Chavez, 1988), where necessary. Next, areas of deep water (> 20m) using the Canadian Hydrographic Bathymetry dataset (Davies et al., 2019), areas of land derived from the lowest tide high-resolution satellite imagery and areas of soft substrate from both the BC Marine Conservation Analysis benthic dataset (Ferdaña, 2006) and the DFO bottom patch model (Gregr

et al., 2013) were masked. Band indices/ratios were then created and linearly enhanced in conjunction with the original bands of the imagery for input into the classification. **Table 7** shows the optimal band indices and/or ratios defined for each image used to enhance the separability between kelp and other classes. Generally, NDVI was used for imagery analysis of Sentinel-2, Landsat, and SPOT satellites as it has been broadly used by the research community for these satellites (Augenstein *et al.*, 1991; Cavanaugh *et al.*, 2010, 2011a, 2013; Reed *et al.*, 2011; Casal *et al.*, 2011; Bell *et al.*, 2015; Nijland *et al.*, 2019; Mora-Soto *et al.*, 2020; **Table 7**). For the other images acquired by RapidEye, PlanetScope, Quickbird-2, GeoEye-1, Worldview-2 satellites, the m-statistic coupled with a visual assessment of the top band indices/ratios and bands were used to select the inputs for the classification step (**Table 7**).

The enhanced indices/ratios and bands imagery were used as inputs (**Table 7**) for a supervised nearest neighbor object-based classification (Trimble eCognition Developer Software V8.64), in which results were validated according to available field and historical data. Considering all sensors included in the validation, the overall global accuracy ranged between 88 to 94 %, with errors primarily associated with sparse, fringing and/or partially submerged kelp forests (Section 2.4.3, Chapter 2). These accuracy scores are in the high range of accuracies documented in the literature, e.g. 83 - 91 % (Schroeder *et al.*, 2019b), 70 – 90 % (Hamilton *et al.*, 2020a), and 59 - 83 % (Nijland *et al.*, 2019) demonstrating good performance by the object-based classification.

Table 7. Summary of medium- to high resolution archived satellite imagery used to build the time series of kelp canopy area where ms resolution refers to the multispectral spatial resolution of imagery, inputs refer to inputs used in object-based image classification and global accuracy refers to the measure of global accuracy attained in the validation of the classification.

SENSOR	MS Resolution	Years	Inputs	Source	Global Accuracy
LANDSAT 1-3	60 m resampled from 80 m	1973-74 1976-77	NDVI Green Red NIR	Freely Available from United States Geological Survey (USGS)	-
LANDSAT 4-5	30 m	1982 1984-86 1988-92			89 %
LANDSAT 7		2001-02			
SPOT 2-4	20 m	2006 2008 2011	NDVI Green Red NIR	Available to researchers through the Centre national d'études spatiales (CNES)	-
SPOT 5-7	10 m	2005-06 2009 2016		SPOT 7 imagery was purchase from Apollo Imaging Corp.	93 %
GEOEYE-1	1.84 m	2017	GNDVI Green Red NIR	Private data sharing agreement	89 %
QUICKBIRD-2	2.62 m	2008 2013	GNDVI Green Red NIR	Private data sharing agreement	92 %
WORLDVIEW-2	1.84 m	2013	RE/Yellow Green Red NIR	Private data sharing agreement	91 %
RAPIDEYE	5 m	2010-12 2014-15	RE/G Green Red RedEdge NIR	Available to researchers through Planet Labs Inc	88 %
PLANETSCOPE	3.7 m	2017-2021	NIR/G Green Red NIR	Available to researchers through Planet Labs Inc	94 %
AERIAL IMAGERY	0.5 m	2007	Red/Green Green Blue	Private data sharing agreement	88 %

Historic kelp forest data - A snapshot of the distribution of kelp forests across BC was digitized from British admiralty charts mapped between 1867-1945 (Costa *et al.*, 2020). These charts mapped areas where kelp forests posed navigational risks to mariners. Consequentially, these data should only be used to denote kelp presence and not be used to represent the absence of kelp forests (Costa *et al.*, 2020b). We performed a qualitative visual comparison between the

historical data and the satellite imagery time series to highlight areas showing kelp resilience and loss across a century.

Environmental driver data

Temporal driver data- Trends in kelp abundance and productivity have been linked to regional climate indicators, including the Pacific Decadal Oscillation (PDO), the El Niño Southern Oscillation (ENSO), the North Pacific Gyre Oscillation (NPGO) and regional SST anomalies (Dayton *et al.*, 1999; Cavanaugh *et al.*, 2011a; Pfister *et al.*, 2018; Schroeder *et al.*, 2019a; Hamilton *et al.*, 2020a; Bell *et al.*, 2020). These climate oscillations can be grouped into two categories based on time scale: high frequency (i.e., ENSO) and low frequency (i.e., the PDO and NPGO). The PDO is a long-term pattern related to the Aleutian low-pressure system over the mid-latitude North Pacific basin, where positive PDOs are characterized by warmer sea surface temperatures and lower primary productivity (Di Lorenzo *et al.*, 2008). The NPGO is another long-term climatic pattern explained by changes in the north-south dipole pattern of sea level pressure driven by the North Pacific Oscillation; in contrast to PDO and ENSO, a negative NPGO indicates warmer temperatures and lower productivity (Di Lorenzo *et al.*, 2008; Franks *et al.*, 2013). Waters of the North Pacific are also influenced by the ENSO, a high-frequency climate oscillation that explains inter-annual variability in conditions controlled by the Southern Oscillation in the western tropical Pacific (Philander, 1983; Zebiak & Cane, 1987). During a strong El Niño year (positive ENSO), warm equatorial waters are transported northwards along the coast of North America, causing low nutrient availability, low phytoplankton productivity and warm SSTs (Philander, 1983; Zebiak & Cane, 1987). Monthly values were obtained and

used to calculate yearly averages of the PDO index[1], the ENSO index[2], and the NPGO index[3]. In addition to climate indices, regional SST anomalies were calculated using *in situ* SST[4] measures from the Bonilla Island lighthouse station (53°29'34.5" N; 130°38'17.0" W, **Figure 13**), the closest long term lighthouse record to the study region. SST anomalies were calculated using a 55-year historical average starting in 1966 and used to represent the regional SST trends in this study. Since the majority of kelp in the region is *Macrocystis*, a perennial species, annual averages were used for all regional indicators of climate. Yearly averages were calculated as the conditions experienced between August of the previous year and July of the acquisition year because most imagers were acquired in July.

Local environmental driver data - The local scale drivers we considered in this study include climatologies of fetch, local SST, wind, and tidal current. Local SST was derived from the thermal infrared band of Landsat satellite imagery (Thomas *et al.*, 2002). All available cloud-free Landsat images covering the entire study region between July and August were selected (1988, 1989, 2007, 2009-11, 2014, 2015, 2017) to create the average of local summer SSTs experienced across the region. To minimize land adjacency impacts, we removed land and water within a 90 meters buffer adjacent to the shoreline for the retrieval of local SST (Wachmann *et al.*, in prep). Fetch[5] was used to represent the gradient of exposure experienced by kelp forests across the study area (Gregr, 2014). In this case, fetch was estimated every 50 m along the coastline and specifically refers to the sum of fetch, which is calculated by summing the distance

1 https://www.ncei.noaa.gov/pub/data/cmb/ersst/v5/index/ersst.v5.pdo.dat
2 https://origin.cpc.ncep.noaa.gov/products/analysis_monitoring/ensostuff/ONI_v5.php
3 http://www.o3d.org/npgo/npgo.php
4 https://open.canada.ca/data/en/dataset/719955f2-bf8e-44f7-bc26-6bd623e82884)
5 https://open.canada.ca/data/en/dataset/412431c4-7363-410e-86a4-76feb9a6dcde

in meters (m) to the nearest land mass at every 5-degree bearing around a point on the shoreline. Fetch was propagated out from the coastline to the 20 m deep water bathymetry line using the Euclidean allocation tool in ArcMap (ArcGIS Desktop Version 10.7.1) to produce a raster of fetch. Mean wind power density (W/m^2) raster (250 m) at 10 m above sea level from the Global Wind Atlas[6] was used to represent local wind conditions, and root mean square average tidal speed (RMS m/s) was obtained from the BC Marine Conservation Analysis (BCMCA) Marine Atlas of Pacific Canada[7] tidal model.

In situ data collection- In addition to validation data for the imagery classification, we collected *in situ* field data, in the form of photo quadrats (1 m^2) and remotely operated vehicle (ROV) footage, in August of 2021 from areas of no kelp, kelp loss, and kelp persistence, as documented in the satellite time series and quantified urchin presence, dominant substrate types, and understory seaweed types present. Substrate type was categorized into 5 classes: sand (0.06-2 mm grain size diameter), granule (2-4 mm), pebble (4-64 mm), cobble (64-256 mm), and boulder (0.25-3 m) based on Greene *et al.* (1999) benthic habitat classification scheme. The seaweed understory was categorized by grouping seaweeds into 3 dominant functional groups present in the study area: turf (any dense short benthic algae), branched (branching algae, i.e., *Desmerestia sp*.), and kelp understory (large brown algae in the order Laminariales). Exploratory video transects using the QYSEA Fifish V6 ROV were used to further explore areas of kelp persistence and loss. For each transect, urchin presence, dominant substrate, and dominant understory type were noted. Due to the small sample size, photo quadrat (n= 44) and ROV (n=4) data for

6 https://globalwindatlas.info/
7 https://bcmca.ca/datafiles/individualfiles/bcmca_eco_physical_hightidalcurrent_atlas.pdf

substrate and understory were grouped and presented together (n=48). *In situ* data collection was used to further support and substantiate the analysis on the drivers of kelp canopy change.

3.2.3 Data analysis

Spatial and temporal scales of analysis

The satellite time series was analyzed at different spatial and temporal scales to understand the spatio-temporal trends in kelp forest across the study region. Specifically, we examined the dataset across (i) the entire satellite time period (1973-2021; a total of 36 out of 48 years due to the availability of good quality data), and (ii) separated into two categories based on the spatial resolution of the imagery: the medium-resolution time series (30-60 m resolution from 1973-2003), and the high-resolution time series (≤ 20 m resolution from 2003-2021). The full time series aimed to capture the long-term trends. The contrast between the two time periods considered uncertainties when comparing across different spatial resolutions.

The spatial component of the analysis considered regional (across the entire study system), subregional (groups of segments experiencing similar environmental conditions) and local (segment) scales. The local scale was set to pre-defined aerial units, called segments. A segment-based approach is often used in kelp remote sensing to minimize errors caused by using data from different sensors and different environmental conditions, including currents, tides, waves, glint, and kelp seasonality (Pfister et al., 2018; Schroeder et al., 2019a; Berry et al., 2021) and can be used to analyze areas with similar conditions. To create the segments, the study region was subdivided into roughly uniform-sized sections to allow for analyses at finer spatial scales. Due to the complex bathymetry of our study system, a methodology for creating segments was adapted from Berry *et al.* (2003). This approach creates segments in two categories based on ocean floor slope calculated as percent rise using the 20-meter bathymetry data from the

Canadian Hydrographic Service (Davies et al., 2019). 'Shoreline segments' (high slope > 3 %), characterized by nearshore kelp beds, were created along 1 km lengths of the shoreline extending to the 20 m bathymetry line. 'Flat segments' (low slope ≤ 3 %), characterized by extensively large kelp beds that extend kilometers offshore, were broken into 1 km segments from the outside boarder of the lower slope areas moving inwards, so that every flat segment was similar in area to an average fringing shoreline segment (segment mean size: shoreline 0.38 +/- 0.19 km^2, flat 0.27 +/- 0.08 km^2). At the local scale, the 1-km segments were used to quantify and visualize the persistence of kelp through time. The kelp persistence metric was measured as a percent of the number of years kelp was present in a given segment compared to the total number of years (n= 36). A kelp persistence metric of 100 % indicates kelp presence in all years included in the satellite time series. Mid persistence metric denotes high variability but accompanied with no directional trend through time represent resilience. Low persistence metrics coupled with declining trends indicate reduced temporal resilience within a given segment.

At the subregion scale, segments were clustered based on shared properties. First, local drivers, including fetch, local SST, wind, and tidal current were averaged per segment. Then, using spearman rank-order correlations, correlated drivers were removed from the clustering analysis to avoid statistical redundancies in the local driver data and overweighing of highly correlated variables (Ketchen & Shook, 1996). Local fetch, wind, and tidal current were highly correlated (fetch and wind $r=0.78$, fetch and tidal current $r=0.86$, wind and tidal current $r=0.80$, $df=237$, $p < 0.001$); only fetch and SST were used in the cluster analysis. Next, a spatially constrained cluster analysis (k nearest neighbors = 4) was performed in ArcMap using the grouping analysis tool. A pseudo-F-statistic, a ratio of between-cluster and within-cluster variation (Milligan and Cooper, 1985), was used to calculate the optimal number of subregions

present in the study system. At the regional scale, we determined the bounds of the study region first based on the proposed marine protected area outlined by MaPP in the Haida Gwaii Marine Plan (2015) for the Cumshewa to Gray Bay region. However, we further needed to constrict the region based on the spatial bounds of the available archived satellite imagery in order to maximize the temporal coverage of the time series.

Statistical analysis of regional drivers at the regional and subregional spatial scales

For all temporal scales (e.g., complete time series: 1973-2021; medium-resolution time series: 1973-2004; and high-resolution time series: 2005-2021), the yearly aerial kelp canopy area was normalized as a percent of the maximum total kelp area occupied across the complete satellite time series. Using linear regressions, we evaluated time series trends and the relationship of normalized kelp area and regional drivers, including SST anomalies, PDO, NPGO and ENSO indices at both the regional and subregional scales. To evaluate the effect of previous years conditions on kelp forest canopy area, we examined two- and three-year averages of regional drivers. Additionally, Spearman rank-order correlations were conducted to understand the correlation between environmental drivers. For all the analysis, the residuals of models were tested for normality using 'residual vs fitted' plots and qqplots (Faraway, 2004). Model selection using the Akaike Information Criteria adjusted for a small sample size (AICc) (Hurvich & Tsai, 1993) was used to define the linear model that best described the relationship between kelp forest area and regional drivers of change. More specifically, we first tested for univariate relationships between each regional driver and kelp forest area. Then, created multivariate models of all significant drivers to assess which overall model performed best. For the historic data, we performed a qualitative analysis, due to the nature of the data, by comparing the snapshot of historical kelp distribution to the subregional and local distribution of kelp forest canopy area

derived from the satellite time series. We then summarized the *in situ* data using stacked bar charts to show the proportion of substrate type and understory type present in different areas of change throughout the study region. All statistical analyses and plots were produced in R Studio Version 1.2.5042.

3.4 Results

3.4.1 Temporal trends in kelp forest area

Regional dynamics

Yearly normalized kelp forest area varied considerably through time (**Figure 14A**, 41.71 ± 20.97 %); however, an overall declining long-term trend of 0.47 % per year occurred across the complete time series (1973-2021, $p<0.05$, $R^2=0.11$, df=1,34, **Table 8**). We observed the maximum kelp forest area (8.18 km^2) in the initial year of the time series in 1973, followed by a large decline in the area at the end of the 70s, resulting in a mean total kelp area of 3.17 ± 1.44 km^2 between 1977 and 2021 (3.03 ± 1.16 km^2 for high-resolution time series 2005-2021). The lowest kelp forest area (0.43 km^2) occurred in 1998, corresponding to 5 % of the maximum kelp forest area. Other notable years of low kelp canopy area were detected in 1977 (2.03 km^2, 25 %), 1982 (1.73 km^2, 21 %), 1986 (1.89 km^2, 23 %), 1991 (2.08 km^2, 25 %), 1992 (1.84 km^2, 23 %), 2007 (1.30 km^2, 16 %), 2015 (1.06 km^2, 13 %) and 2016 (1.38 km^2, 17%).

Time series length affected the direction and magnitude of trends (**Table 8**). The medium resolution time series (1973-2004) showed a declining trend of 1.62 % per year (linear model, $p<0.05$, $R^2=0.17$, df=1,17), approximately 1.2 % higher than declines observed across the full satellite time series. In

Table 8. Linear regression of normalized kelp area by time to show long-term trends. All significant relationships are bolded (p value < 0.1 *, <0.01**, <0.001***)

TOTAL AREA	COEFFICIENT	R^2
YEAR (1973-2021)	**-0.4703***	0.1058
YEAR MED-RES (1973-2004)	**-1.2516***	0.1735
YEAR HIGH RES (2005-2021)	0.3647	0.0158

comparison, no significant trend was detected for the more recent short-term time series from 2005-2021 ($p>0.05$, $df=1,15$, **Table 8**). However, inter-annual variability exists in both time series regardless of trend and period of analysis.

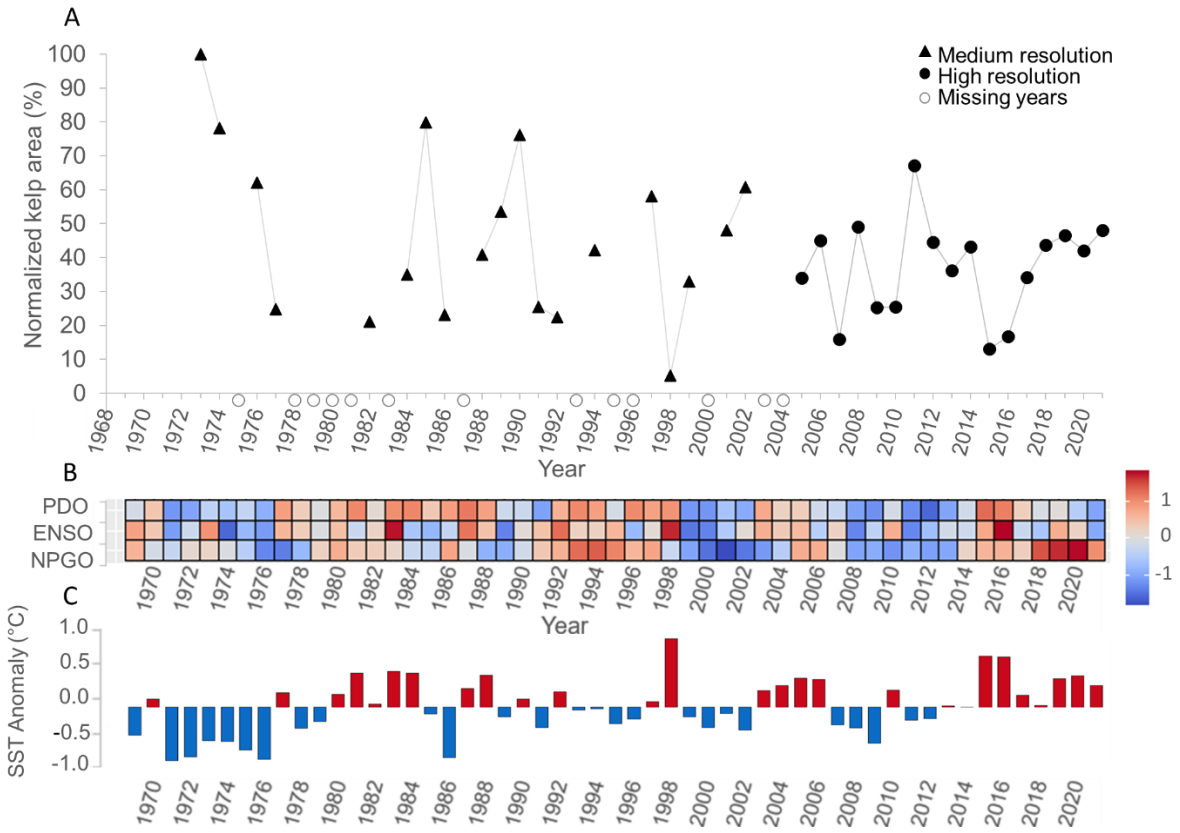

Figure 15. A) The time series of normalized kelp forest canopy area from 1973 to 2021. B) Z-scores of climate indices where PDO represent the Pacific Decadal Oscillation, ENSO represents the El Nino Southern Oscillation and NPGO represents the North Pacific Gyre Oscillation (inverted scale) so that positive values represent warm conditions (red) and negative values (blue) represent cool conditions C) SST anomalies calculated using a 55-year historical average starting in 1966 where bars represent either positive or negative anomalies in degrees Celsius above or below the time series average..

Subregional dynamics

The region shows strong gradients in SST, fetch, wind, and tidal current. In the summer months of July and August, the shallow waters of Gray Bay can often experience water temperatures above 20 °C, while the mouth of the inlet remains cooler (e.g., ~14 °C, **Figure 15A**). In addition to this strong SST gradient, a gradient in fetch, wind and tidal current exists (**Table 9**). The Eastern edge is more exposed to the turbulent waters of Hecate Strait, with high fetch, wind, and tidal currents. The region clustered into 5 subregions based on local SST and

fetch (**Figure 15A**, pseudo-f-statistic: 4 groups = 272.92, 5 groups = 303.61, 6 groups = 279.9233, **Table S1**). Gray Bay (1) experiences the warmest SST and moderate fetch, Flagstaff (2) experiences warm SST and moderate fetch, Cumshewa East (3) experiences the coolest SSTs and highest fetch, Cumshewa West (4) experiences cool SST and low fetch, and Mathers Creek (5) experiences warm SSTs and lowest fetch (**Figure 15A, Table 9**). The kelp forest areas within subregions (**Figure 15B-F**), showed two major patterns: Gray Bay (1) and Flagstaff (2), the warmer subregions, show a clear pattern of loss, whereas Cumshewa East (3), Cumshewa West (4) and Mathers Creek (5) subregions show resilience with high variability, but no declining trends through time.

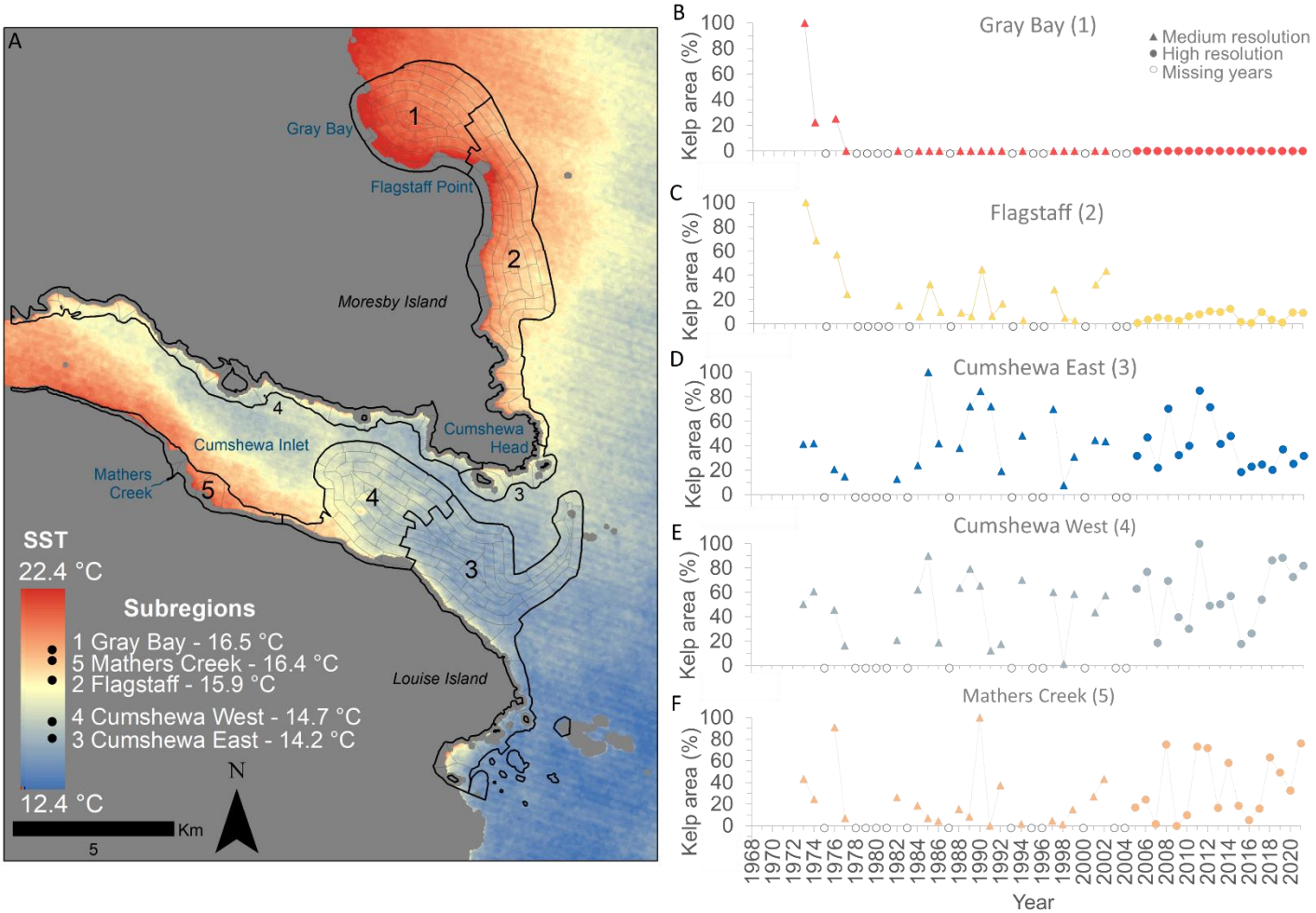

Figure 16. A) Map of subregions derived from the cluster analysis showing the local SST climatology across the region and average temperature experienced in each subregion. B-F) Time series of normalized kelp forest canopy area from 1973 to 2021 for each subregion.

Table 9. Local conditions (mean and standard deviation) experienced in each subregion

SUBREGIONS	Local drivers
GRAY BAY (1)	SST: 16.5 ± 0.4 °C Fetch: 2752474.5 ± 544912.5 m
FLAGSTAFF (2)	SST: 15. 9 ± 0.4 °C Fetch: 4133897.8 ± 740393.9 m
CUMSHEWA EAST (3)	SST: 14.2 ± 0.3 °C Fetch: 2560331.3 ±594121.1 m
CUMSHEWA WEST (4)	SST: 14.7 ± 5 °C 823628.5 ± 395366.7 m
MATHERS CREEK (5)	SST: 16.4 ± 0.4 °C Fetch: 552187.9 ± 206471.4 m

Gray Bay (1) and Flagstaff (2), both located in the Northern portion of the region (**Figure 15A-C**), supported roughly 80% of the total kelp forest area documented in 1973 (6.78 km^2 of 8.18 km^2). Similar to the regional trend, a large decline in kelp forest area occurred in the late 1970s. Specifically in Gray Bay, all of the kelp forest canopy disappeared by 1977 and did not return for the remainder of the timeseries (**Figure 15A**). On the other hand, the Flagstaff subregion followed a very similar pattern of loss to that of Gray Bay but retained some kelp forest area after 1977, despite some years with near-zero canopy coverage (**Figure 15C**). For the Flagstaff subregion, the complete satellite time series (1973-2021) showed a trend of 0.94 % decline per year ($p<0.001$, $R^2=0.34$, df=1,34, **Table 10**) and the medium resolution time series (1973-2004) showed a long-term trend of 1.94 % decline per year ($p<0.01$, $R^2=0.38$, df=1,17, **Table 10**) but no direction significant trend was detected in the high-resolution time series ($p>0.05$, df=1,15, **Table 10**). This trend was driven by an approximate loss of 4.62 km^2 of kelp forest canopy area by 2005, with only a total mean kelp forest canopy area of 0.29 ± 0.59 km^2 (6

± 14 % of the 1973 maximum, **Table 10**) remaining in the short-term time series (2005-2021; **Table 10**).

As opposed to Gray Bay and Flagstaff, the southern subregions showed resilience through time. Although kelp forest canopy area varied considerably in these subregions, no significant positive or negative long-term trends were detected in Cumshewa East (3), Cumshewa West (4) and Mathers Creek (5) subregions (**Figure 15A, D-F, Table 10**). These subregions showed considerable variation in kelp forest area but on average, supported approximately 30 to 52% of their subregion's maximum kelp forest area through time (**Figure 15D-F; Table 10**). Of the three subregions, Cumshewa West (4) supported the largest proportion of kelp area at 3.34 km^2 in 1985. In comparison, Cumshewa East (3) reached a kelp area maximum of 1.87 km^2 in 2011. Although the maximum kelp forest area occurred in different years, both Cumshewa subregions followed a similar pattern of variability through time until 2016, when relatively low kelp forest canopy area was observed (**Figure 15D-E**). Cumshewa West (4) kelp area rebounded quickly to roughly 80 % of the subregion's historic maximum by 2018. However, in Cumshewa East (3) the kelp area remained at approximately 25 % of the subregion's historic maximum. Mathers Creek (5), the smallest of the subregions, supported the smallest proportion of the kelp forest canopy area overall with a maximum of 0.21 km^2 in 1990 (**Figure 15D, Table 10**). Although this subregion showed resilience throughout the time series, the patterns differed from Cumshewa East and West. Overall, Mather's Creek (5) subregion showed more years with low kelp forest canopy area for the medium-resolution time series compared to Cumshewa East and West. However, similarly to Cumshewa West (4), following relatively low years of kelp forest canopy area during 2015/2016, the Mather's Creek (5) subregion did recover to 63% of the subregion's historic maximum by 2018.

Table 10. Maximum total kelp forest canopy area, and trends of each subregion. All significant relationships are bolded (p value < 0.1 *, <0.01**, <0.001***)

SR	Max kelp area	Time series	Norm kelp area (mean ± sd %)	Coeff	R^2
2	4.91 km^2	**Complete**	16 ± 22	**-0.9362 *****	**0.3971**
		Medium	26 ± 27	**-1.936****	**0.3815**
		High	6 ± 14	0.2015	0.0676
3	1.87 km^2	**Complete**	42 ± 23	-0.1334	0.0050
		Medium	44 ± 27	0.4874	0.0240
		High	39 ± 20	-1.3482	0.1138
4	3.34 km^2	**Complete**	52 ± 26	0.3961	0.0492
		Medium	46 ± 26	-0.1058	0.0012
		High	58 ± 25	1.259	0.0594
5	0.21 km^2	**Complete**	30 ± 29	0.2742	0.0190
		Medium	24 ± 29	-1.0075	0.0870
		High	36 ± 29	1.681	0.0841

Local dynamics

At the local scale (i.e., segments within each subregion), the local patterns in the North (**Figure 16A**) reflected the documented subregional disappearance of kelp in the Gray Bay and Flagstaff subregions. At this finer spatial scale, areas where kelp was never found are also documented, as well as finer-grained information on where kelp has disappeared and where its persisted. Within Gray Bay, shallow nearshore segments (depth ~2-5 m), never supported kelp forest canopy (persistence = 0%). The complete disappearance of kelp forests was concentrated in segments further offshore and around Flagstaff point. Just south, in the Flagstaff subregion, kelp forests were much more variable (persistence = 1-34 %) and strongly persistent (25-34 %) further South. For the remainder of the region, high kelp forest persistence occurred in the nearshore segments of Cumshewa East (3), West (4) and Mathers Creek (5). In the offshore areas of Cumshewa East (3) and West (4), a core kelp forest persists through much of the time series

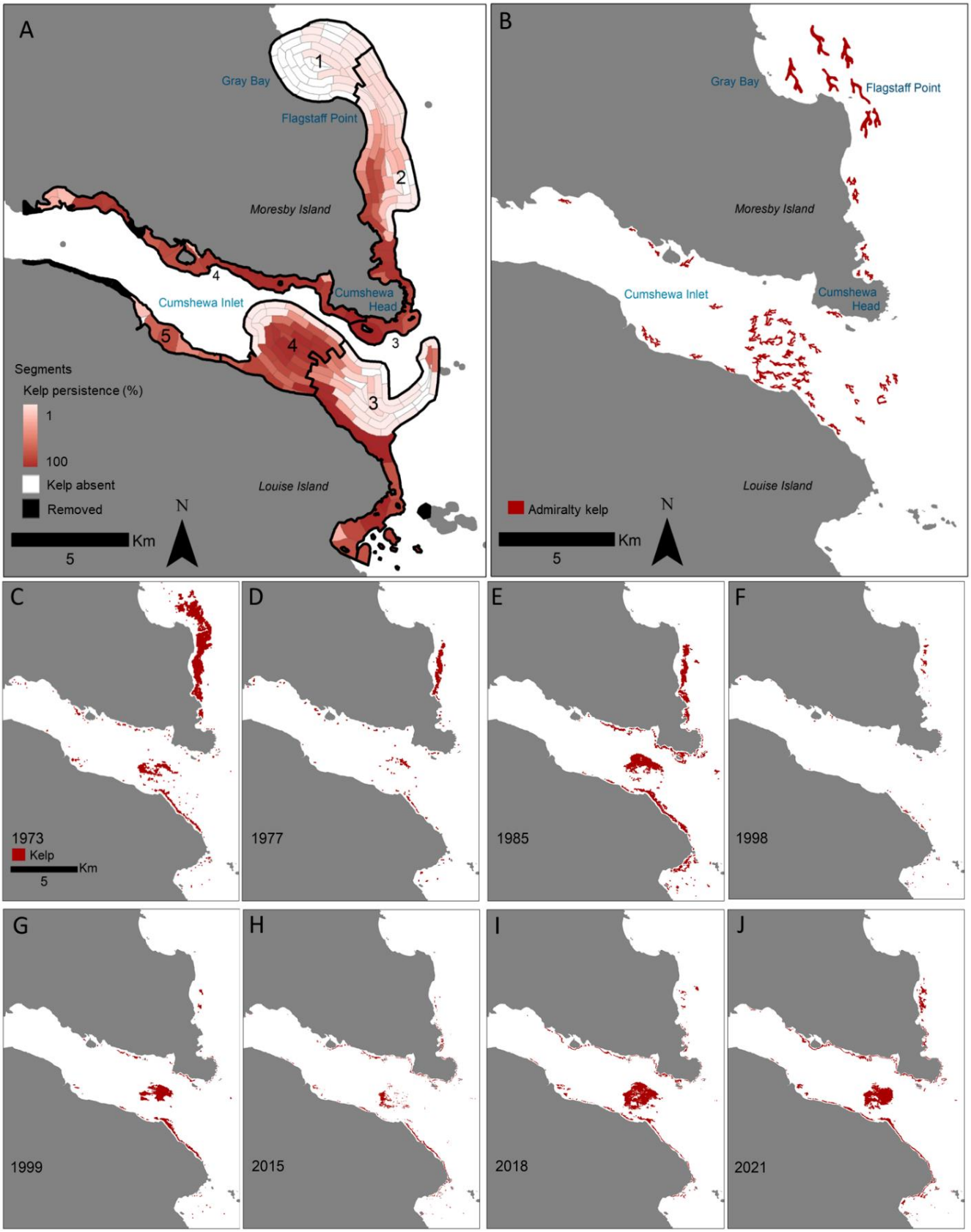

Figure 18. A) Map of local persistence metric on a 1 km segment basis. B) Map of historic distribution of kelp forest derived from British Nautical charts. C-J) Maps of kelp forests from notable years across the time series.

located in the mid-channel area known as Fairbairn shoals. The majority of the core area of the Fairbairn shoals' kelp forest resides in Cumshewa West (4), but often expands into the offshore areas of Cumshewa East (3) in years with high kelp forest canopy area (e.g., **Figure 16C, E, I & J**). However, near the outer coast of Cumshewa East (3) kelp is less persistent, most likely because of the high fetch and deeper depths near the mouth of the inlet. A small cluster of high persistence segments also occurs in Cumshewa East (3) around a small group of islands known as Cumshewa Rocks.

Historic Persistence and Loss

The snapshot of kelp forest presence from historical British Admiralty nautical charts (1867-1945) showed extensive areas of kelp forests with a similar distribution to that documented in 1973 (**Figure 16B & C**). These historical data confirmed the presence of kelp forests in all subregions indicative that kelp forests existed across the entire gradient of conditions in the region over 100 years ago. In particular, a large area of kelp forest canopy was mapped around Gray Bay and Flagstaff Point, indicating that the kelp that disappeared in the 1970s had likely persisted for over a century before disappearing. In contrast, the historical distribution of kelp in Cumshewa Inlet persists similarly to this day (**Figure 16A & B**).

3.4.1 Environmental drivers

Regional Climate Drivers at Regional Scale

The overall temporal pattern of the different regional climate indicators showed that years of positive SST anomalies coincided with warm climate forcing years in the PDO, ENSO and NPGO index (**Table 11**), such as 1977, 1980-84, 1987-88, 1997, 2002-2006, and 2014-2016 and that negative SST anomalies coincide with cooler climate forcing years in the climate indices, such as 1971-1976, 1989, 1999-2002, 2007-2009, 2011-2012 (**Figure 14B & C**). All regional

indicators of climate were highly correlated (**Table 11**) with the expected relationships for this region, in which NPGO is inversely correlated with ENSO, PDO and SST anomalies. Notably, SST anomalies show a warming trend of approximately 0.13 ° C every ten years, culminating in a total increase of 0.62 °C across the time series (**Table 12**).

Table 12. Pearson's correlation coefficient of regional environmental drivers (p value < 0.1 *, <0.01**, <0.001***).

CLIMATE INDICATOR	PDO	ENSO	NPGO	SST
PDO	-			
ENSO	0.59***	-		
NPGO	-0.36*	-0.34.	-	
SST	0.56***	0.56***	-042**	-

Table 13. Linear regression of regional climate indicator through time showing long-term trends (p value < 0.1 *, <0.01**, <0.001***).

CLIMATE INDICATOR	COEFF	R^2
PDO	-0.01154	0.0366
ENSO	0.0035	0.0048
NPGO	**-0.02213***	0.0864
SST	**0.013****	0.1841

Across the complete time series, kelp forest canopy area decreased as SST increased, and years of low kelp forest canopy area coincided with warm conditions represented by positive ENSO and PDO indices (Table 7). In particular, univariate models were ran separately for all predictor variables at the 1-, 2- and 3-year averages for each time series and multivariate models of significant predictors were created to understand what best explained the variation in kelp forest canopy area. Linear models of regional indicators explain anywhere between 15 – 50 % of the variance in kelp forest canopy area across the time series (**Table 13**). Specifically, for the complete time series (1973-2021), the best-fit model included both the 1-year averages of the ENSO and the 2-year averages of SST anomalies, which explained the most variation (31 %) in kelp canopy area (**Table 13**). For the more recent time series (2005-2021), a simple univariate model of the ENSO index (1-year averages) best explained the variability in kelp forest canopy

area and captured the most variation (50%) out of any models across all time periods. For the earlier time series (1973-2002), the 2-year averages of SST anomalies best explained the data at 29 % of the variance.

Table 14. Linear regression of normalized kelp area by regional driver. All significant models are bolded (p value < 0.1 *, <0.01**, <0.001***) and the best overall model determined by AICc for each time series is shown italicized. Each column (1- ,2- and 3-year averages) and row (SST, PDO, ENSO and NPGO) show separate univariate models for each time series, the complete satellite time series (1973-2021), the earlier time series (1973-2005) and the short-term time series (2005-2021).

		1 YEAR AVERAGE			**2 YEAR AVERAGE**			**3 YEAR AVERAGE**		
	Time Series	Coeff	R^2	AICc	Coeff	R^2	AICc	Coeff	R^2	AICc
SST	1973-2021	**-17.4440****	**0.1508**	**312.2439**	**-22.050*****	**0.2003**	**310.0876**	**-23.156****	**0.1745**	**311.2273**
	1973-2005	-19.4000	0.1287	171.7054	***-29.976****	***0.2916***	***167.7993***	**-29.610****	**0.2093**	**169.8669**
	2005-2021	-11.5890	0.1205	142.9154	-4.363	0.0118	145.0189	-8.337	0.0339	144.6084
PDO	1973-2021	**-8.055****	**0.1129**	**313.8096**	-6.567	0.0603	315.8816	-6.859	0.0586	315.9481
	1973-2005	-10.790	0.1222	171.8455	-11.675	0.1102	172.1025	-12.925	0.1319	171.6347
	2005-2021	**-9.680****	0.3497	137.5272	-7.052	0.1458	142.3897	-5.991	0.0856	143.6144
ENSO	1973-2021	**-12.839*****	**0.2052**	**309.8654**	**-16.805****	**0.1582**	**311.9266**	-13.829	0.0710	315.4721
	1973-2005	-11.439	0.1245	171.7939	**-21.211***	**0.1780**	**170.5994**	-14.029	0.0558	173.2319
	2005-2021	***-14.647*****	***0.5168***	***132.2901***	-11.490	0.1555	142.1828	-12.056	0.1011	143.3069
NPGO	1973-2021	1.496	0.0061	317.905	2.144	0.0100	317.7603	2.168	0.0080	317.8351
	1973-2005	1.517	0.0034	174.2629	3.125	0.0106	174.1249	4.933	0.0187	173.968
	2005-2021	0.001	0	145.2334	0.2393	0.0003	145.2274	-0.08945	0	145.2326
***BEST OVERALL MODEL FOR 1973-2021: ENSO** (1 YEAR AVERAGE) + **SST** (2 YEAR AVERAGE) R^2= **0.3078** AIC_C= **307.8057** P<0.01*										

The most significant disappearance of kelp forest coincided with a temperature shift in the late 1970s, where the region transitioned from a cool period to a warm period indicated by the PDO, the ENSO and SST anomalies (**Figure 2A-C**). Following this disappearance, 26 years out of the 43 years expressed above average SST in association with lower kelp forest area (e.g., observed in 1982, 1984, 1988, 1992, 1989, 2007, 2015 and 2016 (**Figure 2**). Specifically in 1998, the lowest kelp forest canopy area (0.43 km^2, 5% of the time series maximum) was documented, following the strongest SST anomaly recorded (1977: 0.93 °C above the historical average). In addition, the second and third highest SST anomalies occurred during the well documented 2014-2016 marine heatwave (Di Lorenzo *et al.*, 2008; Gentemann *et al.*, 2017;

Fewings & Brown, 2019; Starko *et al.*, 2022), and led to the lowest kelp forest area documented in the recent time series (1.07 km^2, 13 % of the time series maximum).

Regional Climate Drivers at the Subregional Scale

At the subregional scale, the change in kelp extent in response to regional climate indicators showed a general negative relationship with the ENSO, PDO and SST anomalies (**Table 14**). Specifically in Flagstaff, two models performed well, including both the univariate SST anomaly (3-year average) and the multivariate model that included SST anomalies and the ENSO index (both at 3-year averages). With inclusion of the ENSO index, 4 % more variation in kelp canopy area (50 % in comparison to 45%) was explained. For Cumshewa West and East, the ENSO index (2-year average and 1-year averages, respectively) were the best models, explaining 21 % and 32 % of the variation, respectively (**Table 14**). The main difference between subregions was that PDO best explained the variability of the kelp canopy area in the Mathers Creek subregion.

Table 16. Best linear model for each subregion the complete time series (p value < 0.1 *, <0.01**, <0.001***).

SUBREGION	BEST PREDICTOR MODEL	REGRESSION COEFFICIENT	R^2	AICC
FLAGSTAFF (2)	SST (3-year average)	-38.57***	0.4582	298.4063
	ENSO (3-year average) & SST3 (3-year average)		0.4945	299.0246
CUMSHEWA EAST (3)	ENSO (2-year average)	-21.29***	0.2080	316.7684
CUMSHEWA WEST (4)	ENSO (1-year average)	-19.78***	0.3209	318.9754
MATHERS CREEK (5)	PDO (1-year average)	-15.25***	0.2145	331.7842

In situ drivers

From the *in situ* exploration of modern-day drivers, only one urchin occurred in the photoquadrats; another four were seen in the ROV video footage (**Figure 17A**). We did not observe urchins in the regions where kelp forests had been lost. Pebble was the dominant substrate found in areas where kelp was never present. In areas where kelp was present and lost, substrate did not differ and was largely made up of cobble and boulders mixed with soft sediment (**Figure 17B**). The analysis of the understory data showed that both turf and eelgrass dominated shallow areas where kelp was never detected within Gray Bay, while turfs and branched brown algae (*Desmerestia sp.*) dominated the understory community in the regions where kelp was lost. Only one site within the area where kelp was lost supported an understory kelp forest community - that site was the closest in proximity to the remaining kelp forests. A lush understory community of kelp occurred in areas where canopy kelp persisted (**Figure 17B**).

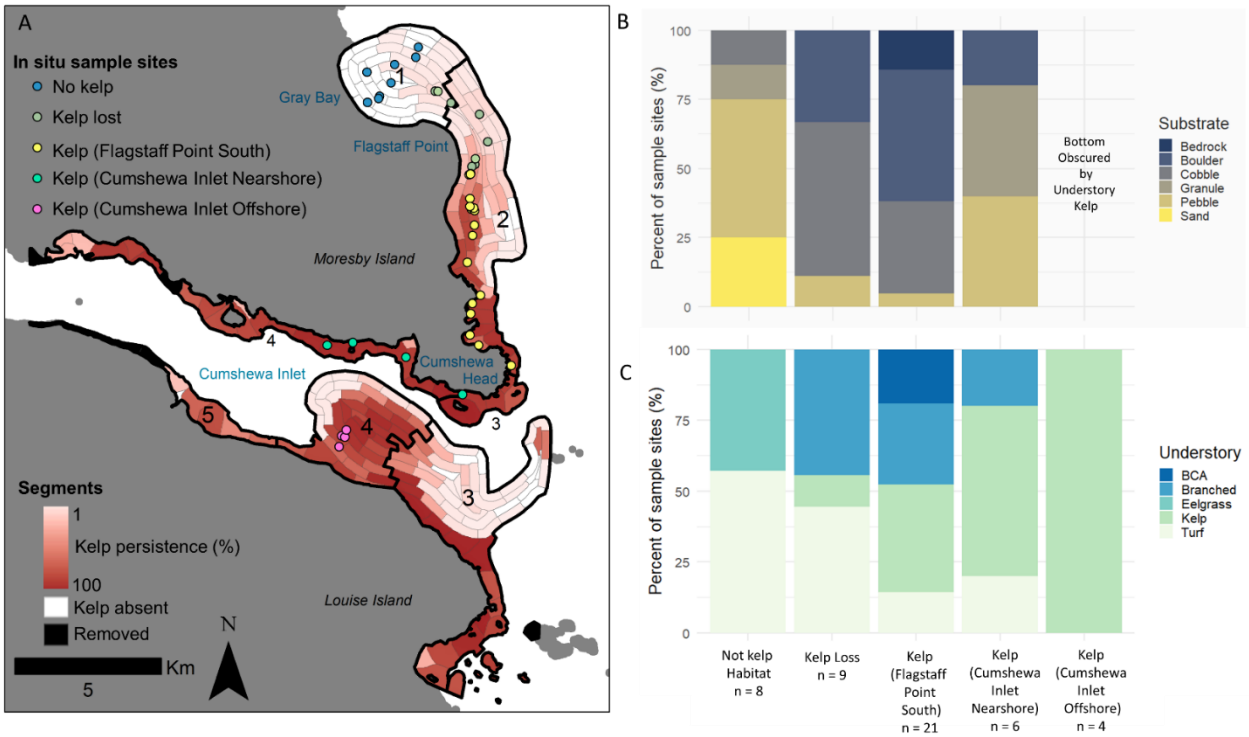

Figure 20. A) Locations of in situ survey sites overlayed over a map of the local persistence metric. B-C) Stacked bar plot showing the percent of substrate classes B) and dominant understory algae class C) documented in areas of no kelp, kelp loss and kelp persistence.

3.5 Discussion

Through the use of medium- to high-resolution archived satellite imagery (1973-2021) and historical data (1867-1945), this study presents the longest and most continuous dataset of kelp canopy area on the Pacific Coast of Canada for the assessment of long-term trends and drivers of change. We identify a long-term declining trend across the region primarily driven by losses in the kelp canopy area in the late 1970s followed by substantial variability and associated with high-frequency and low-frequency climate oscillations. Subregional and local scales of variability were striking, with the greatest losses observed in the late 1970s for kelp forests in the warmer waters of the northern portion of the region (Gray Bay and Flagstaff). Kelp forests further to the South (Cumshewa East, West and Mathers Creek), however, demonstrated overall resilience and remained relatively unchanged since the late 1800s/early 1900s. Across multiple spatial scales of analysis, local gradients in SST coupled with regional climate anomalies, are associated with the observed spatial differentiation in trends. At finer spatial scales, depth, substrate type and fetch played a role in where kelp forests persisted throughout the region. The major influence of top-down trophic level controls such as urchins, may be important in other regions, but do not appear to account for modern-day trends observed in this study as they were not prevalent.

3.5.1 Temporal trends

We observed substantial declines, and local/subregional variability, however, these patterns are not new to the Pacific coast of North America. Similar losses of kelp habitat occurred in the Southern Puget Sound area of Washington State during the late 1970s, however, a lack of sufficient temporal resolution in the time series hinder the ability to pinpoint the exact timing of the loss (Berry *et* al., 2020). Additionally, the aerial scale of losses documented herein are more

comparable in size to some of the kelp forests lost in Northern California during the 2014-2016 marine heatwave and sea star wasting epidemic (Rogers-Bennett & Catton, 2019; McPherson *et al.*, 2021) than those documented in Washington State. In comparison, the Mather's Creek, Cumshewa West and Cumshewa East subregions showed similar trends to those documented by Hamilton *et al*., (2019) in Oregon and Bell *et al*., (2020) in Southern California, where Landsat-derived time series showed relative stability in kelp forest biomass since 1984. However, these papers lack temporal coverage dating to the 1970s and may have missed early losses in kelp forest canopy area that we were able to capture with the multi-satellite imagery time series.

In British Columbia, other studies of different lengths and geographic scales show highly variable patterns of change (Sutherland *et al.*, 2008; Watson & Estes, 2011; Schultz *et al.*, 2016; Burt *et al.*, 2018; Schroeder *et al.*, 2019a; Starko *et al.*, 2022). A long time series (1988-2009) of local sites within Kyuquot Sound (about 300 kilometers south of Haida Gwaii) showed a contrary pattern, where the re-introduction of otters led to a significant regime shift from urchin barrens to productive kelp forest (Watson & Estes, 2011). Other studies on the coastline of BC show no directional trend, and may be indicative of kelp forest resilience, but are limited in geographic and temporal scope (Sutherland *et al.*, 2008; Schroeder *et al.*, 2019a). Additional recent studies have highlighted local declines in kelp forest abundance along the BC coast as a result of direct and indirect effects of the 2014-2016 marine heatwave and sea star wasting epidemic (Schultz *et al.*, 2016; Burt *et al.*, 2018; Starko *et al.*, 2022). Our study showed similar trends with declines observed during the 2014-2016 marine heatwave. However, this area unlike those documented in Howe Sound, (Schultz *et al*, 2016), the central coast (Burt *et al.*, 2018), and Barkley Sound (Starko *et al.*, 2022), showed recovery to pre-heatwave kelp forest canopy area as documented in the short-term time series (2005-2014), demonstrating resilience to large-scale

climate forcing in the 21st century. Our analysis highlights the importance of considering historic losses associated with climate regime shifts in the 1970s as a backdrop for more recent changes observed along the Pacific coast of North America. Without this long-term time series, including indicators of kelp presence since the late 1800s, modern-day mapping may not capture longer term, more dramatic declines in kelp coverage.

Temporally, declines in kelp forest ecosystems are most commonly observed in long time series (20 – 50 years) (Wernberg *et al.*, 2016; Krumhansl *et al.*, 2016; Bell *et al.*, 2020). Specifically related to *Nereocystis* and *Macrocystis*, long-term time series data are required to define resilience given kelp forests' large inter-annual variability and susceptibility to large-scale low-frequency climate oscillations (Dayton *et al.*, 1998; Bell *et al.*, 2020). The length of the time series may have severe implications on the considerations about the "normal state of the environment", with further consequences for management and modelling approaches. The term 'shifting baseline syndrome' refers to the concept that the perceived normal state of the environment changes based on the availability of information and can shift through time based on a lack of experience of previous conditions or length of study period used to define 'normal' (Papworth *et al.*, 2009; Soga & Gaston, 2018). As an example of 'shifting baseline syndrome', our data shows no trend ($p>0.05$, df=1,15, **Table 8**) in the short-term time series (2005-2021), demonstrating that without the careful inclusion of medium-resolution satellite imagery from 1973-2004 the results would have led to the conclusions that kelp forests, although variable, were resilient in the region; even though the long time series showed a differing story of loss (a declining long-term trend of 0.47 % per year 1973-2021, $p<0.05$, $R^2=0.11$, df=1,34, **Table 8**). This highlights the importance of reconstructing long time series for kelp forest ecosystems and centering data within the broader context of the region.

Even with the inclusion of data from the nautical charts (1867-1945), our time series does not capture the distribution of kelp forests prior to the influence of large-scale anthropogenic activities. The maritime fur trade (1785-1840) led to the functional wide-spread extirpation of sea otters on the Pacific Coast of North America by the mid to late 1800s. The timing of the nautical charts likely corresponds with the first otter-free period in this region, which is likely associated with a contraction of kelp forest extent (Estes & Duggins, 1995; Watson & Estes, 2011) A reduction in kelp-derived carbon in rockfish bones of archaeological sites in Southern Haida Gwaii was found during the time period associated with the extirpation of otters, likely indicating a decline in kelp forest abundance (Szpak *et al.*, 2013). This may indicate that the long-term declining trend documented in this study is also an artifact of shifting baselines, with historical distributions of kelp forest canopy area likely larger than the historic maximum documented here, and the potential for even steeper declines, if the time series were extended to times when sea otters were present.

3.5.2 Environmental drivers

Regional climate drivers

At the regional scale, high-frequency climate indicators, i.e., SST anomalies (2-year average) and the ENSO (1-year average) were most strongly related to changes in kelp area, with less kelp during warmer conditions. Throughout the time series, large-scale events such as strong El Nino years, which positively correlate with warm SST anomalies, led to a decrease in the area of kelp forest canopy, similarly to the relationship many describe across the Pacific Coast of North America (Cavanaugh *et al.*, 2011a, 2019b; Bell *et al.*, 2015; Pfister *et al.*, 2018; Burt *et al.*, 2018; Arafeh-Dalmau *et al.*, 2019; Starko *et al.*, 2022). Warmer SST often coincides with lower nutrient availability and lower salinity (Druehl, 1978; Schiel & Foster, 2015; Pfister *et al.*, 2018;

Hamilton *et al.*, 2020a), which, generally, slows growth, weakens tissue and diminishes reproduction (Gerard, 1982; Zimmerman & Kremer, 1986; Brown *et al.*, 1997; Simonson *et al.*, 2015; Stephens & Hepburn, 2016; Starko *et al.*, 2022). Salinity and nutrient data for this region were unavailable for the entire time series, and therefore, relationships with these specific drivers were not disentangled from temperature effects in this study. Additional, drivers included in this study did not account for all the variation observed in the data and other drivers such as wave height, storms frequency and duration, turbidity (i.e., erosion from logging), bryozoan coverage and upwelling (Dayton *et al.*, 1998, 1999; Foster & Schiel, 2010; Reed *et al.*, 2011; Krumhansl *et al.*, 2011; Pfister *et al.*, 2018; Hamilton *et al.*, 2020a) most likely control aspects of kelp forest canopy area through time but were unavailable for inclusion in this study.

In addition to SST anomalies and the ENSO, the inter-annual variability of canopy area showed a significant relationship to the PDO index, indicating that although high-frequency climate forcing best describe kelp forest area variation, long-term climate oscillations also play a role. Specifically in this study, the kelp area relationship to PDO is likely driven by the kelp declines in the late 1970s, which coincided with the PDO-driven climate regime shift in 1976-1977 (Isaacs, 1976). In the Southern Puget Sound region in Washington, a markedly significant decline around the time of this regime shift was documented (Berry *et al.*, 2021), in southern California , following this shift, conditions changed from a nitrate-rich to nitrate depleted environment, resulting in less resilience *Macrocystis* kelp forests (North *et al.*, 1993b; Parnell *et al.*, 2010). Contrary to other work in California (Cavanaugh *et al.*, 2011a; Bell *et al.*, 2020) and Washington (Pfister *et al.*, 2018), kelp forests in Haida Gwaii did not show a significant relationship to the NPGO, suggesting that the Aleutian low-pressure system that drives the PDO has more influence at Haida Gwaii's high latitudinal range than the NPGO. Generally,

unfavourable warmer conditions were expressed by all climate indices (**Figure 14B**; ENSO, PDO, and NPGO) at the end of the 70s, mid 90s (similar to Johnstone & Mantua, 2014), and throughout the 2000s (Di Lorenzo & Mantua, 2016; Oliver *et al.*, 2018, 2019). Specifically, these conditions were associated with a general decrease in kelp area (**Figures 14 and 15**) and are better expressed when multiple years play a role in prediction of kelp distribution. In particular, SST anomalies at 2-, and 3-year averages, and the ENSO index at 2-, and 3-year averages explained more variation in the kelp forest area than 1-year averages (depending on area) demonstrating that conditions across multiple years influence kelp forest health. The response of kelp forests to conditions across multiple years are likely related to changes in reproduction, recruitment, and mortality, whereas, year to year variability is likely driven by surface die back, slowed growth and mortality, which then leads to the lasting impacts on standing stock and reproductive output even once favorable conditions return (Tegner *et al.*, 1997; Dayton *et al.*, 1999; Cavanaugh *et al.*, 2011a; Pfister *et al.*, 2018; Schroeder *et al.*, 2019a).

Spatially Dependent Kelp Forest Dynamics

Spatial heterogeneity in drivers can lead to variable responses in kelp forests at local scales (Krumhansl *et al.*, 2016; Pfister *et al.*, 2018; Smale, 2020; Starko *et al.*, 2022). Here, we corroborate these findings, and show that in Haida Gwaii, variable responses to climate drivers occurred at both the subregional and local spatial scale. We found that the spatial pattern of loss documented in these subregions and the local persistence data act in synchronicity with the local spatial patterns of SST in addition to regional climate oscillations. Here we demonstrate that local gradients can exacerbate the impacts of regional climate anomalies, which result in the local extinctions. As the coastline moves northward on the Pacific Coast of North America, complexity increases, leading to more heterogeneity in the seascape (Cavanaugh *et al.*, 2021),

thus leading to higher variability in response to shifting environments (Starko *et al.*, 2019, 2022). Similarly, this dynamic has led to other instances of local extinctions on the coast of British Columbia in Barkley Sound along a similar local SST gradient (Starko *et al.*, 2019, 2022).

In contrast, local gradients can also moderate the impact of regional SST anomalies. The lower temperatures in the Cumshewa East and West subregions likely moderated the effects of anonymously warm SST events and the regime shift that occurred in the late 1970s. Both Cumshewa Inlet subregions (East and West) follow a similar pattern of kelp variability through time, mainly explained by the ENSO, however, no overall declining trend was observed, demonstrating resilience to environmental perturbations. These subregions also differ in the recent recovery following the 2014-2016 marine heatwave. Cumshewa West, characterized by relatively warmer and more sheltered conditions shows quick recovery to pre-heat wave kelp area. Cumshewa East, however, characterized by temperatures on average 0.5 °C cooler shows slow recovery, with kelp forest area not returning to pre-heat wave amounts by 2021. This may hint to possible higher temperature tolerance of the Cumshewa East kelp population. This subregion is further inside the inlet, with decreased fetch and warmer temperatures over time, but still below the lethal temperature thresholds. When compared with 12 other clades, *Macrocystis*, which primarily makes up the kelp forest canopy area within our study region, was adaptable to warm waters throughout their lifecycle. However, many possible explanations could exist for the higher recovery rate within the warmer Cumshewa West subregion, such as higher standing stock available to replenish losses in the subregion or possible variations in nutrient availability and susceptibility to winter storms, and erosion from logging which we were unable to quantify within this study. Further west in the inlet, kelp area also showed quick recovery following the

2014-2016 marine heatwave in the Mather's Creek subregion, which is exposed to even warmer conditions than Cumshewa West, approximately 1.7 °C warmer on average.

Another mechanism that controlled kelp recovery following the 2014-2016 marine heatwave along the Pacific coast of North America was the co-occurring sea star wasting epidemic, which led to an increased abundance of urchins and the establishment of urchin barrens (Schultz *et al.*, 2016; Burt *et al.*, 2018; Arafeh-Dalmau *et al.*, 2019; McPherson *et al.*, 2021; Starko *et al.*, 2022). Although we could not collect *in situ* urchin data during the 2014-2016 marine heatwave, we were able to evaluate the presence of urchin barrens in 2021. Urchin barrens are known to persist for years to decades because urchins are able to reduce their metabolic activity when food sources become limited (Dolinar & Edwards, 2021), so our observations are likely indicative of conditions during the recent heatwave years. Urchins are often found in the nearshore waters of Haida Gwaii; normally below the wave driven urchin exclusion zones on rocky reefs through out kelp forested regions, often creating urchin barrens (Lee *et al.*, 2021). During our field surveys, no urchin barrens were present where losses were documented in the Northern subregions (Gray Bay and Flagstaff), and very few urchins were found where kelp forest persisted and throughout the remainder of the study region. In addition to the lack of urchins present, the region was composed mostly of mixed sediment substrate, including sand and pebble in the shallows of Gray Bay where the attachment of kelp holdfasts and their subsequent growth to canopy heights is rare. A mix of sand and cobble were observed from subregions where kelp was lost, which urchins normally avoid (Laur *et al.*, 1986). Recently, kelp forest refugia were found in sandy mixed substrate coves that limited urchin grazing in Barkley Sound, supporting the idea that urchins are not a significant contributor to kelp forest dynamics within regions dominated by soft and mixed sediment substrate types.

Additionally, turf and branched algae are often associated with gradual warming and heatwaves (Filbee-Dexter & Wernberg, 2018). This algae cover was found in areas where kelp disappeared in the Gray Bay and Flagstaff subregions, further supporting our hypothesis of temperature-driven kelp forest loss opposed to trophic-driven loss.

3.6 Conclusion

Kelp forests provide the foundation of the environment in temperate nearshore ecosystems of the Pacific Coast of North America; however, the variable dynamics of these systems mean that reliable long-term data is needed to monitor changes. Here, we present the longest, most continuous dataset of kelp forest canopy area to date on the coast of BC by using medium- to high-resolution archived imagery and historical data to lend insight into the environmental drivers of change from local to regional scales. Previous studies highlight the feasibility of using both medium-resolution (Cavanaugh *et al.*, 2011a; Bell *et al.*, 2015; Rogers-Bennett & Catton, 2019; Hamilton *et al.*, 2020a; McPherson *et al.*, 2021; Houskeeper *et al.*, 2022) and high-resolution (Schroeder *et al.*, 2019a; Mora-Soto *et al.*, 2020) satellite imagery to monitor kelp forests canopy through time; however, this study presents a novel application of combining multiple resolutions of satellite imagery to understand long term trends as far back as possible in order to shift historical baselines of kelp forest canopy dynamics on the coast of BC. Landsat 1-3 imagery acquired since 1973, with coarser spatial resolution, was fundamental to define the presence of large kelp areas, similar to the presence of kelp documented in the 1850s. Here, the medium-resolution time series although highly variable shows a declining trend, whereas the high-resolution time series shows similar variability but no directional trend. The multidecadal declining trend seen across the complete satellite time series was largely driven by losses in the 1970s, which would not have been captured with the use of the shorter time series

of high-resolution data (2005-2021) or even Landsat medium-resolution satellite imagery back to 1984.

The strength of environmental drivers varied across regional, subregional, and local scales. Across the region, the canopy area was mostly driven by SST anomalies, high-frequency (ENSO) and low-frequency (PDO) climate oscillations, similar to those observed in California (Cavanaugh *et al.*, 2011a; Bell *et al.*, 2020; McPherson *et al.*, 2021), and Washington (Pfister *et al.*, 2018; Berry *et al.*, 2021). At the subregion and local scales, we show that differences in local conditions, specifically SST, resulted in variable resilience to climate perturbations. Warmer subregions lost extensive coverage of kelp forests in comparison to cooler, more resilient areas. These contrasting spatial trends within a North-South expanse of 23 km are similar to other complex coastal regions of BC (Starko *et al.*, 2019, 2022). Our area presents a unique environment to study kelp forest dynamics outside of the influence of modern-day otter-urchin trophic effects and highlights the importance of long-term data at various spatial scales to examine the role of climate on shaping kelp forest ecosystems globally. This understanding of how local-scale variation leads to spatial resilience will deepen managers' and researchers' abilities to make informed decisions on conserving, monitoring, and managing kelp forests into the future.

4.0 Summary and Conclusions

4.1 Thesis Overview

The main goal of this research was to quantify the distribution, variability, and drivers of change of Haida Gwaii kelp forests. We defined two research objectives to achieve this goal:

(1) In the second chapter (2.0), we develop a methodological framework that enables the creation of a long-term dataset of kelp canopy area using archived multispectral satellite imagery from multiple satellite sensors that vary in their spatial resolution (0.5 m – 60 m) and temporal coverage (1973-2021).

We define the MSKM framework through the use of simple, standardized remote sensing practices, including imagery quality criteria, geometric and Rayleigh corrections, accompanied with adjustable image-based methods such as defining specific band indices/ratios for each sensor and applying an object-based image analysis approach for the classification of kelp forests. Through the application of these methods, we achieved high levels of global accuracy (88-94 %) in the classification of kelp forest canopy produced from the range of resolutions used within the time series. However, we showed that the ability to map kelp forests at different spatial resolutions can vary based on ocean floor slope (as a proxy for kelp bed size), suggesting the use of this metric to define areas of high uncertainties in the output kelp maps. Specifically in our region, we suggest that areas, where the slope is greater than 11.4 %, should be excluded from the time series analysis that includes high- and medium-resolution imagery due to the observed discrepancies of up to 50% in kelp forest canopy area when degrading the resolution of imagery from 2.6 m to 6 m and 10 m, and from 10 m to 20 m, 30 m and 60 m Also, our results suggested that yearly kelp area changes up to 7 % may be attributed to errors associated with resolution when comparing kelp forest area from imagery at different resolutions.

(2) In chapter three (3.0), we define changes in Haida Gwaii kelp forest canopy and associated drivers of change over the last 100 years using historical data (1867-1945) and medium- to high-resolution archived satellite imagery (1973-2021) at regional to local scales of analysis.

By comparing the long-term satellite time series of kelp forest canopy area derived in chapter two (2.0) with historical data and regional to local environmental drivers at the regional, subregional, and local (segment) spatial scales, we highlight areas of high resilience and loss. Broadly, we showed that kelp forest area is related to high-frequency climate indicators, i.e., SST anomalies and ENSO, and to a lesser degree, the PDO low-frequency climate index where warm conditions lead to less kelp forest canopy area overall. More specifically, a significant disappearance of kelp forest canopy area was documented in the relatively warmer Northern portion of the study region, causing an approximate 60 % decrease in the total kelp forest area recorded in the time series. This loss coincides with the cool-to-warm regime shift in the PDO in the late 1970s, most likely exacerbated by the warmer end of a strong local SST gradient experienced across the region. Contrarily, we found that in the remainder of the region, kelp forest area remained at a similar distribution to that of the historical data from over a century prior, highlighting high resilience in the cooler, more sheltered areas of the study region even following the recent 2015-2016 marine heatwave. Moreover, we showed a lack of urchin barrens and an abundance of turf and branching understory algae in 2021 where kelp forests disappeared supporting the hypothesis of scale-dependent environmental responses to drivers of change in the Cumshewa and Gray Bay region of Haida Gwaii.

4.2 Contributions of the research

Beyond the contributions highlighted throughout the previous chapters, this work contributes to the broader literature on the remote sensing of coastal nearshore ecosystems and fills a gap in the geographic coverage of kelp forest research. Importantly, this work builds a better understanding of the dynamics at play in British Columbia which lacks long-term, large-scale spatio-temporal kelp forest data, adding to the growing body of research on the monitoring of foundation species in the face of rapid global change. Additionally, this research shows that archived satellite imagery from throughout the evolution of remote sensing technology at different spatial resolutions can be used to reconstruct kelp forest trends. In particularly, the length of the time series compiled in this study highlights the importance of reconstructing long-term data to capture changes and extend historical baselines in hopes of minimizing shifting baseline syndrome in highly variable ecosystems and is one of the first to highlight drastic climate driven losses as far back as the 1970s. Overall, the variable spatial patterns of change shown in this work emphasize the importance of understanding the intersection between local and regional drivers of kelp forest dynamics and sets a solid underpinning for the future widespread monitoring, management, and protection of kelp forests globally which benefit the overall health of human and non-human communities alike.

4.3 Limitations and Future Research

Several limitations exist within this research, many of which have already been outlined in previous chapters. First, limitations arose from the availability of good quality archived satellite imagery and driver data for the region. Specifically, one to two good images were selected per year meaning time series analysis may be influenced by differences in the timing of peak biomass due to variability in growing conditions year to year. However, no directional trend was

found when comparing the influence of acquisition time on the amount of kelp forest canopy area in imagery, researcher should still be aware of this limitation when using the MSKM framework. Another major limitation of this work is the lack of driver data available for the region. In particular, continuous data of biotic drivers such as urchins, sunflower sea stars, and bryozoan, in addition to further environmental data like nutrient concentrations, water turbidity, salinity, and storm frequency would have deepened the understanding of the complex dynamics present in the system that remain unexplained by the drivers included in this study.

Of consideration to researchers when applying the MSKM framework, is the time needed to compile data from different sources and to process imagery. Also, because of temporal gaps in coverage of freely available high-resolution satellite imagery, some high-resolution satellite images were purchased, which can be cost prohibitive to certain groups, such as non-government organizations or other academics when using the MSKM framework in the future. Lastly, even though this study presents a time series that spans approximately 800 km^2 on the coast of Haida Gwaii, it is but a small proportion of the over 24 000 km long complex coastline of BC meaning the patterns of change observed herein cannot and should not be equated to the entire coast. However, the patterns here do highlight the importance of understanding the intersection between local to regional scale drivers which can then be used at the scale of the entire BC coastline to highlight possible areas of expected vulnerability or resilience. Future work can continue to fill geographic gaps in coverage across the globe in data poor regions using the MSKM framework and once the drivers of kelp forests area robustly understood, these time series can be coupled with climate prediction modelling in the future to predict changes of these dynamic and significant ecosystems.

5.0 References

Alavipanah SK, Matinfar HR, Emam AR, Khodaei K, Bagheri RH, Panah Y. **2010**. Criteria of selecting satellite data for studying land resources. 83–102.

Anderson R, Rand A, Rothman M, Share A, Bolton J. **2007**. Mapping and quantifying the South African kelp resource. *African Journal of Marine Science* **29**: 369–378.

Arafeh-Dalmau N, Montaño-Moctezuma G, Martínez JA, Beas-Luna R, Schoeman DS, Torres-Moye G. **2019**. Extreme Marine Heatwaves Alter Kelp Forest Community Near Its Equatorward Distribution Limit. *Frontiers in Marine Science* **6**.

Augenstein E, Stow D, Hope A. **1991**. Evaluation of Spot Hrv-Xs Data for Kelp Resource Inventories. *Photogrammetric Engineering and Remote Sensing* **57**: 501–509.

Ayoub F, Leprince S, Binet R, Lewis KW, Aharonson O, Avouac J-P. **2008**. Influence of camera distortions on satellite image registration and change detection applications. In: IGARSS 2008 - 2008 IEEE International Geoscience and Remote Sensing Symposium. II-1072-II–1075.

Bannari A, Morin D, Bénié GB, Bonn FJ. **1995**. A theoretical review of different mathematical models of geometric corrections applied to remote sensing images. *Remote Sensing Reviews* **13**: 27–47.

Baraldi A, Boschetti L. **2012**. Operational Automatic Remote Sensing Image Understanding Systems: Beyond Geographic Object-Based and Object-Oriented Image Analysis (GEOBIA/GEOOIA). Part 1: Introduction. *Remote Sensing* **4**: 2694–2735.

Beas-Luna R, Micheli F, Woodson CB, Carr M, Malone D, Torre J, Boch C, Caselle JE, Edwards M, Freiwald J, *et al.* 2020. Geographic variation in responses of kelp forest communities of the California Current to recent climatic changes. *Global Change Biology* **00**: 1–17.

Bell TW, Allen JG, Cavanaugh KC, Siegel DA. **2020**. Three decades of variability in California's giant kelp forests from the Landsat satellites. *Remote Sensing of Environment* **238**: 110811.

Bell TW, Cavanaugh KC, Siegel DA. **2015**. Remote monitoring of giant kelp biomass and physiological condition: An evaluation of the potential for the Hyperspectral Infrared Imager (HyspIRI) mission. *Remote Sensing of Environment* **167**: 218–228.

Bennion M, Fisher J, Yesson C, Brodie J. **2019**. Remote Sensing of Kelp (Laminariales, Ochrophyta): Monitoring Tools and Implications for Wild Harvesting. *Reviews in Fisheries Science & Aquaculture* **27**: 127–141.

Berry HD, Mumford TF, Christiaen B, Dowty P, Calloway M, Ferrier L, Grossman EE, VanArendonk NR. **2021**. Long-term changes in kelp forests in an inner basin of the Salish Sea. *PLOS ONE* **16**: e0229703.

Berry HD, Sewell AT, Wyllie-Echeverria S, Reeves BR, Mumford TF, Skalski JR, Zimmerman RC, Archer J. **2003**. Puget Sound Submerged Vegetation Monitoring Project: 2000 - 2002 Monitoring Report. : 170.

Blakley BB, Chalmers WT. **1973**. *Masset Kelp Inventory*.

Boldt JL, Canada, Department of Fisheries and Oceans. **2020**. *State of the physical, biological and selected fishery resources of Pacific Canadian Marine Ecosystems in 2019*.

Britton-Simmons K, Eckman J, Duggins D. **2008**. Effect of tidal currents and tidal stage on estimates of bed size in the kelp Nereocystis luetkeana. *Marine Ecology Progress Series* **355**: 95–105.

Brown MT, Nyman MA, Keogh JA, Chin NKM. **1997**. Seasonal growth of the giant kelp Macrocystis pyrifera in New Zealand. *Marine Biology* **129**: 417–424.

Burt JM, Tinker MT, Okamoto DK, Demes KW, Holmes K, Salomon AK. **2018**. Sudden collapse of a mesopredator reveals its complementary role in mediating rocky reef regime shifts. *Proceedings of the Royal Society B: Biological Sciences* **285**: 20180553.

Butler C, Lucieer V, Wotherspoon S, Johnson C. **2020**. Multi-decadal decline in cover of giant kelp Macrocystis pyrifera at the southern limit of its Australian range. *Marine Ecology Progress Series* **653**: 1–18.

Camacho M. **2006**. Depth Analysis of Midway Atoll using QuickBird Multi-Spectral Imaging over Variable Substrates.

Cameron FK. **1915**. *Potash from Kelp*. U.S. Government Printing Office.

Carnell PE, Keough MJ. **2019**. Reconstructing Historical Marine Populations Reveals Major Decline of a Kelp Forest Ecosystem in Australia. *Estuaries and Coasts* **42**: 765–778.

Casado-Amezúa P, Araújo R, Bárbara I, Bermejo R, Borja Á, Díez I, Fernández C, Gorostiaga JM, Guinda X, Hernández I, *et al.* 2019. Distributional shifts of canopy-forming seaweeds from the Atlantic coast of Southern Europe. *Biodiversity and Conservation* **28**: 1151–1172.

Casal G, Sánchez-Rodríguez E, Freire J. **2011**. Remote sensing with SPOT-4 for mapping kelp forests in turbid waters on the south European Atlantic shelf. *Estuarine, Coastal and Shelf Science* **91**: 371–378.

Cavanaugh KC, Bell T, Costa M, Eddy NE, Gendall L, Gleason MG, Hessing-Lewis M, Martone R, McPherson M, Pontier O, *et al.* 2021. A Review of the Opportunities and Challenges for Using Remote Sensing for Management of Surface-Canopy Forming Kelps. *Frontiers in Marine Science* **8**: 1536.

Cavanaugh KC, Dangremond EM, Doughty CL, Williams AP, Parker JD, Hayes MA, Rodriguez W, Feller IC. **2019a**. Climate-driven regime shifts in a mangrove–salt marsh ecotone over the past 250 years. *Proceedings of the National Academy of Sciences* **116**: 21602–21608.

Cavanaugh KC, Kendall BE, Siegel DA, Reed DC, Alberto F, Assis J. **2013**. Synchrony in dynamics of giant kelp forests is driven by both local recruitment and regional environmental controls. *Ecology* **94**: 499–509.

Cavanaugh KC, Reed DC, Bell TW, Castorani MCN, Beas-Luna R. **2019b**. Spatial Variability in the Resistance and Resilience of Giant Kelp in Southern and Baja California to a Multiyear Heatwave. *Frontiers in Marine Science* **6**: 413.

Cavanaugh K, Siegel D, Kinlan B, Reed D. **2010**. Scaling giant kelp field measurements to regional scales using satellite observations. *Marine Ecology Progress Series* **403**: 13–27.

Cavanaugh K, Siegel D, Reed D, Dennison P. **2011a**. Environmental controls of giant-kelp biomass in the Santa Barbara Channel, California. *Marine Ecology Progress Series* **429**: 1–17.

Chang K-T. **2009**. *Introduction to Geographic Information Systems*. McGraw-Hill Higher Education.

Chavez PS. **1988**. An improved dark-object subtraction technique for atmospheric scattering correction of multispectral data. *Remote Sensing of Environment* **24**: 459–479.

Coleman MA, Reddy M, Nimbs MJ, Marshell A, Al-Ghassani SA, Bolton JJ, Jupp BP, De Clerck O, Leliaert F, Champion C, *et al.* 2022. Loss of a globally unique kelp forest from Oman. *Scientific Reports* **12**: 5020.

Congalton RG. **1991**. A review of assessing the accuracy of classifications of remotely sensed data. *Remote Sensing of Environment* **37**: 35–46.

Cooley T, Anderson GP, Felde GW, Hoke ML, Ratkowski AJ, Chetwynd JH, Gardner JA, Adler-Golden SM, Matthew MW, Berk A, *et al.* 2002. FLAASH, a MODTRAN4-based atmospheric correction algorithm, its application and validation. In: IEEE International Geoscience and Remote Sensing Symposium. 1414–1418 vol.3.

Coon LM, Roland W, Field EJ, Clayton WEL. **1979**. *Kelp Inventory 1976. Part 3. North & West Coasts Graham Island (Q.C.I)*. Marine Resources Branch, Ministry of Environment, Province of British Columbia.

Coon LM, Roland W, Sutherland IR, Hall R. **1978**. *Kelp Inventory 1978 NorthWest Coast of Vancouver Island*.

Costa M, Barona N, Tenhunen K, Nephin J, Willis P, Mortimorc JP, Dudas S, Rubidge E. **In press**. Historical distribution to kelp forests on the coast of British Columbia: 1858-1956.

Costa M, Le Baron N, Tenhunen K, Nephin J, Willis P, Mortimor JP, Dudas S, Rubidge E. **2020**. Historical distribution of kelp forests on the coast of British Columbia: 1858–1956. *Applied Geography* **120**: 102230.

Crain CM, Halpern BS, Beck MW, Kappel CV. **2009**. Understanding and Managing Human Threats to the Coastal Marine Environment. *Annals of the New York Academy of Sciences* **1162**: 39–62.

Cui T-W, Zhang J, Sun L-E, Jia Y-J, Zhao W, Wang Z-L, Meng J-M. **2012**. Satellite monitoring of massive green macroalgae bloom (GMB): imaging ability comparison of multi-source data and drifting velocity estimation. *International Journal of Remote Sensing* **33**: 5513–5527.

Davies SC, Pacific Biological Station (1972-), Canada, Department of Fisheries and Oceans. **2019**. *Coastal digital elevation models integrating ocean bathymetry and land topography for marine ecological analyses in Pacific Canadian waters*.

Dayton PK. **1985**. Ecology of Kelp Communities. *Annual Review of Ecology and Systematics* **16**: 215–245.

Dayton PK, Tegner MJ, Edwards PB, Riser KL. **1998**. Sliding Baselines, Ghosts, and Reduced Expectations in Kelp Forest Communities. *Ecological Applications* **8**: 309–322.

Dayton PK, Tegner MJ, Edwards PB, Riser KL. **1999**. Temporal and Spatial Scales of Kelp Demography: The Role of Oceanographic Climate. *Ecological Monographs* **69**: 219–250.

Dean TA, Schroeter SC, Dixon JD. **1984**. Effects of grazing by two species of sea urchins (Strongylocentrotus franciscanus and Lytechinus anamesus) on recruitment and survival of two species of kelp (Macrocystis pyrifera and Pterygophora californica). *Marine Biology* **78**: 301–313.

Deysher LE. **1993**. Evaluation of remote sensing techniques for monitoring giant kelp populations. *Hydrobiologia* **260**: 307–312.

DFO. **2015**. *Report on the Progress of Recovery Strategy Implementation for Northern Abalone (Haliotis kamtschatkana) in Pacific Canadian Waters for the Period 2007-2012*. Fisheries and Oceans Canada.

Di Lorenzo E, Mantua N. **2016**. Multi-year persistence of the 2014/15 North Pacific marine heatwave. *Nature Climate Change* **6**: 1042–1047.

Di Lorenzo E, Schneider N, Cobb KM, Franks PJS, Chhak K, Miller AJ, McWilliams JC, Bograd SJ, Arango H, Curchitser E, *et al.* 2008. North Pacific Gyre Oscillation links ocean climate and ecosystem change. *Geophysical Research Letters* **35**.

Dierssen HM, Chlus A, Russell B. **2015**. Hyperspectral discrimination of floating mats of seagrass wrack and the macroalgae Sargassum in coastal waters of Greater Florida Bay using airborne remote sensing. *Remote Sensing of Environment* **167**: 247–258.

Dogliotti AI, Ruddick KG, Nechad B, Doxaran D, Knaeps E. **2015**. A single algorithm to retrieve turbidity from remotely-sensed data in all coastal and estuarine waters. *Remote Sensing of Environment* **156**: 157–168.

Dolinar D, Edwards M. **2021**. The metabolic depression and revival of purple urchins (Strongylocentrotus purpuratus) in response to macroalgal availability. *Journal of Experimental Marine Biology and Ecology* **545**: 151646.

Druehl LD. **1970**. The pattern of Laminariales distribution in the northeast Pacific. *Phycologia* **9**: 237–247.

Druehl LD. **1978**. The distribution of *Macrocystis integrifolia* in British Columbia as related to environmental parameters. *Canadian Journal of Botany* **56**: 69–79.

Duncan C, Owen HJF, Thompson JR, Koldewey HJ, Primavera JH, Pettorelli N. **2018**. Satellite remote sensing to monitor mangrove forest resilience and resistance to sea level rise. *Methods in Ecology and Evolution* **9**: 1837–1852.

Easterling DR. **2000**. Climate Extremes: Observations, Modeling, and Impacts. *Science* **289**: 2068–2074.

Eger A, Marzinelli E, Baes R, Blain C, Blamey L, Carnell P, Choi CG, Hessing-Lewis M, Kim KY, Lorda J, *et al.* 2021. The economic value of fisheries, blue carbon, and nutrient cycling in global marine forests.

Estes JA, Duggins DO. **1995**. Sea Otters and Kelp Forests in Alaska: Generality and Variation in a Community Ecological Paradigm. *Ecological Monographs* **65**: 75–100.

Evans TL, Costa M, Tomas W, Camilo AR. **2013**. A SAR FINE AND MEDIUM SPATIAL RESOLUTION APPROACH FOR MAPPING THE BRAZILIAN PANTANAL. *A. R.* **38**: 19.

Faraway JJ. **2004**. *Linear Models with R*. Chapman and Hall/CRC.

Ferdaña Z. **2006**. Case Study: Pacific Northwest Coast (PNWC) Ecoregion Offshore Classification Methodology. 12.

Fewings MR, Brown KS. **2019**. Regional Structure in the Marine Heat Wave of Summer 2015 Off the Western United States. *Frontiers in Marine Science* **6**.

Field EJ, Clark EAC. **1978**. *Kelp Inventory, 1976, Part 2. The Dundas Group. British Columbia Marine Resources Branch,*. British Columbia Marine Resources Branch.

Field EJ, Coon LM, Clayton WEL, Clark EAC. **1977**. *Kelp Inventory, 1976, Part 1. The Estevan Group and Campania Island*. British Columbia Marine Resources Branch.

Filbee-Dexter K, Feehan C, Scheibling R. **2016**. Large-scale degradation of a kelp ecosystem in an ocean warming hotspot. *Marine Ecology Progress Series* **543**: 141–152.

Filbee-Dexter K, Wernberg T. **2018**. Rise of Turfs: A New Battlefront for Globally Declining Kelp Forests. *BioScience* **68**: 64–76.

Finger DJI, McPherson ML, Houskeeper HF, Kudela RM. **2021**. Mapping bull kelp canopy in northern California using Landsat to enable long-term monitoring. *Remote Sensing of Environment* **254**: 112243.

Foster MS, Schiel DR. **2010**. Loss of predators and the collapse of southern California kelp forests (?): Alternatives, explanations and generalizations. *Journal of Experimental Marine Biology and Ecology* **393**: 59–70.

Franks P, Di Lorenzo E, Goebel N, Chenillat F, Riviere P, Edwards C, Miller A. **2013**. Modeling Physical-Biological Responses to Climate Change in the California Current System. *Oceanography* **26**: 26–33.

Frazier AE, Hemingway BL. **2021**. A Technical Review of Planet Smallsat Data: Practical Considerations for Processing and Using PlanetScope Imagery. *Remote Sensing* **13**: 3930.

Friedlander AM, Ballesteros E, Bell TW, Caselle JE, Campagna C, Goodell W, Hüne M, Muñoz A, Salinas-de-León P, Sala E, *et al.* 2020. Kelp forests at the end of the earth: 45 years later. *PLOS ONE* **15**: e0229259.

Gentemann CL, Fewings MR, García-Reyes M. **2017**. Satellite sea surface temperatures along the West Coast of the United States during the 2014–2016 northeast Pacific marine heat wave. *Geophysical Research Letters* **44**: 312–319.

Gerard VA. **1982**. IN SITU RATES OF NITRATE UPTAKE BY GIANT KELP, MACROCYSTZS PYRZFERA (L.) C. Agardh: TISSUE DIFFERENCES, ENVIRONMENTAL EFFECTS, AND PREDICTIONS OF NITROGEN-LIMITED GROWTH. **Vol. 62**: 211–224.

Giannini F, Hunt BPV, Jacoby D, Costa M. **2021**. Performance of OLCI Sentinel-3A satellite in the Northeast Pacific coastal waters. *Remote Sensing of Environment* **256**: 112317.

Greene HG, Yoklavich MM, Starr RM, O'Connell VM, Wakefield WW, Sullivan DE, McRea JE, Cailliet GM. **1999**. A classification scheme for deep seafloor habitats. *Oceanologica Acta* **22**: 663–678.

Gregr EJ, Lessard J, Harper J. **2013**. A spatial framework for representing nearshore ecosystems. *Progress in Oceanography* **115**: 189–201.

Gregr EJ, Palacios DM, Thompson A, Chan KMA. **2019**. Why less complexity produces better forecasts: an independent data evaluation of kelp habitat models. *Ecography* **42**: 428–443.

Gupta N, Bhaudauria HS. **2014**. Object based Information Extraction from High Resolution Satellite Imagery using eCognition - ProQuest. **11**: 139–144.

Guujaaw. **2002**. *Statement of Claim*.

Haegele CW, Hamey MJ. **1981**. *Shoreline Vegetation on Herring Spawning Grounds for Cumshewa Inlet, Queen Charlotte IslandsCanadian*. Department of Fisheries and Oceans Resource Services Branch Pacific Biological Station Nanaimo, British Columbia V9R 5K6.

Haggan N, Neis B, Baird I (Eds.). **2007**. *Fishers' knowledge in fisheries science and management*. Paris: UNESCO Publishing.

Haida Marine Traditional Knowledge Study Participants, Council of the Haida Nation, Haida Oceans Technical Team, Winbourne J. **2011**. *Haida Marine Traditional Knowledge Volume I, II, III*.

Hamilton SL, Bell TW, Watson JR, Grorud-Colvert KA, Menge BA. **2020**. Remote sensing: generation of long-term kelp bed data sets for evaluation of impacts of climatic variation. *Ecology*: e03031.

Hamilton SL, Gleason MG, Godoy N, Eddy N, Grorud-Colvert K. **2022**. Ecosystem-based management for kelp forest ecosystems. *Marine Policy* **136**: 104919.

Hodgson D, McDonald JL, Hosken DJ. **2015**. What do you mean, 'resilient'? *Trends in Ecology & Evolution* **30**: 503–506.

Hossain MS, Bujang JS, Zakaria MH, Hashim M. **2015**. The application of remote sensing to seagrass ecosystems: an overview and future research prospects. *International Journal of Remote Sensing* **36**: 61–114.

Houskeeper HF, Rosenthal IS, Cavanaugh KC, Pawlak C, Trouille L, Byrnes JEK, Bell TW, Cavanaugh KC. **2022**. Automated satellite remote sensing of giant kelp at the Falkland Islands (Islas Malvinas). *PLOS ONE* **17**: e0257933.

Howes D, Harper J, Owens E. **2001**. BC Biophysical Shore-Zone Mapping System— A Systematic Approach to Characterize Coastal Habitats in the Pacific Northwest. : 11.

Hurvich CM, Tsai C-L. **1993**. A Corrected Akaike Information Criterion for Vector Autoregressive Model Selection. *Journal of Time Series Analysis* **14**: 271–279.

Isaacs JD. **1976**. SOME IDEAS AND FRUSTRATIONS ABOUT FISHERY SCIENCE. : 10.

Jenkins BW, Britt I. **1972**. *Seaweed inventory of two Queen Charlotte inlets*. Department of Environment, Fisheries Service, Vancouver, B.C.

Jensen JR. **1980**. Remote Sensing Techniques for Kelp Surveys. *PHOTOGRAMMETRIC ENGINEERING*: 13.

Jensen JR. **2005**. *Introductory Digital Image Processing: A Remote Sensing Perspective*. Prentice Hall.

Johnson CR, Banks SC, Barrett NS, Cazassus F, Dunstan PK, Edgar GJ, Frusher SD, Gardner C, Haddon M, Helidoniotis F, *et al.* 2011. Climate change cascades: Shifts in

oceanography, species' ranges and subtidal marine community dynamics in eastern Tasmania. *Journal of Experimental Marine Biology and Ecology* **400**: 17–32.

Johnson SW, Murphy ML, Csepp DJ, Harris PM, Thedinga JF. **2003**. *A survey of fish assemblages in eelgrass and kelp habitats of southeastern Alaska*. U.S Department of Commerce.

Johnstone JA, Mantua NJ. **2014**. Atmospheric controls on northeast Pacific temperature variability and change, 1900–2012. *Proceedings of the National Academy of Sciences* **111**: 14360–14365.

Kaufman YJ, Remer LA. **1994**. Detection of forests using mid-IR reflectance: an application for aerosol studies. *IEEE Transactions on Geoscience and Remote Sensing* **32**: 672–683.

Ketchen DJ, Shook CL. **1996**. The Application of Cluster Analysis in Strategic Management Research: An Analysis and Critique. *Strategic Management Journal* **17**: 441–458.

Klemas V. **2010**. Remote Sensing Techniques for Studying Coastal Ecosystems: An Overview. *Journal of Coastal Research* **27**: 2–17.

Krumhansl KA, Lee JM, Scheibling RE. **2011**. Grazing damage and encrustation by an invasive bryozoan reduce the ability of kelps to withstand breakage by waves. *Journal of Experimental Marine Biology and Ecology* **407**: 12–18.

Krumhansl KA, Okamoto DK, Rassweiler A, Novak M, Bolton JJ, Cavanaugh KC, Connell SD, Johnson CR, Konar B, Ling SD, *et al.* 2016. Global patterns of kelp forest change over the past half-century. *Proceedings of the National Academy of Sciences* **113**: 13785–13790.

Kumagai NH, García Molinos J, Yamano H, Takao S, Fujii M, Yamanaka Y. **2018**. Ocean currents and herbivory drive macroalgae-to-coral community shift under climate warming. *Proceedings of the National Academy of Sciences* **115**: 8990–8995.

Ladah LB, Zertuche-González JA, Hernández-Carmona G. **1999**. Giant Kelp (macrocystis Pyrifera, Phaeophyceae) Recruitment Near Its Southern Limit in Baja California After Mass Disappearance During Enso 1997–1998. *Journal of Phycology* **35**: 1106–1112.

Laur DR, Ebeling AW, Reed DC. **1986**. Experimental evaluations of substrate types as barriers to sea urchin (Strongylocentrotus spp.) movement. *Marine Biology* **93**: 209–215.

Layton C, Coleman MA, Marzinelli EM, Steinberg PD, Swearer SE, Vergés A, Wernberg T, Johnson CR. **2020**. Kelp Forest Restoration in Australia. *Frontiers in Marine Science* **7**.

Lee LC, Daniel McNeill G, Ridings P, Featherstone M, Okamoto DK, Spindel NB, Galloway AWE, Saunders GW, Adamczyk EM, Reshitnyk L, *et al.* 2021. Chiixuu Tll iinasdll: Indigenous Ethics and Values Lead to Ecological Restoration for People and Place in Gwaii Haanas. *Ecological Restoration* **39**: 45–51.

Lin C, Wu C-C, Tsogt K, Ouyang Y-C, Chang C-I. **2015**. Effects of atmospheric correction and pansharpening on LULC classification accuracy using WorldView-2 imagery. *Information Processing in Agriculture* **2**: 25–36.

Lu Y, Yuan J, Lu X, Su C, Zhang Y, Wang C, Cao X, Li Q, Su J, Ittekkot V, *et al.* 2018. Major threats of pollution and climate change to global coastal ecosystems and enhanced management for sustainability. *Environmental Pollution* **239**: 670–680.

MaPP, Marine Working Group, Marine Planning Partnership for the North Pacific Coast (B.C.), North Coast--Skeena First Nations Stewardship Society, British Columbia, Ministry of Forests L and NRO. **2015**. *Haida Gwaii Marine Plan*. Victoria, B.C.: MaPP.

Markham BL, Storey JC, Williams DL, Irons JR. **2004**. Landsat sensor performance: history and current status. *IEEE Transactions on Geoscience and Remote Sensing* **42**: 2691–2694.

Matthew MW, Adler-Golden SM, Berk A, Richtsmeier SC, Levine RY, Bernstein LS, Acharya PK, Anderson GP, Felde GW, Hoke ML, *et al.* 2000. Status of atmospheric correction using a MODTRAN4-based algorithm. In: Algorithms for Multispectral, Hyperspectral, and Ultraspectral Imagery VI. International Society for Optics and Photonics, 199–207.

McPherson ML, Finger DJI, Houskeeper HF, Bell TW, Carr MH, Rogers-Bennett L, Kudela RM. **2021**. Large-scale shift in the structure of a kelp forest ecosystem co-occurs with an epizootic and marine heatwave. *Communications Biology* **4**: 1–9.

Mora-Soto A, Palacios M, Macaya EC, Gómez I, Huovinen P, Pérez-Matus A, Young M, Golding N, Toro M, Yaqub M, *et al.* 2020. A High-Resolution Global Map of Giant Kelp (Macrocystis pyrifera) Forests and Intertidal Green Algae (Ulvophyceae) with Sentinel-2 Imagery. *Remote Sensing* **12**: 694.

Mumford TF. **2007**. *Kelp and Eelgrass in Puget Sound*. Fort Belvoir, VA: Washington State Department of Natural Resources.

Nahirnick NK, Costa M, Schroeder S, Sharma T. **2020**. Long-Term Eelgrass Habitat Change and Associated Human Impacts on the West Coast of Canada. *Journal of Coastal Research* **36**: 30–40.

Nahirnick NK, Reshitnyk L, Campbell M, Hessing-Lewis M, Costa M, Yakimishyn J, Lee L. **2019**. Mapping with confidence; delineating seagrass habitats using Unoccupied Aerial Systems (UAS). *Remote Sensing in Ecology and Conservation* **5**: 121–135.

Nelson MD, McRoberts RE, Holden GR, Bauer ME. **2009**. Effects of satellite image spatial aggregation and resolution on estimates of forest land area. *International Journal of Remote Sensing* **30**: 1913–1940.

Nichol LM, Watson JC, Committee on the Status of Endangered Wildlife in Canada. **2007**. *COSEWIC assessment and status report on the sea otter, Enhydra lutris, in Canada*. Ottawa: Committee on the Status of Endangered Wildlife in Canada.

Nijland W, Reshitnyk L, Rubidge E. **2019**. Satellite remote sensing of canopy-forming kelp on a complex coastline: A novel procedure using the Landsat image archive. *Remote Sensing of Environment* **220**: 41–50.

North WJ, James DE, Jones LG. **1993a**. History of kelp beds (Macrocystis) in Orange and San Diego Counties, California. : 7.

North WJ, James DE, Jones LG. **1993b**. History of kelp beds (Macrocystis) in Orange and San Diego Counties, California. *Hydrobiologia* **260**: 277–283.

Oliver ECJ, Burrows MT, Donat MG, Sen Gupta A, Alexander LV, Perkins-Kirkpatrick SE, Benthuysen JA, Hobday AJ, Holbrook NJ, Moore PJ, *et al.* 2019. Projected Marine Heatwaves in the 21st Century and the Potential for Ecological Impact. *Frontiers in Marine Science* **6**.

Oliver ECJ, Donat MG, Burrows MT, Moore PJ, Smale DA, Alexander LV, Benthuysen JA, Feng M, Sen Gupta A, Hobday AJ, *et al.* 2018. Longer and more frequent marine heatwaves over the past century. *Nature Communications* **9**: 1–12.

Olivero J, Ferri F, Acevedo P, Lobo JM, Fa JE, Farfán MÁ, Romero D, Amazonian communities of Cascaradura, Niñal, Curimacare, Chapazón, Solano and Guzmán Blanco, Real R. **2016**. Using indigenous knowledge to link hyper-temporal land cover mapping with land use in the Venezuelan Amazon: 'The Forest Pulse'. *Revista De Biologia Tropical* **64**: 1661–1682.

Papworth S k., Rist J, Coad L, Milner-Gulland E j. 2009. Evidence for shifting baseline syndrome in conservation. *Conservation Letters* **2**: 93–100.

Parnell PE, Miller EF, Cody CEL, Dayton PK, Carter ML, Stebbinsd TD. **2010**. The response of giant kelp (Macrocystis pyrifera) in southern California to low-frequency climate forcing. *Limnology and Oceanography* **55**: 2686–2702.

Peterson TD, Toews HNJ, Robinson CLK, Harrison PJ. **2007**. Nutrient and phytoplankton dynamics in the Queen Charlotte Islands (Canada) during the summer upwelling seasons of 2001–2002. *Journal of Plankton Research* **29**: 219–239.

Pfister CA, Berry HD, Mumford T. **2018**. The dynamics of Kelp Forests in the Northeast Pacific Ocean and the relationship with environmental drivers (A Randall Hughes, Ed.). *Journal of Ecology* **106**: 1520–1533.

Pflug B, Main-Knorn M. **2014**. Validation of atmospheric correction algorithm ATCOR. In: Comerón A, Kassianov EI, Schäfer K, Picard RH, Stein K, Gonglewski JD, eds. Amsterdam, Netherlands, 92420W.

Philander SGH. **1983**. El Niño Southern Oscillation phenomena. *Nature* **302**: 295–301.

Piñeiro-Corbeira C, Barreiro R, Cremades J. **2016**. Decadal changes in the distribution of common intertidal seaweeds in Galicia (NW Iberia). *Marine Environmental Research* **113**: 106–115.

Rayleigh, Lord. **1899**. XXXIV. On the transmission of light through an atmosphere containing small particles in suspension, and on the origin of the blue of the sky. *The London, Edinburgh, and Dublin Philosophical Magazine and Journal of Science* **47**: 375–384.

Reed DC, Rassweiler A, Carr MH, Cavanaugh KC, Malone DP, Siegel DA. **2011**. Wave disturbance overwhelms top-down and bottom-up control of primary production in California kelp forests. *Ecology* **92**: 2108–2116.

Richter R, Schlapfer D. Atmospheric / Topographic Correction for Satellite Imagery. : 203.

Rinde E, Christie H, Fagerli CW, Bekkby T, Gundersen H, Norderhaug KM, Hjermann DØ. **2014**. The Influence of Physical Factors on Kelp and Sea Urchin Distribution in Previously and Still Grazed Areas in the NE Atlantic. *PLOS ONE* **9**: e100222.

Rogers-Bennett L, Catton CA. **2019**. Marine heat wave and multiple stressors tip bull kelp forest to sea urchin barrens. *Scientific Reports* **9**: 15050.

Sani DA, Hashim M, Hossain MS. **2019**. Recent advancement on estimation of blue carbon biomass using satellite-based approach. *International Journal of Remote Sensing* **40**: 7679–7715.

Sawaya K. **2003**. Extending satellite remote sensing to local scales: land and water resource monitoring using high-resolution imagery. *Remote Sensing of Environment*.

Schiel DR, Foster MS. **2015**. *The Biology and Ecology of Giant Kelp Forests*. Univ of California Press.

Schroeder SB, Boyer L, Juanes F, Costa M. **2019a**. Spatial and temporal persistence of nearshore kelp beds on the west coast of British Columbia, Canada using satellite remote sensing. *Remote Sensing in Ecology and Conservation*.

Schroeder SB, Dupont C, Boyer L, Juanes F, Costa M. **2019b**. Passive remote sensing technology for mapping bull kelp (Nereocystis luetkeana): A review of techniques and regional case study. *Global Ecology and Conservation* **19**: e00683.

Schultz JA, Cloutier RN, Côté IM. **2016**. Evidence for a trophic cascade on rocky reefs following sea star mass mortality in British Columbia. *PeerJ* **4**: e1980.

Simonson E, Scheibling R, Metaxas A. **2015**. Kelp in hot water: I. Warming seawater temperature induces weakening and loss of kelp tissue. *Marine Ecology Progress Series* **537**: 89–104.

Sloan NA, Bartier PM. **2000**. *Living Marine Legacy of Gwaii Haanas. I: Marine Plant Baseline to 1999 and Plant-related Management Issues*. Parks Canada.

Sloan NA, Dick L, Relations H-O, Gwaii H. **2015**. SEA OTTERS, AQUAPELAGOS & ECOSYSTEM SERVICES. **9**: 7.

Smale DA. **2020**. Impacts of ocean warming on kelp forest ecosystems. *New Phytologist* **225**: 1447–1454.

Smale DA, Burrows MT, Moore P, O'Connor N, Hawkins SJ. **2013**. Threats and knowledge gaps for ecosystem services provided by kelp forests: a northeast Atlantic perspective. *Ecology and Evolution* **3**: 4016–4038.

Smale DA, Wernberg T. **2013**. Extreme climatic event drives range contraction of a habitat-forming species. *Proceedings of the Royal Society B: Biological Sciences* **280**: 20122829–20122829.

Smale DA, Wernberg T, Oliver ECJ, Thomsen M, Harvey BP, Straub SC, Burrows MT, Alexander LV, Benthuysen JA, Donat MG, *et al.* 2019. Marine heatwaves threaten global biodiversity and the provision of ecosystem services. *Nature Climate Change* **9**: 306–312.

Soga M, Gaston KJ. **2018**. Shifting baseline syndrome: causes, consequences, and implications. *Frontiers in Ecology and the Environment* **16**: 222–230.

Springer Y, Hays C, Carr M, Mackey MM. **2007**. *Ecology and Management of Bull Kelp (Harvest)*. Pacific Marine Conservation Council.

Starko S, A Bailey L, Creviston E, A James K, Warren A, K Brophyid M, Danasel A, Fass M, A Townsend J, Neufeld C. **2019**. Environmental heterogeneity mediates scale- dependent declines in kelp diversity on intertidal rocky shores. *PLoS ONE*.

Starko S, Neufeld CJ, Gendall L, Timmer B, Campbell L, Yakimishyn J, Druehl L, Baum JK. **2022**. Microclimate predicts kelp forest extinction in the face of direct and indirect marine heatwave effects. *Ecological Applications* **n/a**: e2673.

Stekoll MS, Deysher LE, Hess M. **2006**. A remote sensing approach to estimating harvestable kelp biomass. *Journal of Applied Phycology* **18**: 323–334.

Stephens TA, Hepburn CD. **2016**. A kelp with integrity: Macrocystis pyrifera prioritises tissue maintenance in response to nitrogen fertilisation. *Oecologia* **182**: 71–84.

Suchy KD, Le Baron N, Hilborn A, Perry RI, Costa M. **2019**. Influence of environmental drivers on spatio-temporal dynamics of satellite-derived chlorophyll a in the Strait of Georgia. *Progress in Oceanography* **176**: 102134.

Suchy KD, Young K, Galbraith M, Perry RI, Costa M. **2022**. Match/Mismatch Between Phytoplankton and Crustacean Zooplankton Phenology in the Strait of Georgia, Canada. *Frontiers in Marine Science* **9**.

Sutherland IR. **1990**. *Kelp Inventory, 1989, The Vancouver Island and Malcolm Island Shores of Queen Charlotte Strait.* Aquaculture and Commercial Fisheries Branch Ministry of Agriculture and Fisheries Province of British Columbia.

Sutherland IR. **1998**. *Kelp Inventory, 1996 Porcher Island, Groschen Island, Banks Island, and The Estevan Group*. Aquaculture and Commercial Fisheries Branch Ministry of Agriculture, Fisheries and Food Province of British Columbia.

Sutherland IR. **1999**. *Kelp Inventory, 1995 Nootka Sound*. Ministry of Fisheries Sustainable Economic Development Branch.

Sutherland IR, Karpouzi V, Mamoser M, Carswell B. **2008**. *Kelp inventory, 2007 : Areas of the British Columbia Central Coast from Hakai Passage to the Bardswell Group*. Oceans and Marine Fisheries Branch, B.C., Ministry of Environment, Fisheries and Oceans Canada B.C., Ministry of Agriculture and Lands and Heiltsuk Tribal Council.

Szpak P, Orchard TJ, Salomon AK, Gröcke DR. **2013**. Regional ecological variability and impact of the maritime fur trade on nearshore ecosystems in southern Haida Gwaii (British Columbia, Canada): evidence from stable isotope analysis of rockfish (Sebastes spp.) bone collagen. *Archaeological and Anthropological Sciences* **5**: 159–182.

Tanaka K, Taino S, Haraguchi H, Prendergast G, Hiraoka M. **2012**. Warming off southwestern Japan linked to distributional shifts of subtidal canopy-forming seaweeds. *Ecology and Evolution* **2**: 2854–2865.

Tarpley JD, Schneider SR, Money RL. **1984**. Global Vegetation Indices from the NOAA-7 Meteorological Satellite. *Journal of Climate and Applied Meteorology* **23**: 491–494.

Teagle H, Hawkins SJ, Moore PJ, Smale DA. **2017**. The role of kelp species as biogenic habitat formers in coastal marine ecosystems. *Journal of Experimental Marine Biology and Ecology* **492**: 81–98.

Tegner M, Dayton P, Edwards P, Riser K. **1997**. Large-scale, low-frequency oceanographic effects on kelp forest succession:a tale of two cohorts. *Marine Ecology Progress Series* **146**: 117–134.

Teillet PM, Ren X. **2008**. Spectral band difference effects on vegetation indices derived from multiple satellite sensor data. **34**: 16.

Thomas A, Byrne D, Weatherbee R. **2002**. Coastal sea surface temperature variability from Landsat infrared data. *Remote Sensing of Environment* **81**: 262–272.

Thomson RE. **1981**. *Oceanography of the British Columbia coast*. Ottawa: Dept. of Fisheries and Oceans.

Thurstan RH, McClenachan L, Crowder LB, Drew JA, Kittinger JN, Levin PS, Roberts CM, Pandolfi JM. **2015**. Filling historical data gaps to foster solutions in marine conservation. *Ocean & Coastal Management* **115**: 31–40.

Tian J, Zhu X, Wu J, Shen M, Chen J. **2020**. Coarse-Resolution Satellite Images Overestimate Urbanization Effects on Vegetation Spring Phenology. *Remote Sensing* **12**: 117.

Timmer B, Reshitnyk LY, Hessing-Lewis M, Juanes F, Costa M. **2022**. Comparing the Use of Red-Edge and Near-Infrared Wavelength Ranges for Detecting Submerged Kelp Canopy. *Remote Sensing* **14**: 2241.

Titus J, Geroge S. **2013**. A Comparison Study On Different Interpolation Methods Based On Satellite Images. *International Journal of Engineering Research* **2**: 4.

Trishchenko AP, Cihlar J, Li Z. **2002**. Effects of spectral response function on surface reflectance and NDVI measured with moderate resolution satellite sensors. *Remote Sensing of Environment* **81**: 1–18.

Turner N. **2001**. *Coastal peoples and marine plants on the northwest coast.*

Vega JMA, Broitman BR, Vásquez JA. **2014**. Monitoring the sustainability of Lessonia nigrescens (Laminariales, Phaeophyceae) in northern Chile under strong harvest pressure. *Journal of Applied Phycology* **26**: 791–801.

Venello TA, Sastri AR, Suchy KD, Galbraith MD, Dower JF. **2022**. Drivers of variation in crustacean zooplankton production rates differ across regions off the west coast of Vancouver Island and in the subarctic NE Pacific. *ICES Journal of Marine Science* **79**: 741–760.

Vergés A, Doropoulos C, Malcolm HA, Skye M, Garcia-Pizá M, Marzinelli EM, Campbell AH, Ballesteros E, Hoey AS, Vila-Concejo A, *et al.* 2016. Long-term empirical evidence of ocean warming leading to tropicalization of fish communities, increased herbivory, and loss of kelp. *Proceedings of the National Academy of Sciences* **113**: 13791–13796.

Watson J, Estes JA. **2011**. Stability, resilience, and phase shifts in rocky subtidal communities along the west coast of Vancouver Island, Canada. *Ecological Monographs* **81**: 215–239.

Wernberg T, Bennett S, Babcock RC, de Bettignies T, Cure K, Depczynski M, Dufois F, Fromont J, Fulton CJ, Hovey RK, *et al.* 2016. Climate-driven regime shift of a temperate marine ecosystem. *Science* **353**: 169–172.

Wernberg T, Krumhansl K, Filbee-Dexter K, Pedersen MF. **2019**. Chapter 3 - Status and Trends for the World's Kelp Forests. In: Sheppard C, ed. World Seas: an Environmental Evaluation (Second Edition). Academic Press, 57–78.

Wernberg T, Smale DA, Tuya F, Thomsen MS, Langlois TJ, de Bettignies T, Bennett S, Rousseaux CS. **2013**. An extreme climatic event alters marine ecosystem structure in a global biodiversity hotspot. *Nature Climate Change* **3**: 78–82.

Wolter PT, Johnston CA, Niemi GJ. **2005**. Mapping submergent aquatic vegetation in the US Great Lakes using Quickbird satellite data. *International Journal of Remote Sensing* **26**: 5255–5274.

Yang M, Hu Y, Tian H, Khan FA, Liu Q, Goes JI, Gomes H do R, Kim W. **2021**. Atmospheric Correction of Airborne Hyperspectral CASI Data Using Polymer, 6S and FLAASH. *Remote Sensing* **13**: 5062.

Yesson C, Bush LE, Davies AJ, Maggs CA, Brodie J. **2015**. The distribution and environmental requirements of large brown seaweeds in the British Isles. *Journal of the Marine Biological Association of the United Kingdom* **95**: 669–680.

Young NE, Anderson RS, Chignell SM, Vorster AG, Lawrence R, Evangelista PH. **2017**. A survival guide to Landsat preprocessing. *Ecology* **98**: 920–932.

Zebiak SE, Cane MA. **1987**. A Model El Niño–Southern Oscillation. *Monthly Weather Review* **115**: 2262–2278.

Zhu Z. **2019**. Science of Landsat Analysis Ready Data. *Remote Sensing* **11**: 2166.

Zimmerman R, Kremer J. **1986**. In situ growth and chemical composition of the giant kelp, Macrocystis pyrifera: response to temporal changes in ambient nutrient availability. *Marine Ecology Progress Series* **27**: 277–285.